



HAL
open science

Nicotine inhibits the VTA-to-amygdala dopamine pathway to promote anxiety

Claire Nguyen, Sarah Mondoloni, Tinaïg Le Borgne, Ines Centeno, Maxime Come, Joachim Jehl, Clément Solié, Lauren M. Reynolds, Romain Durand-de Cuttoli, Stefania Tolu, et al.

► To cite this version:

Claire Nguyen, Sarah Mondoloni, Tinaïg Le Borgne, Ines Centeno, Maxime Come, et al.. Nicotine inhibits the VTA-to-amygdala dopamine pathway to promote anxiety. *Neuron*, 2021, 109 (16), pp.2604-2615.e9. 10.1016/j.neuron.2021.06.013 . pasteur-03300623

HAL Id: pasteur-03300623

<https://pasteur.hal.science/pasteur-03300623>

Submitted on 24 Nov 2021

HAL is a multi-disciplinary open access archive for the deposit and dissemination of scientific research documents, whether they are published or not. The documents may come from teaching and research institutions in France or abroad, or from public or private research centers.

L'archive ouverte pluridisciplinaire **HAL**, est destinée au dépôt et à la diffusion de documents scientifiques de niveau recherche, publiés ou non, émanant des établissements d'enseignement et de recherche français ou étrangers, des laboratoires publics ou privés.



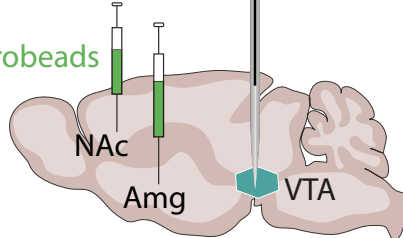
Distributed under a Creative Commons Attribution - NonCommercial - NoDerivatives 4.0 International License

IP Nic
(0.5 mg/kg)



Nicotine-evoked
anxiety

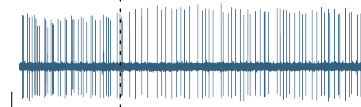
Retrobeads



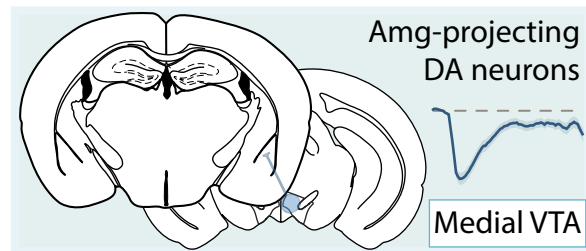
DA firing activation



Nicotine



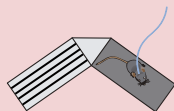
DA firing inhibition



NAc DA terminal activation or inhibition



No change in anxiety



Preference

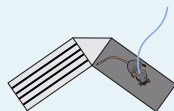


No effect on
nicotine-evoked anxiety

Amg DA terminal activation or inhibition



Decreased or Increased
anxiety



Avoidance



Suppresses
nicotine-evoked anxiety

1 Nicotine inhibits the VTA to Amygdala dopamine pathway to promote 2 anxiety

3 Authors

4 Nguyen C^{1,2}, Mondoloni S², Le Borgne T^{1,2}, Centeno I², Come M^{1,2}, Jehl J^{1,2}, Solié C^{1,2}, Reynolds LM^{1,2},
5 Durand-de Cuttoli R², Tolu S², Valverde S², Didienne S^{1,2}, Hanneke B², Fiancette JF³, Pons S⁴, Maskos
6 U⁴, Deroche-Gamonet V³, Dalkara D⁵, Hardelin JP^{1,2}, Mourot A^{1,2}, Marti F^{1,2##} & Faure P^{1,2##}

7 Affiliations

8 ¹ ESPCI, Laboratoire de plasticité du cerveau UMR8249, 10 rue Vauquelin, 75005 Paris, France.

9 ² Sorbonne Université, Inserm, UMR8246 CNRS, Neuroscience Paris Seine - IBPS, 75005 Paris, France

10 ³ Neurocentre Magendie, Inserm U1215, Université de Bordeaux, 146 rue Léo Saignat, Bordeaux F33077, France

11 ⁴ Institut Pasteur, Unité Neurobiologie intégrative des systèmes cholinergiques, Département de neuroscience,
12 75724 Paris cedex, France.

13 ⁵ Sorbonne Université, Inserm, CNRS, Institut de la Vision, Paris, France.

14 # equal contributions

15 * Correspondence to fabio.marti@upmc.fr, phfaure@gmail.com

16 Lead contact: phfaure@gmail.com

17 Summary

18 Nicotine stimulates dopamine (DA) neurons of the ventral tegmental area (VTA) to establish and maintain
19 reinforcement. Nicotine also induces anxiety, through an as yet unknown circuitry. We found that nicotine
20 injection drives opposite functional responses of two distinct populations of VTA DA neurons with
21 anatomically segregated projections: it activates neurons that project to the nucleus accumbens (NAc),
22 whereas it inhibits neurons that project to the amygdala nuclei (Amg). We further show that nicotine
23 mediates anxiety-like behavior by acting on $\beta 2$ subunit-containing nicotinic acetylcholine receptors of the
24 VTA. Finally, using optogenetics, we bidirectionally manipulate the VTA-NAc and VTA-Amg pathways to
25 dissociate their contributions to anxiety-like behavior. We show that inhibition of VTA-Amg DA neurons
26 mediates anxiety-like behavior, while their activation prevents the anxiogenic effects of nicotine. These
27 distinct subpopulations of VTA DA neurons with opposite responses to nicotine may differentially drive
28 the anxiogenic and the reinforcing effects of nicotine.

29 Keywords

30 nicotinic acetylcholine receptors; dopamine circuits; addiction; juxtacellular recordings; optogenetics;
31 amygdala; nucleus accumbens; ventral tegmental area

32 Introduction

33 Nicotine is the principal addictive component that drives continued tobacco use. The initiation of addiction
34 involves the mesocorticolimbic dopamine (DA) system, which contributes to the processing of rewarding
35 stimuli during the overall shaping of successful behaviors (Schultz, 2007). Addictive drugs such as
36 nicotine are assumed to hijack the mechanisms of reinforcement learning, leading to an overvaluation of
37 the drug reward at the expense of natural rewards. While drug-induced reinforcement learning generally
38 involves an increase in extracellular DA concentration in the nucleus accumbens (NAc), the underlying
39 molecular and cellular mechanisms are drug dependent (Changeux, 2010; Di Chiara and Imperato, 1988;
40 Luscher, 2016). Nicotine exerts its reinforcing effects through the direct activation of nicotinic acetylcholine
41 receptors (nAChR), a family of pentameric ligand-gated ion channels (Changeux et al., 1998), expressed
42 on midbrain DA and GABA neurons, thus increasing the activity of both neuronal populations (Maskos et
43 al., 2005; Morel et al., 2014; Tolu et al., 2013). Cell type-specific optogenetic manipulations have
44 confirmed that DA cell activation is sufficient to drive the transition toward addiction, and established
45 causal links between DA neuron activation and drug-adaptive behaviors (Pascoli et al., 2015). However,
46 such a view does not take into account the heterogeneity of midbrain DA neurons and the possibility that
47 different messages can be transmitted in parallel from DA neurons of the ventral tegmental area (VTA DA
48 neurons). Indeed, VTA DA neurons belong to anatomically distinct circuits, differ in their molecular
49 features, and show diverse responses to external stimuli (Lammel et al., 2008; Poulin et al., 2018). DA
50 neurons transmit signals related not only to salience and reward, but also to aversive stimuli (Brischoux
51 et al., 2009; de Jong et al., 2019), including the “negative” effects of nicotine at high doses (Grieder et al.,
52 2019; 2010). However, how DA neurons simultaneously drive opposite outcomes in response to the same
53 stimuli remains unclear. While the vast majority of research groups that have examined nicotine-evoked
54 responses report a homogenous activation of DA neurons and an increase in DA release in their projection
55 areas (Di Chiara and Imperato, 1988; Grenhoff et al., 1986; Mansvelder and McGehee, 2000; Maskos et
56 al., 2005; Picciotto et al., 1998; Zhao-Shea et al., 2011), other reports suggest that the responses of VTA
57 DA neurons to nicotine are more heterogeneous than previously thought (Eddine et al., 2015; Mameli-
58 Engvall et al., 2006; Zhao-Shea et al., 2011). Therefore, a key issue is how the multiple effects of nicotine
59 map onto DA cell diversity, and whether nAChR or other features can define different neuronal
60 subpopulations that, through their response to nicotine, can influence specific behaviors.

61 Results

62 Distinct VTA DA neuron populations show opposite responses to acute nicotine injection

63 We recorded the response of VTA DA neurons to an intravenous (IV) injection of nicotine using single-
64 cell electrophysiological recordings in anesthetized mice. We used a dose of nicotine (30 µg/kg) that has
65 been shown to be reinforcing in the context of IV self-administration (Morel et al., 2014). These neurons
66 were first identified during the recordings based on their electrophysiological properties (i.e., firing rate
67 and action potential width) (Mameli-Engvall et al., 2006; Ungless and Grace, 2012), and then filled with
68 neurobiotin (NB) by the juxtacellular labeling technique (Eddine et al., 2015; Pinault, 1996). All neurons
69 were confirmed as DA neurons by *post hoc* immunofluorescence with co-labeling for tyrosine hydroxylase
70 (TH) and NB (Figure 1A). Acute IV nicotine injections induced a significant variation of DA neuron firing
71 rates, producing either an increase or a decrease in firing rate that was absent in control experiments with

72 saline. Indeed, the variations in firing frequency had a unimodal distribution for saline injections (n = 233
73 neurons) but a bimodal distribution for nicotine injections (n = 245, Figure 1B, comparison of distribution,
74 Kolmogorov-Smirnov test, $p < 0.001$, see also Figure S1). Among the 245 identified DA neurons, some
75 were activated (Nic +, n = 155) whereas others were inhibited Nic -, n = 88) by the nicotine injection
76 (Figure 1C), in line with our previous findings (Eddine et al., 2015). Nicotine-induced increases or
77 decreases in DA neuron firing rate were of similar amplitude (about 35% from baseline for a dose of 30
78 $\mu\text{g}/\text{kg}$), and were higher in amplitude than saline-evoked responses (Figure 1D). In addition, nicotine-
79 induced changes in DA neuron firing rate were dose-dependent and, importantly, maintained the polarity
80 of their response (i.e. either an increase or decrease) at all doses tested (Figure 1E). Finally, to rule out
81 potential confounding effects of anesthesia on the activity of VTA DA neurons, putative VTA DA neurons
82 (n = 16) were recorded in freely-moving mice (Figure S2A-B), and nicotine or saline was injected into the
83 tail vein (IV 30 $\mu\text{g}/\text{kg}$, see methods). We observed VTA DA neurons that were either activated (Nic +, n
84 = 8) or inhibited (Nic -, n = 8) by the nicotine injection (Figure 1F), replicating the results we found in
85 anesthetized mice (comparisons between saline-induced and nicotine-induced firing rate variations by
86 Student's t-test with Bonferroni correction, * $p = 0.02$ for activated neurons and *** $p < 0.001$ for inhibited
87 neurons). Therefore, the nature of nicotine-evoked responses (i.e. activation or inhibition) constitutes a
88 marker that allows the robust segregation of VTA DA neurons into two populations.

89 We then sought to determine whether the spontaneous activity of these two populations of DA neurons
90 differ in anesthetized mice. The basal activity of VTA DA neurons is characterized by the firing rate and
91 the percentage of spikes within a burst (% SWB) (Mameli-Engvall et al., 2006). Bursts are classically
92 identified as discrete events consisting of a sequence of spikes with (1) a burst onset defined by two
93 consecutive spikes within an interval < 80 ms and (2) the end of a burst defined by an inter-spike interval
94 > 160 ms (Grace and Bunney, 1984a; Ungless and Grace, 2012). We found that nicotine-activated and
95 nicotine-inhibited DA neurons had similar firing rates ($\Delta = 0.26$ Hz, $p = 0.0506$) and bursting activities (Δ
96 = 3.5%, $p = 0.064$ Figure S2C). An analysis of the distribution of burst time intervals also highlighted
97 different profiles in the distribution of inter-spike intervals depending on the burst length (Figure S2C).
98 Other parameters describing cell spontaneous activity (e.g. coefficient of variation or bursting frequency)
99 were analyzed, but none of them revealed a difference between nicotine-activated and nicotine-inhibited
100 DA neurons. Finally, a multiple logistic regression was used to predict the probability of response type
101 (inhibited/activated) based on predictor variables (the firing frequency, the coefficient of variation, %SWB
102 and bursting frequency). Only the spontaneous firing frequency was statistically associated to the
103 outcome ($p = 0.007$) and the classification prediction was very low (about 36%). Overall, differences
104 between the two groups could be detected, yet nicotine-evoked responses could not be predicted based
105 upon the sole analysis of spontaneous activity.

106 We next asked whether these two populations were anatomically segregated. Neurobiotin-filled cell
107 bodies of each responding neuron (n = 243) were positioned onto mouse brain atlas plates (Paxinos and
108 Franklin, 2004) (Figure S3) to study their anatomical location. As illustrated by a single atlas plate
109 schematic (bregma - 3.3 mm), anatomical coordinates suggest that the inhibited neurons were located
110 more medially within the VTA than the activated neurons, independently of their antero-posterior or dorso-
111 ventral positions (Figure 1G).

112

113 **Nicotine-activated VTA DA neurons project to the nucleus accumbens, while nicotine-inhibited**
114 **VTA DA neurons project to the amygdala**

115 The DA system is heterogeneous, and is increasingly thought about in terms of anatomically and
116 functionally distinct sub-networks (Watabe-Uchida et al., 2012). DA neurons in the VTA have been
117 reported to project to different terminal regions based on their localization along the mediolateral axis
118 (Beier et al., 2019; 2015; Lammel et al., 2008). Therefore, we next investigated whether these two
119 subpopulations belong to anatomically distinct dopamine circuits by probing nicotine-evoked responses
120 of DA neurons with identified projection sites. To do so, we first targeted the nucleus accumbens (NAc)
121 by simultaneously injecting green retrobeads (RB), a retrograde tracer, in 3 sub-nuclei: the lateral shell
122 (NAcLSh), the medial shell (NAcMSh) and core (Figure S4A). Two weeks later, spontaneous and nicotine-
123 evoked activities of VTA DA neurons were recorded *in vivo* in anesthetized mice, and neurons were then
124 labeled with neurobiotin. Triple labeling immunofluorescence allowed us to confirm *post hoc* the DA nature
125 (TH+), projection site (RB+ / RB-), and position (NB+) of all recorded neurons (Figure 2A, Figure S4B).
126 We recorded and labeled 32 nicotine-activated and 17 nicotine-inhibited neurons in mice with RB injected
127 in the NAc (all shell+core), among which 30 neurons were further identified as NAc-projecting (RB+, TH+)
128 neurons. Out of the NAc-projecting DA neurons 93% (28/30) were activated by nicotine, while only 7%
129 (2/30) of neurons were inhibited. In contrast, the remaining 19 DA neurons showed no evidence of
130 projection to the NAc (RB-, TH+), and 79% (15/19) of these neurons were inhibited by a nicotine injection,
131 while 21% (4/19) were activated (Figure 2B-C). The proportion of nicotine-activated neurons in NAc-
132 projecting cells was thus significantly greater than what would be expected from the entire population of
133 RB+ and RB- neurons (Pearson's Chi-squared test, $p < 0.001$). A similar analysis was carried out on mice
134 with a single RB injection site of either the NAcMSh or the NAcLSh to examine whether this effect was
135 driven by a specific NAc sub-nucleus. Analysis of the nicotine-evoked responses on NAcMSh-projecting
136 DA neurons ($n = 14$ RB+, TH+ and $n = 8$ RB- TH+) and NAcLSh-projecting DA neurons ($n = 6$ RB+, TH+
137 and $n = 6$ RB- TH+) leads to the same conclusion that the majority of DA neurons that project to the NAc
138 are activated by nicotine, regardless of the specific NAc sub-nucleus they project to (Figure S5).
139 In a second series of experiments, RB were injected in the amygdala nuclei (Amg), targeting both the
140 basolateral (BLA) and central (CeA) amygdala (Figure S4C). All recorded neurons were once again
141 labeled with NB and confirmed as DA *post hoc* by triple labeling immunofluorescence (TH+, NB+, RB+/-,
142 Figure 2D, Figure S4D). We recorded and labeled 26 nicotine-activated and 26 nicotine-inhibited neurons
143 in mice with RB injected in the Amg (BLA + CeA) (Figure 2E-F), among which 22 VTA DA neurons were
144 confirmed as Amg-projecting (RB+, TH+) neurons. Out of the Amg-projecting DA neurons, 86% (19/22)
145 were nicotine-inhibited, while only 14% (3/22) were activated. In contrast, DA neurons without evidence
146 of projection to the Amg (RB-, TH+) were mainly nicotine-activated (77%, 23/30), with 23% (7/30) of
147 neurons inhibited (Figure 2E-F). The proportion of inhibited neurons in Amg-projecting cells was thus
148 significantly greater than what would be expected from the entire population of RB+ and RB- neurons
149 (Pearson's Chi-squared test, $p < 0.001$). Analysis of the distribution of the nicotine-evoked variation in
150 firing frequency for NAc-projecting ($n = 30$) and Amg-projecting neurons ($n = 22$) revealed two different
151 distributions (Kolmogorov-Smirnov test, $p < 0.001$) with opposite modes (i.e positive and negative
152 variations, Figure 2G). Overall, these results indicate that the majority of VTA DA neurons activated by
153 an IV nicotine injection project to the NAc (core or shell), whereas the majority of nicotine-inhibited
154 neurons project to the Amg (comparison of the percentages of inhibited and activated neurons in Amg-
155 projecting neurons and NAc-projecting neurons by Pearson's Chi-squared test: $p < 0.001$). Notably, in
156 line with previous reports (Lammel et al., 2008), further anatomical analysis of triple-labeled VTA sections
157 revealed that Amg-projecting DA neurons are located more medially in the VTA than NAc-projecting DA
158 neurons (Figure S4E). We found that NAc-projecting and Amg-projecting DA neurons had similar firing

159 rates ($p = 0.8$) but Amg-projecting neurons tend to have higher bursting activity ($p = 0.28$), in line with
160 what we had previously observed for nicotine-activated and nicotine-inhibited VTA DA neurons (Figure
161 S4F, and see Figure S2C).

162 We then probed how these opposite changes in the firing of VTA DA neurons in response to nicotine
163 injection translate into dopamine release in the NAc and Amg. Using *in vivo* fiber photometry and a
164 genetically-encoded dopamine sensor (GRAB_{DA2m}, (Sun et al., 2018; 2020)) we assessed the real-time
165 dynamics of DA release in the NAcLSh and in the BLA after IV nicotine injection (30 $\mu\text{g}/\text{kg}$) in the tail vein
166 of freely-moving mice (Figure 2H). We found that nicotine injection evoked an increase of DA release in
167 the NAcLSh, whereas it produced a decrease of DA release in the BLA (Figure 2I), in agreement with our
168 electrophysiological results at the cell body level. Together, these results confirm that nicotine drives
169 opposite functional responses within two distinct DA pathways from the VTA.

170 Finally, we took advantage of the anatomical distinction between these two pathways to analyze the
171 respective electrophysiological properties of their VTA DA neurons in *ex vivo* patch-clamp recordings.
172 NAc-projecting (MSh+LSh+core) or Amg-projecting (BLA+CeA) DA neurons were labeled with RB (Figure
173 S6A-B). Amg-projecting DA neurons showed higher excitability (Figure S6C-D) than NAc-projecting DA
174 neurons, but no difference in nicotine-evoked currents was found between these two populations (Figure
175 S6E-F). These results indicate that these two VTA DA cell populations have different membrane
176 properties, but do not markedly differ in the functional expression of somatodendritic nAChR.

177 **The anxiogenic effect of nicotine requires $\beta 2$ subunit-containing nAChR in the VTA**

178 We next asked whether these two distinct dopamine sub-circuits are associated with different behavioral
179 outcomes after an acute injection of nicotine. Nicotine is known to have rewarding properties, which
180 require the activation of VTA DA neurons (Durand-de Cuttoli et al., 2018; Maskos et al., 2005; Tolu et al.,
181 2013). However, nicotine can also induce negative outcomes such as anxiety-like behaviors and stress-
182 induced depressive-like states (Kutlu and Gould, 2015; Morel et al., 2017; Picciotto and Mineur, 2013),
183 for which the underlying circuitry remains elusive. We hypothesized that the activation and inhibition of
184 the different DA neuron pathways have distinct roles in nicotine-induced behavior. We first aimed to
185 establish the role of the VTA in the anxiogenic effects of acute nicotine exposure. To this end, mice were
186 placed in an elevated-O-maze (EOM) after an acute injection of either saline or nicotine (intra-peritoneal,
187 IP, 0.5 mg/kg, injected one minute before the test), and we found that nicotine, but not saline, reduced
188 exploration of the open arms over time (Figure 3A and Figure S7A for individual data). Mice that received
189 nicotine injections also showed fewer entries into the open arms (Figures S7A), and this anxiety-like
190 phenotype was not related to a detectable effect of nicotine on locomotor activity in an open field (OF,
191 Figure S7B). Next, to probe the specific role of the VTA in this anxiogenic effect, we locally infused nicotine
192 into this brain region (Figure S7C) one minute before the EOM test, using bilaterally implanted cannulas.
193 As with IP injections, we found that the infusion of nicotine, but not saline, directly into the VTA decreased
194 exploration of the EOM open arms over time (Figure 3B and Figure S7D for individual data). Finally, we
195 assessed the involvement of VTA $\beta 2$ subunit-containing nAChR ($\beta 2^* \text{nAChR}$) in the anxiogenic effect of
196 nicotine, as nicotine-evoked responses have been shown to be mainly mediated by $\beta 2^* \text{nAChR}$ present
197 on the soma of both DA and VTA GABA neurons (Tolu et al., 2013). *In vivo* juxtacellular recordings of
198 VTA DA neurons in mutant mice lacking the $\beta 2$ subunit of nAChR ($\beta 2^{-/-}$ mice) demonstrated the absence
199 of a response to nicotine injection (Figure 3C left). Lentiviral re-expression of the $\beta 2$ subunit selectively in
200 the VTA of $\beta 2^{-/-}$ mice ($\beta 2^{-/-}$ Vec mice) globally restored the response to nicotine injection (Figure 3C and

201 Figure S8), allowing the reemergence of nicotine-induced increases or decreases in DA neuron firing
202 (Figure 3C left). Regarding behavior, $\beta 2^{-/-}$ mice were insensitive to the anxiogenic effect of nicotine
203 injection in the EOM test and lentiviral re-expression of $\beta 2$ in the VTA ($\beta 2^{-/-}$ -Vec mice) restored this effect
204 (Figure 3D and see Figure S7G for individual data). Together, these results indicate that the anxiogenic
205 effect of an acute nicotine injection requires signaling through $\beta 2^*nAChR$ in the VTA, but do not allow us
206 to conclude whether the activation and/or inhibition of specific VTA DA neuron populations is required.

207 **Manipulating the VTA-Amg DA pathway modulates basal and nicotine-induced anxiety**

208 Ideally, dissociating whether nicotine-evoked activation or inhibition of VTA DA neurons is necessary for
209 the behavioral effects of nicotine would require to isolate these responses in DA neurons, as well as in
210 VTA GABA neurons, which also express nAChR (Grieder et al., 2019; Tolu et al., 2013). However,
211 because nicotine-induced activation and inhibition of DA neurons are concomitant and inextricably linked
212 to one another (since nicotine cannot directly inhibit neurons), and because the responses of VTA DA
213 and GABA neurons to nicotine are also tightly linked (Tolu et al., 2013), we decided to manipulate the two
214 populations of DA neurons independently, using optogenetics. DAT-Cre mice expressing CatCh, Jaws
215 (Figure S9) or YFP with no opsin (Figure S10A-B) were implanted in the BLA (Figure S10C) or in the
216 NAcLSH (Figure S10D) to restrict the effects of the optogenetic stimulation to DA terminals within that
217 region.

218 We first examined the effect of optogenetic manipulations of DA terminals in the amygdala. When
219 compared to YFP controls, photo-inhibiting DA neuron terminals in the BLA of Jaws-expressing mice
220 reduced the percentage of time spent in the open arms of the EOM, (Figure 4A, and see Figure S11A for
221 individual data). There were also no detectable effects of the light-stimulation on the number of entries in
222 the open arms (Figure S11A-B) or on locomotor activity (Figure S11C). Conversely, photo-activating DA
223 terminals in the BLA of CatCh-expressing mice increased the percentage of time spent in the open arms
224 of the EOM in comparison to mice expressing YFP (Figure 4B, and see Figure S11B for individual data).
225 Moreover, we also noticed that the position of the animal at the onset of the stimulation did not impact
226 any of the behavior observed in the EOM (Figure S11A-B). To determine whether the anxiogenic effect
227 observed during inhibition of DA neuron terminals in the BLA was specific to the BLA nucleus, we used
228 another group of WT mice injected with either Jaws or GFP in the VTA, and implanted bilateral optical
229 fibers either in the BLA or in the CeA (Figure S12A-B). We found that optogenetically inhibiting VTA
230 neuron terminals in Jaws-expressing WT mice decreased the percentage of time spent in the open arms
231 of the EOM when optical fibers were implanted in the BLA, but not when they were implanted in the CeA
232 (Figure S12C-D). There was not a detectable effect of stimulation on locomotor activity in an OF (Figure
233 S12E-F). We next asked whether optogenetically activating the terminals of BLA-projecting VTA DA
234 neurons could prevent the anxiogenic effect of nicotine injection. DAT-Cre mice expressing CatCh or YFP
235 only in the VTA received an IP injection of nicotine one minute before the EOM test, and received light
236 stimulation in the BLA throughout the 9-minute test. Indeed, we found that the light-evoked activation of
237 BLA terminals of DA neurons during the EOM test abolished the anxiogenic effect of the nicotine injection,
238 as the percentage of time spent by CatCh-expressing mice in the EOM open arms did not decrease during
239 the test, and was significantly higher in these mice than in YFP-expressing controls during the last 3-
240 minute period of the test (Figure 4C). We next explored the behavioral outcome of manipulating the
241 terminals of BLA-projecting VTA DA neurons on motivational valence by using a real-time place

242 preference paradigm (RTPP). Photo-inhibiting DA terminals in the BLA resulted in a significant avoidance
243 for the compartment where animals were photo-stimulated, in keeping with our previous findings that
244 inhibition of this pathway produces an anxiogenic effect in the EOM test, while photo-activating these
245 terminals had no behavioral effect (Figure 4D). Inhibition of BLA-projecting VTA DA neurons therefore
246 plays a central role in mediating the anxiogenic effect of nicotine.

247 **The VTA-NAc DA pathway is not involved in nicotine-induced anxiety-like behavior**

248 DA in the NAc has been suggested to be involved in the modulation of anxiety-like behavior (Radke and
249 Gewirtz, 2012; Zarrindast et al., 2012). We thus next assessed whether NAc-projecting neurons also
250 participate in the anxiogenic effects of acute nicotine administration. We examined the behavioral
251 outcome of optogenetic manipulations of DA neuron terminals in the NAc during the EOM test. Light-
252 evoked activation (CatCh-expressing mice, Figure 5A) or inhibition (Jaws-expressing mice, Figure 5B) of
253 DA neuron terminals in the NAcLSh had no effect on the time spent in the open arms of the EOM (see
254 Figure S13A-B for individual data). There was also no detectable effect of the light-stimulation on the
255 number of entries in the open arms (Figure S13A-B), or on locomotor activity (Figure S13C). Moreover,
256 the position of the animal at the onset of the stimulation did not reveal any impact on the behavior
257 observed in the EOM (Figure S13A-B). Selectively inhibiting NAcLSh DA terminals using Jaws produced
258 a slight change in basal anxiety levels but, more importantly, did not attenuate the anxiogenic effect of
259 nicotine in the EOM test, as the drug reduced the exploration of the open arms over time in both control
260 and opsin group (Figure 5C). NAcLSh-projecting VTA DA neurons are therefore not involved in mediating
261 the anxiogenic effect of nicotine. In contrast, activation of DA neuron terminals in the NAcLSh induced
262 significant place preference in the RTPP protocol, indicating that stimulating this pathway is rewarding
263 (Figure 5D). Because medial and lateral NAc areas have different functional roles (de Jong et al., 2019),
264 we further investigated the effect of optogenetic modulation of VTA neuron terminals in the NAcMSH in a
265 separate group of WT mice (Figure S14A). Stimulating these terminals produced an increased number of
266 entries and time spent in the EOM open arms, but this likely results from an increase of locomotor activity,
267 as the distance traveled in an open field was likewise increased (Figure S14B-C). Inhibiting these
268 terminals produced a slight decrease in basal anxiety levels but did not induce behavioral change in the
269 EOM test nor prevented the reduction of time spent in open arms over time induced by nicotine (Figure
270 S14B-D). Finally, we did not observe a significant effect of activating or inhibiting these terminals on the
271 place preference score in the RTPP (Figure S14E). Our results thus demonstrate that NAcMSH and
272 NAcLSh projections of VTA DA neurons are not involved in the nicotine-induced anxiety-like behavior
273 observed in the EOM test.

274 **Discussion**

275 The VTA has long been perceived as a structure that broadly disseminates DA in the brain, with the
276 different time courses of DA release providing a phenomenological account for the functional involvement
277 of DA neurons in different behavioral processes (Schultz, 2007). This temporal account of DA neuron
278 function was gradually replaced or extended by the notion that the DA system, in particular the VTA, is
279 divided into subpopulations of DA neurons, each associated with distinct appetitive, aversive, or
280 attentional behaviors (Lammel et al., 2012). However, we are only beginning to appreciate how the
281 functional activation/inhibition dynamics within these subpopulations impact behavioral processes. Here,

282 we show that (1) activation and inhibition of VTA DA neurons appear concurrently as a consequence of
283 nicotine injection, and (2) they correspond to two anatomically and functionally distinct circuits, which
284 mediate contrasting behavioral effects. Our results argue for a functional dissociation of VTA to Amg and
285 VTA to NAc DA pathways: inhibition of Amg-projecting VTA DA neurons is anxiogenic, while activation of
286 NAcLSh-projecting VTA DA neurons is rewarding. We cannot completely rule out the possibility that
287 optogenetic excitation of axon terminals produces backpropagation of action potentials and activation of
288 other pathways. However, as the VTA projections to the NAc and Amg are anatomically segregated (i.e.
289 neurons do not send collaterals to these two regions (Beier et al., 2015), it is unlikely that this would
290 directly affect the functional dissociation between the two pathways studied in this paper. Furthermore,
291 the fact that photoactivation of NAcLSh terminals is reinforcing, but not those of the NAcMSh or BLA,
292 argues against this possibility.

293 VTA DA neurons are known to be heterogeneous in their axonal projections, electrophysiological
294 properties, and in several molecular features. For example, they show striking differences in their
295 expression of hyperpolarization-activated cyclic nucleotide-gated cation channels (HCN), of the dopamine
296 transporter (DAT), of the dopamine receptor D2R, and vesicular glutamate transporters (VGLUTs)
297 (Lammel et al., 2008; Margolis et al., 2008; Morales and Margolis, 2017). However, the functional
298 consequences of this heterogeneity on behavior remain poorly understood. Here, we demonstrate that
299 nicotine injection evokes opposite responses in two distinct subpopulations of VTA DA neurons: a large
300 majority of those with axons projecting to the NAc are activated, while a large majority of those with axons
301 projecting to the Amg are inhibited. In addition to their functional and anatomical segregation, we found
302 that these subpopulations display different excitabilities *in vitro* and different bursting activities *in vivo*.
303 However, they cannot be distinguished solely on the basis of their spontaneous firing pattern in
304 anesthetized mice. Are there specific intrinsic differences between these two neuronal populations, beside
305 their projection sites, that would underlie their opposing responses to nicotine injection? NAcMSh-
306 projecting VTA DA neurons exhibit smaller I_h currents than BLA-projecting VTA DA neurons, but both
307 have similar input resistances and capacitances (Ford et al., 2006), and NAc core- and BLA-projecting
308 neurons have similar expressions of DAT, D2R and TH (Su et al., 2019). We have previously reported
309 that nicotine activated and inhibited VTA DA cells react similarly to D2R agonist or antagonist injection *in*
310 *vivo*, in agreement with similar D2R expression levels in the two neuronal populations (Eddine et al.,
311 2015). Finally, there is no clear variation in nicotine-evoked currents in Amg-projecting or NAc-projecting
312 VTA neurons, suggesting that nAChR expression does not differ markedly between these populations.

313 While intrinsic differences may still exist, it is also possible that the emergence of either nicotine-evoked
314 activation or inhibition of these neurons by nicotine arises from network dynamics. Nicotine's primary
315 action is to activate nAChR, which are well-characterized ligand gated cation channels, and cause
316 neuronal depolarization. Within the VTA, nicotine directly activates both DA and GABA neurons, which
317 both express nAChR (Klink et al., 2001; Tolu et al., 2013). In particular, β_2^* nAChR of the VTA neurons
318 are key mediators of the reinforcement effects of nicotine, as previously shown by re-expressing the β_2
319 subunit of nAChR locally in the VTA of $\beta_2^{-/-}$ mice (Maskos et al., 2005; Tolu et al., 2013), or by rendering
320 β_2^* nAChR insensitive to nicotine using light (Durand-de Cuttoli et al., 2018). Here, we show that
321 β_2^* nAChR of VTA neurons are also required to evoke, after systemic nicotine injection, the anxiogenic
322 properties of nicotine as well as the inhibition of the subpopulation of DA neurons projecting to Amg.
323 Therefore, nicotine acting through β_2^* nAChR activates VTA GABAergic interneurons and DA neurons

324 projecting to the NAc, while concurrently inhibiting DA neurons projecting to the Amg. The inhibitory effect
325 of nicotine may be mediated by inhibition through local DA release (Eddine et al., 2015), although no
326 difference in D2R-mediated inhibitory postsynaptic currents or in DA reuptake between NAcMSh-
327 projecting and BLA-projecting DA neurons has been reported (Ford et al., 2006). Alternatively, it could
328 involve either local (interneurons) or long-range GABAergic inhibition of the Amg-projecting DA neuron
329 subpopulation primarily, which is compatible with the recent demonstration of distinct inhibitory networks
330 resulting in specific feedback loops between VTA and NAc sub-regions (Yang et al., 2018).

331 Nicotine is highly reinforcing, but also produces aversive and anxiogenic effects at various doses (Balerio
332 et al., 2006; Kutlu and Gould, 2015; Picciotto and Mineur, 2013; Wolfman et al., 2018). Importantly, as
333 the doses of nicotine used in this study are known to be rewarding in different paradigms in mice, an effect
334 attributable to VTA DA neuron activation (Durand-de Cuttoli et al., 2018; Maskos et al., 2005; Tolu et al.,
335 2013), we demonstrate that the same dose of nicotine can concurrently induce a rewarding effect by
336 activating the VTA to NAc DA pathway, and a “negative” emotional state by inhibiting the VTA to Amg DA
337 pathway. Yet, we find that neither the activating effects nor the inhibiting effects of nicotine injection on
338 VTA DA neurons can override each other, that is to say that both types of responses occur at each dose
339 of nicotine along the dose-response curve, with neither response taking precedence at any specific dose.
340 Thus, depending on the context, the exact same dose of nicotine can trigger anxiety or reinforcement.
341 Aversion for high doses of nicotine and anxiety associated with nicotine withdrawal have been attributed
342 to nicotinic and glutamatergic signaling in the habenulo-interpeduncular axis (Fowler et al., 2011; Frahm
343 et al., 2011; Molas et al., 2017; Zhao-Shea et al., 2013). There is also evidence that nAChR of neurons
344 located in the Amg modulate depressive-like states (Mineur et al., 2016). However, a role for DA in
345 aversion to nicotine has also been proposed. D1R and D2R antagonists prevent conditioned-place
346 aversion induced by an acute high-dose nicotine injection (Grieder et al., 2012), and $\beta 2^*$ nAChR have
347 been shown to be necessary for both the aversive and rewarding effects of nicotine by a strategy of $\beta 2$
348 subunit re-expression in DA and GABAergic neurons of the VTA in $\beta 2^{-/}$ mice (Grieder et al., 2019).
349 However, the mechanism underlying these opposite effects of the drug has not yet been established.
350 Here, we show that activation of $\beta 2^*$ nAChR of VTA neurons is necessary for nicotine to inhibit Amg-
351 projecting DA neurons and induce anxiety-like behavior. This indicates that VTA signaling is critically
352 involved in the acute anxiogenic effect of nicotine, and suggests that it could also mediate aversion to
353 nicotine. Our experiments also demonstrate that inhibition of the VTA to Amg DA pathway allows the
354 expression of anxiety-like behavior, and that a reduction of this inhibition relieves nicotine-induced
355 anxiety-like behavior. These experiments strongly suggest a driving role for the inhibition of this pathway
356 in nicotine-induced anxiety behavior, yet they do not exclude the possibility that other pathways also
357 transmit the anxiogenic effect of nicotine.

358 Our findings emphasize the complex role of the DA system in not only positive but also negative
359 motivational processes, proposing a more nuanced view of the effects of reinforcing doses of nicotine on
360 VTA DA neurons. Opposing responses of DA neurons to drug exposure have also been observed with
361 cocaine (Mejias-Aponte et al., 2015), ethanol (Doyon et al., 2013), and morphine (Margolis et al., 2014).
362 Notably, the inhibition of VTA DA neurons induced by opioids differs according to their NAc or BLA
363 projection zone (Ford et al., 2006), suggesting that the behavioral effects of opioid drugs could also result
364 from a specific pattern of inhibition in these two pathways. Since our results demonstrate that both
365 rewarding and anxiogenic messages occur simultaneously upon nicotine exposure and are conveyed by

366 distinct subpopulations of VTA DA neurons, the question then arises as to how the concurrent
367 engagement of two circuits with opposing messages could compete to produce nicotine reinforcement,
368 and whether an imbalance between the two could lead to addiction. Indeed, this question may prove
369 critical when it comes to medical strategies aimed at smoking cessation. While the optogenetic strategies
370 used in this study are well suited to mimic the individual effects of a drug that also produces strong and
371 synchronized neuronal activity, the translational value of these effects is perhaps not to be sought in the
372 specific activation or inhibition of a given neuronal pathway, but rather in the functional imbalance that
373 this creates between the target structures of VTA neurons. Nevertheless, a detailed understanding of the
374 multiple pathways engaged in nicotine-evoked responses and of their respective behavioral contributions
375 can still help us to understand the mechanisms leading to nicotine addiction. In this respect, the activation
376 and inhibition processes which appear in VTA DA neurons as a consequence of systemic nicotine
377 injection call for further mechanistic studies, since they correspond to discrete neuronal circuits and
378 mediate distinct behavioral effects, both of which are relevant to the understanding of addiction.

379 **Acknowledgements:**

380 We are grateful to France Lam and the imaging platform facility (IBPS), the animal facilities (IBPS), Victor
381 Gorgievski for behavioral data acquisition, and Jérémie Naudé for technical and statistical advices. We
382 are grateful to Yulong Li laboratory (Peking University, Beijing) for providing us with GRAB_{DA} sensor
383 plasmids. We are grateful to Mélissa Desrosiers, Camille Robert, and AAV production facility of Paris
384 Vision Institute for viral production and purification.

385 This work was supported by *Centre national de la recherche scientifique* (CNRS UMR 8246), *Institut*
386 *nationale de la santé et de la recherche médicale* (Inserm U1130), *Fondation pour la recherche médicale*
387 (FRM DEQ2013326488 to PF, FRM FDT201904008060 to SM, FRM ECO201806006688 to JJ, FRM
388 SPF202005011922 to CS), French National Cancer Institute Grant TABAC-16-022 et TABAC-19-020 (to
389 PF), French state funds managed by *Agence nationale de la recherche* (ANR-16 Nicostress to PF, ANR-
390 19 Vampire to FM), and LabEx Bio-Psy (to PF, and doctoral fellowship to CN), and LMR was supported
391 by a NIDA–Inserm Postdoctoral Drug Abuse Research Fellowship. PF and UM are members of LabEx
392 Bio-Psy.

393 **Author contributions:**

394 C.N., F.M. and P.F. designed the study. C.N., F.M. and P.F. analyzed the data. C.N. and F.M. performed
395 *in vivo* electrophysiological recordings. L.M.R, S.T. and S.V. contributed to *in vivo* electrophysiological
396 recordings. T.L.B. contributed to *in vivo* electrophysiological data analyses. S.M. designed, performed
397 and analyzed *ex vivo* patch-clamp recordings. C.N. performed stereotaxic injections (with the contribution
398 of S.M. and T.L.B.), fiber/cannula/catheter implantations and behavioral experiments. C.N., S.M., T.L.B.,
399 I.C. and F.M. performed immunostaining experiments. M.C., C.S. and S.D. designed and performed
400 tetrode implantation, and signal analysis for *in vivo* recordings on freely moving animals. S.M., T.L.B. I.C.
401 M.C., J.J., C.S. and B.H. contributed to behavioral experiments. J.J. performed signal treatment and
402 analysis for fiber photometry experiments. R.D.C. and A.M. contributed to optogenetic experiments. D.D.,
403 S.P. and U.M. provided viruses. U.M. provided ACNB2 KO mice. J.F.F. and V.D.G. contributed to
404 behavioral experiments and to design protocols. C.N., L.M.R. J.P.H., A.M., F.M. and P.F. wrote the
405 manuscript.

406 **Declaration of Interests:**

407 Authors declare no competing financial interests.

408

409 **Figure legends**

410 **Figure 1: Nicotine injection evokes opposing responses in distinct VTA DA neuron populations**
411 **(A)** Intravenous (IV) injections of nicotine (Nic, 30 µg/kg) induce activation or inhibition of distinct VTA DA
412 neurons in anesthetized mice (representative recordings). Post-recording identification of neurobiotin
413 (NB)-labeled VTA DA neurons by immunofluorescence (TH = tyrosine hydroxylase, NB = streptavidin-
414 AMCA against neurobiotin). **(B)** Response density after IV injection of either saline (Sal, grey, n = 233) or
415 nicotine (Nic, black, n = 245) expressed as percentage of firing frequency variation induced by the injection
416 (Kolmogorov-Smirnov test, *** p < 0.001). **(C)** Time course for the average change in firing frequency
417 upon nicotine injection for activated (Nic+ in red, n = 155, maximum variation $+33.75 \pm 52.52$ %) and
418 inhibited (Nic- in blue, n = 88, minimum variation -35.43 ± 23.63 %) VTA DA neurons. **(D)** Firing rate
419 variation (Δ) from baseline (Bas) induced by Nic or Sal injection in nicotine-activated and nicotine-inhibited
420 DA neurons. Comparison between mean firing rate during baseline and maximal firing rate after injection
421 for activated neurons, and between mean firing rate during baseline and minimal firing rate after injection
422 for inhibited neurons (paired Wilcoxon test, *** p < 0.001, ns p > 0.05), and comparisons between saline-
423 induced and nicotine-induced firing rate variations (Wilcoxon test, *** p < 0.001). Mean scores are
424 represented in black and individual scores in grey. **(E)** Dose-response curves in Nic+ (red) and Nic- (blue)
425 DA neurons. Responses to different doses of nicotine (0, 10, 15, 30, 60, 90 µg/kg with n = 48, 9, 27, 51,
426 33, 17 for activated neurons, and n = 11, 3, 3, 12, 9, 5 for inhibited neurons) are expressed as percentage
427 of variation from baseline. Neurons are classified as activated or inhibited on the basis of their response
428 to the injection at at least 30 µg/kg nicotine (one-way ANOVA dose effect, Nic+ $F_{(5,179)} = 7.54$ *** p < 0.001
429 and Nic- $F_{(5,37)} = 4.78$, ** p = 0.002). **(F)** Time course for the average change in firing frequency upon saline
430 (grey, n = 16) or nicotine injection for Nic+ (red, n = 8) and Nic- (blue, n = 8) VTA DA neurons recorded
431 with tetrodes in freely moving mice with examples of traces for a Nic+ (red) and a Nic- (blue) neuron. **(G)**
432 Localization of NB-labeled, Nic+ and Nic- DA neurons (n=243), positioned on the Paxinos atlas at bregma
433 - 3.3 mm. Nic- neurons had a more medial distribution within the VTA than Nic+ neurons (Wilcoxon test,
434 *** p < 0.001), but neither antero-posterior (Wilcoxon test, p = 0.4) nor dorso-ventral (Wilcoxon test, p =
435 0.56) differences in their distribution were observed.

436 **Figure 2: VTA DA neuron populations activated or inhibited by nicotine belong to anatomically**
437 **segregated projection pathways**

438 **(A)** Retrobeads (RB) were injected in the nucleus accumbens (NAc, injection in the lateral shell (LSH) +
439 medial shell (MSh) + core), and *in vivo* recordings of VTA DA neuron responses to an IV nicotine injection
440 were performed on anesthetized mice. *Post hoc* identification of NAc-projecting DA neurons by
441 immunofluorescent co-labeling of tyrosine hydroxylase (TH), neurobiotin (NB) and retrobeads (RB). **(B)**
442 Localization of NB-labeled DA neurons (NB+ TH+, n = 49) following RB injection (●RB+, ○RB-) into the
443 NAc. Red and blue colors denote nicotine-activated (Nic+) and nicotine-inhibited (Nic-) neurons,
444 respectively. (RB+ Nic+, n = 28; RB+ Nic-, n = 2; RB- Nic+, n = 4; RB- Nic-, n = 15). **(C)** *Left*: Percentage
445 and number of Nic+ (red) and Nic- (blue) cells among NAc-projecting DA neurons (RB+, *top*) or non-RB-
446 labeled neurons (RB-, *bottom*), with mean change in firing frequency in response to IV injection of either
447 nicotine (red or blue, 30 µg/kg) or saline (black). *Right*: Firing rate variation (Δ) from baseline (Bas)
448 induced by nicotine (Nic) injection in RB+ (mean Δ = +0.52 Hz) or RB- (mean Δ = -0.61 Hz) or RB- DA
449 neurons following RB injection into the NAc. (Comparison between mean firing rate during baseline and
450 maximum/minimum firing rate after injection: paired Wilcoxon test *** p (RB+) < 0.001, * p (RB-) = 0.017,
451 comparison between nicotine-induced firing rate variation evoked in RB+ and RB- DA neurons: Wilcoxon
452 test *** p < 0.001. Mean scores are represented in black, and individual scores in red or blue). **(D)** Same
453 as in (A) but with RB injected in the amygdala (Amg: injection in central nucleus (CeA) + basolateral
454 amygdala (BLA)). **(E)** Localization of NB+ DA neurons (NB+ TH+, n = 52) following RB injection into the
455 Amg (RB+ Nic+, n = 3; RB+ Nic-, n = 19; RB- Nic+, n = 23; RB- Nic-, n = 7). **(F)** *Left*: Percentage and
456 number of Nic+ (red) and Nic- (blue) cells among Amg-projecting DA neurons (RB+, *top*) or non-RB-
457 labeled neurons (RB-, *bottom*). *Right*: Firing rate variation (Δ) from baseline (Bas) induced by nicotine
458 (Nic) injection in RB+ (mean Δ = -0.32 Hz) or RB- (mean Δ = +0.79 Hz) DA neurons following RB injection
459 into the Amg. (Comparison between mean firing rate during baseline and maximum/minimum firing rate
460 after injection: paired Wilcoxon test * p (RB+) = 0.027, ** p (RB-) = 0.002, comparison between nicotine-
461 induced firing rate variation evoked in RB+ and RB- DA neurons: Wilcoxon test *** p < 0.001). **(G)** Density
462 of responses evoked by nicotine in NAc-projecting (gold) and Amg-projecting (purple) DA neurons.
463 Responses expressed as percentage of firing variation induced by nicotine (Kolmogorov-Smirnov test ***
464 p < 0.001). **(H)** AAV-mediated delivery of the genetically encoded GPCR-activation-based-DA sensor
465 (GRAB_{DA}) in the BLA and the NAcLSH of wild-type (WT) mice. One optic fiber was implanted in the BLA
466 of one brain hemisphere and a second fiber was implanted in the NAcLSH of the other hemisphere.
467 Examples of fluorescence variation of GRAB_{DA} expression (as $\Delta F/F$) induced by IV Nic or Sal injection
468 and fiber implantation sites (*Left*) in the BLA and (*Right*) in the NAcLSH with *post hoc* verification of both
469 implantations. **(I)** (*Left*) Mean fluorescence variation of GRAB_{DA} (expressed as $\Delta F/F$, transparent curves
470 (mean $\Delta F/F$), bold curves (kernel fit of $\Delta F/F$)) induced by saline (grey) or nicotine IV injection (30 µg/kg)
471 in freely moving mice recorded by fiber photometry in the NAcLSH (gold, n = 8 injections in 6 mice) and
472 the BLA (purple, n = 7 injections in 6 mice). (*Right*) Difference in peak $\Delta F/F$ between nicotine and saline
473 (Paired Student's t-test, *** p < 0.001 and * p = 0.011 for NAcLSH and BLA ; difference in $\Delta F/F$ (Nicotine –
474 Saline) between NAcLSH and BLA, Student's t-test, *** p < 0.001)

475 **Figure 3: $\beta 2$ subunit-containing nAChR mediate VTA DA neuron responses to nicotine injection**
476 **and nicotine-induced anxiety-like behavior.**

477 **(A)** Nicotine (Nic, 0.5 mg/kg) or saline (Sal) was injected intraperitoneally (IP) 1 minute before the 9-
478 minute elevated O-maze (EOM) test. Nic injection in a group of wild-type (WT) mice (n = 21) decreased
479 the time they spent in the open arms of the EOM compared to the group injected with Sal (n = 23) (two-
480 way RM ANOVA treatment x time interaction $F_{(2,84)} = 5.37$, ** p = 0.006, main effect of time $F_{(2,84)} = 3.84$, *
481 p = 0.025; *post hoc* Wilcoxon test with Bonferroni corrections: * p (3 vs 9 minutes) = 0.03 ; p(3 vs 6
482 minutes) = 0.1 ; p (6 vs 9') = 0.2; *post hoc* Wilcoxon test Sal vs Nic at 9 minutes, *** p < 0.001). **(B)** Mice
483 implanted with intracranial (IC) bilateral guide cannulas were injected either with Sal or with Nic (100 ng
484 in 100 nl infusion) over 1 minute before the 9-minute EOM test. The Nic-injected mice (n = 7) spent less
485 time in the open arms over time, but not the control mice (n = 6) (two-way RM ANOVA treatment x time
486 interaction $F_{(2,22)} = 9.66$ *** p < 0.001, main effect of time *** p < 0.001; *post hoc* Student's t-test with
487 Bonferroni corrections: *** p (3 vs 9 minutes) < 0.001; * p (3 vs 6 minutes) = 0.025; * p (6 vs 9 minutes) =
488 0.02; *post hoc* Student's t-test Sal vs Nic at 9 minutes, p = 0.054). **(C)** *Top left*: Representative juxtacellular
489 recording traces of VTA DA neurons in mice lacking the $\beta 2$ nAChR subunit ($\beta 2^{-/-}$) and in $\beta 2^{-/-}$ -vectorized
490 mice, in which the $\beta 2$ subunit has been virally re-expressed together with a GFP marker in the VTA ($\beta 2^{-/-}$ -
491 Vec). *Bottom left*: Individual and mean responses (expressed as percentage of firing frequency variation)
492 indicate that there were no Nic-evoked responses in VTA DA neurons of $\beta 2^{-/-}$ mice (n = 46 cells from 12
493 mice), and that both Nic-evoked activation (n = 51 cells from 18 mice) and inhibition (n = 39 cells from 19
494 mice) of VTA DA neurons were restored in $\beta 2^{-/-}$ -Vec mice. *Top right*: Immunofluorescence for TH and GFP
495 on $\beta 2^{-/-}$ -Vec mice. *Bottom right*: Cumulative distribution of Nic-evoked response amplitude of VTA DA
496 neurons in $\beta 2^{-/-}$ mice (n = 46 cells from 12 mice, grey) and $\beta 2^{-/-}$ -Vec mice (n = 90 cells from 24 mice, black)
497 (Kolmogorov-Smirnov test ** p = 0.008). Bar plots show the maximum firing variation induced by Nic (filled
498 bars) and saline (unfilled bars) in the two groups. Nic injection did not alter the firing frequency of VTA DA
499 neurons in $\beta 2^{-/-}$ mice, however it induced a significant increase (mean 12.45 ± 13.37) or decrease (mean
500 -13.16 ± 16.31) in the firing frequency of VTA DA neurons in $\beta 2^{-/-}$ -Vec mice compared to saline (**p <
501 0.001, *** p < 0.001) or (**p < 0.001, ** p = 0.005) (Wilcoxon paired test with Bonferroni corrections) **(D)**
502 EOM test after IP Nic injection (0.5 mg/kg) in a control group of $\beta 2^{-/-}$ mice some of which were sham-
503 transduced with GFP in the VTA (see methods, $\beta 2^{-/-}$ n = 23) and in $\beta 2^{-/-}$ -Vec mice (n = 18). Re-expression
504 of $\beta 2$ subunit in the VTA ($\beta 2^{-/-}$ -Vec) restored the nicotine-evoked anxiogenic effects in the EOM test, which
505 was absent in the $\beta 2^{-/-}$ mice (two-way RM ANOVA interaction treatment x time $F_{(2,78)} = 3.43$, * p = 0.04,
506 main time effect $F_{(2,78)} = 6.87$, ** p = 0.002; *post hoc* Student's t-test with Bonferroni corrections: ** p(3 vs
507 9 minutes) = 0.003; * p(3 vs 6 minutes) = 0.03; p(6 vs 9 minutes) = 0.2; *post hoc* Student's t-test $\beta 2^{-/-}$ and
508 $\beta 2^{-/-}$ -GFP vs $\beta 2^{-/-}$ -Vec mice at 9 minutes, p = 0.06).

509 **Figure 4: Inhibition of BLA- projecting DA neurons drive anxiety-like behavior, but not place**
510 **preference.**

511 **(A)** *Left:* AAVs for Cre-dependent expression of Jaws (orange, n = 18) or YFP (green, n = 19) were
512 injected into the VTA of DAT-Cre mice, and optical fibers were placed in the BLA. *Right:* Percentage of
513 time spent in the EOM open arms for mice stimulated continuously at 520 nm over a 5-minute period (ON)
514 in the BLA (Two-way RM ANOVA time x opsin interaction $F_{(2,70)} = 3.32$, * $p = 0.04$; *post hoc* Student's t-
515 test for Jaws vs YFP mice: * $p(\text{ON}) = 0.04$; *post hoc* Student's t-test with Bonferroni corrections for Jaws
516 mice, * $p(5 \text{ vs } 10 \text{ minutes}) = 0.01$, * $p(10 \text{ vs } 15 \text{ minutes}) = 0.02$). **(B)** *Left:* AAVs for Cre-dependent
517 expression of CatCh (blue, n = 18) or YFP (green, n = 19) were injected into the VTA of DAT-Cre mice,
518 and optical fibers were placed in the BLA. *Right:* Percentage of time spent in the EOM open arms for mice
519 stimulated at 470 nm over a 5-minute period (ON) at 10 Hz, 5 ms-pulses in the BLA (Two-way RM ANOVA
520 main effect of time $F_{(2,70)} = 4.41$, * $p = 0.02$, time x opsin interaction $F_{(2,70)} = 4.43$, * $p = 0.015$; *post hoc*
521 Student's t-test for CatCh vs YFP mice, ** $p(\text{ON}) = 0.009$, *post hoc* Student's t-test with Bonferroni
522 corrections for CatCh mice, ** $p(5 \text{ vs } 10 \text{ minutes}) = 0.001$; * $p(10 \text{ vs } 15 \text{ minutes}) = 0.01$). **(C)** *Left:* AAVs
523 for Cre-dependent expression of CatCh (blue, n = 13) or YFP (green, n = 9) were injected into the VTA of
524 DAT-Cre mice, and optical fibers were placed in the BLA. Nicotine (Nic, 0.5 mg/kg) was injected
525 intraperitoneally (IP) 1 minute before the 9-minute elevated O-maze (EOM) test. *Right:* Percentage of
526 time spent in the EOM open arms for mice stimulated in the BLA throughout the test at 10 Hz, 5-ms light-
527 pulses after IP nicotine injection (Two-way RM ANOVA main effect of time $F_{(2,40)} = 4.92$, * $p = 0.01$, time
528 x opsin interaction $F_{(2,40)} = 3.74$, * $p = 0.03$; *post hoc* Student's t-test for CatCh vs YFP mice at 9 minutes
529 ** $p = 0.006$). **(D)** Preference score in a 20 min-real-time place preference test (RTPP) defined by the %
530 of time spent in the compartment where animals are photo-stimulated compared to the compartment
531 where they are not (ON-OFF). Optical inhibition of the VTA-BLA pathway (orange, n = 17 mice) induced
532 online place avoidance compared to the control mice (YFP, green, n = 20) (Student's t-test, * $p = 0.017$).
533 Mice with optical activation of the VTA-BLA pathway (blue, n = 12) did not display any difference compared
534 to the control mice (YFP, green, n = 13) (Student's t-test, $p = 0.5$).

535 **Figure 5: Activation of NAcLSH-projecting VTA DA neurons drives real-time place preference**
536 **behavior, but has no effect on anxiety-like behavior**

537 **(A)** *Left:* AAVs for Cre-dependent expression of CatCh (blue, n = 13) or YFP (green, n = 14) were injected
538 into the VTA of DAT-Cre mice, and optical fibers were placed in the NAcLSH. *Right:* Percentage of time
539 spent in the EOM open arms for mice stimulated at 470 nm over a 5-minute period (ON) at 10 Hz, 5 ms-
540 pulses in the NAcLSH (Two-way RM ANOVA no time or opsin effect, nor interaction $F_{(2,50)} = 0.8$, $p = 0.5$).

541 **(B)** *Left:* AAVs for Cre-dependent expression of Jaws (orange, n = 12) or YFP (green, n = 12) were
542 injected into the VTA of DAT-Cre mice, and optical fibers were placed in the NAcLSH. *Right:* Percentage
543 of time spent in the EOM open arms for mice stimulated continuously at 520 nm over a 5-minute period
544 (ON) in the NAcLSH (Two-way RM ANOVA no time or opsin effect, nor interaction $F_{(2,44)} = 0.16$, $p = 0.8$).

545 **(C)** *Left:* AAVs for Cre-dependent expression of Jaws (orange, n = 11) or YFP (green, n = 12) were
546 injected into the VTA of DAT-Cre mice, and optical fibers were placed in the NAcLSH. Nicotine (Nic, 0.5
547 mg/kg) was injected intraperitoneally (IP) 1 minute before the 9-minute elevated O-maze (EOM) test.
548 *Right:* Percentage of time spent in the EOM open arms for mice stimulated continuously in the NAcLSH
549 throughout the test after IP nicotine injection (Two-way RM ANOVA main time effect $F_{(2,42)} = 12.6$, *** $p <$
550 0.001 , opsin effect $F_{(1,21)} = 5.08$, * $p = 0.03$, no interaction $F_{(2,42)} = 0.55$, $p = 0.6$).

551 **(D)** Preference score in a 20 min-RTPP test defined by the % of time spent in the compartment where animals are photo-
552 stimulated compared to the compartment where they are not (ON-OFF). Mice with optical inhibition of the
553 VTA-NAcLSH pathway (orange, n = 12) did not display any difference compared to the control mice (YFP,
554 green, n = 12) (Student's t-test, $p = 0.5$). Optical activation of the VTA-NAcLSH pathway (blue, n = 13)
555 induced online place preference compared to the control mice (YFP, green, n = 14) (Student's t-test, * p
556 $= 0.04$).

557 **STAR Methods**

558 **LEAD CONTACT**

559 Further information and requests for resources and reagents should be directed to and will be fulfilled by
560 the Lead Contact, Philippe Faure (phfaure@gmail.com) or Fabio Marti (fabio.marti@upmc.fr).

561 **MATERIALS AVAILABILITY**

562 This study did not generate new unique reagents.

563 **DATA AND CODE AVAILABILITY**

564 All the data are available from the corresponding authors upon request.

565 **EXPERIMENTAL MODEL AND SUBJECT DETAILS**

566 Wild-type (WT) C57BL/6J (Janvier Labs, France), ACNB2 KO ($\beta 2^{-/-}$) and DAT^{CRE} (DAT-Cre) male mice,
567 weighing 25-35 grams, were used in this study. $\beta 2^{-/-}$ mice were generated using standard homologous
568 recombination procedures. Founders were backcrossed onto a C57BL/6J background for a least 20
569 generations and bred on site. DAT^{CRE} mice were provided by François Tronche (IBPS Paris, France).
570 They were bred on site and genotyped as described (Turiault et al., 2007).

571 Mice were kept in an animal facility where temperature ($20 \pm 2^{\circ}\text{C}$) and humidity were automatically
572 monitored, and a circadian light-dark cycle of 12/12 hours was maintained. All experiments were
573 performed on 8-to-16-week-old mice. All experiments were performed in accordance with the
574 recommendations for animal experiments issued by the European Commission directives 219/1990,
575 220/1990 and 2010/63, and approved by Sorbonne University.

576 **METHOD DETAILS**

577 **Viral production**

578 AAV vectors were produced as previously described (Khabou et al., 2018) using the co-transfection
579 method, and purified by iodixanol gradient ultracentrifugation (Choi et al., 2007). AAV vector stocks were
580 titrated by quantitative PCR (qPCR) (Aurnhammer et al., 2012) using SYBR Green (Thermo Fischer
581 Scientific). Lentiviruses were prepared as previously described (Maskos et al., 2005; Tolu et al., 2013),
582 with a titer of either 380 ng of p24 protein per μL or 764 ng/ μL for the AChR $\beta 2$ -expressing vector, and
583 150 ng of p24 protein per μL or 361 mg per 2 μL for GFP-expressing vector.

584 **Drugs**

585 The nicotine (Nic) used for all experiments is a nicotine hydrogen tartrate salt (Sigma-Aldrich, USA). For
586 juxtacellular recordings, we performed an intravenous injection (IV) of Nic at a dose of 30 $\mu\text{g}/\text{kg}$ (4.16
587 mg/kg, free base) or saline solution (H_2O with 0.9% NaCl). For the behavioral test, in elevated O-maze
588 (EOM) or open-field (OF), mice were injected intra-peritoneally (IP) with Nic at 0.5 mg/kg, 1-minute before
589 the test. For intra-cranial (IC) experiments in EOM, saline solution or 100ng of Nic tartrate, in a volume of

590 100 nl, were infused over 1 minute before the beginning of the test. All solutions were prepared in the
591 laboratory.

592 **Stereotaxic surgeries**

593 For virus and RB injections, intracranial cannulas, fibers, catheters and micro-drive implantations, mice
594 were anesthetized with a gas mixture of oxygen (1 L/min) and 3% isoflurane (Vetflurane®, Virbac) for the
595 induction of anesthesia, and then placed in a stereotaxic frame (David Kopf) maintained under anesthesia
596 throughout the surgery at 1% isoflurane. A local anesthetic (100 µL Lurocaine®) was applied at the
597 location of the scalp incision or the catheter implant before the procedure. At the end of the surgery, 0.1
598 mL of buprenorphine (BupreCare®, 1 mg/kg) was injected subcutaneously to prepare awakening.

599 **Retrobead injection**

600 Green fluorescent retrograde tracer, retrobeads (RB, LumaFluor Inc., Naples, FL), were injected (200 nL
601 per site, 0.1 µL/min) in WT animals either in the NAc (NAc lateral shell NAcLSH: bregma 1.45 mm, lateral
602 1.75 mm, ventral 4.0 mm; NAc medial shell NAcMSH: bregma 1.78 mm, lateral 0.45 mm, ventral 4.1 mm;
603 NAc core: bregma 1.55 mm, lateral 1.0 mm, ventral 4.0 mm) or in the Amg (BLA: bregma -1.61 mm, lateral
604 3.18 mm, ventral 4.7 mm; CeA: bregma -0.78 mm, lateral 2.3 mm, ventral 4.8 mm) with a 10 µL Hamilton
605 syringe (Hamilton) coupled with a polyethylene tubing to a 36G injection cannulas (Phymep). Note that
606 these empirically derived stereotaxic coordinates do not precisely match those given in the mouse brain
607 atlas (Paxinos and Franklin, 2004), which we used as references for the injection-site images. To enable
608 retrograde transport of the RB into the somas of midbrain DA neurons, we waited for an adequate time to
609 perform the electrophysiology experiments, depending on the injection zone: 3 weeks after injection into
610 the NAc and 2 weeks after injection into the Amg.

611 **Intracranial infusion**

612 Bilateral guide cannulas (Bilaney) were implanted in the VTA (bregma 3.1 mm, lateral 0.5 mm, ventral 4.3
613 mm) of WT mice under anesthesia 1 week before the EOM experiment, in order to enable local infusion
614 of drugs. Before each experiment session a double injection cannula (4.5 mm length, 1 mm interval) was
615 inserted into the implanted bilateral guide cannulas (length under pedestal 4.0 mm), 0.5 mm beyond the
616 tip of the guide cannulas. The day of the experiment, the cannulas were connected to a multi-syringe
617 pump (Univentor) allowing saline or nicotine (100 ng) injection over 1 minute (injected volume of 100 nL).

618 **Virus injection and optogenetic experiments**

619 For lentiviral re-expression of the $\beta 2$ subunit, we performed bilateral injections of 1 µL of PGK- $\beta 2$ -IRES-
620 GFP ($\beta 2^{-/-}$ Vec mice) or sham PGK-IRES-GFP into the VTA of $\beta 2^{-/-}$ mice (coordinates from bregma 3.1
621 mm, lateral 0.5 mm, ventral 4.5 mm).

622 To perform DA neuron-specific optogenetic experiments, intracranial (IC) injections were performed
623 bilaterally into the VTA (bregma 3.1 mm, lateral 0.5 mm, ventral 4.5 mm) of 8-week-old DAT-Cre mice, in
624 which Cre recombinase expression is restricted to DA neurons without disrupting endogenous dopamine
625 transporter (DAT) expression (Turiault et al., 2007; Zhuang et al., 2005), with 0.5 µL of AAV per
626 hemisphere (AAV5.EF1 α .DIO.CatCh.YFP 2.46e¹² or 6.53e¹³ vg/mL used in the BLA and
627 AAV9.EF1 α .DIO.hChR2.YFP 9.59e¹³ vg/mL used in the NAcLSH, AAV5.EF1 α .DIO.Jaws.eGFP 1.16e¹³
628 vg/mL, AAV5.EF1 α .DIO.YFP 6.89e¹³ or 9.10e¹³ vg/mL). A double-floxed inverse open reading frame
629 (DIO) allowed restraining to VTA DA neurons the expression of CatCh, a channelrhodopsin mutant with

630 enhanced light sensitivity and Ca²⁺ permeability (Kleinlogel et al., 2011) for activation, or Jaws a red-
631 shifted cruxhalorhodopsin Jaws (Chuong et al., 2014) for inhibition (Figure S9). Optical fibers (200 µm
632 core, NA = 0.39, Thor Labs) coupled to a zirconia ferule (1.25 mm) were implanted bilaterally in the
633 different target sites of the VTA (coordinates for BLA implantation: bregma -1.6 mm, lateral 3.18 mm,
634 ventral 4.5 mm) (coordinates for NAcLSh implantation: bregma 1.5 mm, lateral 1.75 mm, ventral 3.90
635 mm), and fixed to the skull with dental cement (SuperBond, Sun medical). An ultra-high-power LED (470
636 nm for Catch, 520 nm for Jaws, Prizmatix) coupled to a patch cord (500 µm core, NA = 0.5, Prizmatix)
637 was used for optical stimulation (output intensity of 10 mW, frequency of 10 Hz, 5 ms-pulse for CatCh,
638 continuous stimulation at 520 nm for Jaws).

639

640 To perform non-conditional expression in different subnuclei of the amygdala (Amg), an AAV2-CAG-Jaws-
641 GFP (1.45 e¹² ng/µL) or AAV2-7m8-CAG-GFP (5.70 e¹² ng/µL) were injected bilaterally into the VTA
642 (same coordinates as previously indicated) of distinct groups of 8-week-old WT mice. Optical fibers were
643 bilaterally implanted in those mice either in the basolateral amygdala (BLA: bregma -1.6 mm, lateral 3.18
644 mm, ventral 4.5 mm) or in the central amygdala (CeA: bregma -0.78 mm, lateral 2.3 mm, ventral 4.8 mm).
645 To perform non-conditional expression in the NAc medial shell (NAcMSh), a
646 AAV5.hSyn.hChr2(H134R).eYFP (2.4e¹³) or AAV5.hsyn.Jaws.KGC.GFP.ER2 (1.3e¹³) or
647 AAV5.hSyn.eGFP.WPRE.bGH (2.2e¹³) was injected bilaterally in the VTA of distinct groups of 8 week-
648 old WT male mice. Optical fibers were bilaterally implanted in those mice in the NAcMSh with 12° angle
649 (NAcMSh: bregma 1.5 mm, lateral 1.5 mm, ventral 4.5 mm).

650

651 All experiments were conducted at least 4 weeks after viral injection, to enable expression of the different
652 constructs. The optical stimulation cable was plugged onto the ferule during all experimental sessions
653 when on purpose, to habituate the animals and control for latent experimental effects.

654 **Fiber photometry experiments**

655 8-week-old WT mice were injected with 0.5 µl of AAV-hSyn-GRAB_{DA2m} (1.23e¹⁴ vg/mL) in the BLA
656 (bregma -1.61 mm, lateral 3.18 mm, ventral 4.7 mm) or NAcLSh (bregma 1.5 mm, lateral 1.55 mm, ventral
657 3.95 mm). Optical fibers (200 µm core, NA = 0.39, Thor Labs) coupled to a stainless-steel ferule (1.25
658 mm) were implanted after virus injection at the same coordinates, and fixed to the skull with dental cement
659 (SuperBond, Sun medical). Two weeks after surgeries, animals begin a habituation period to the plastic
660 cylinder used for photometry recordings.

661 Before the measurements, the animals were implanted in one of the tail veins with a catheter (30G needle
662 connected to PE10 tubing). Venous return and the absence of tail swelling after a saline injection ensured
663 a good positioning of the catheter, which was then glued and taped to the animal's tail. During awakening,
664 the mouse was placed into a 7 cm-diameter plastic cylinder from which its tail can protrudes on the outside
665 via a hole (see schematic on Figure S2B).

666 Fluorescence measurements of DA levels in the NAcLSh and BLA were recorded using a Doric Lenses
667 1-site 2-color fiber photometry system. The fiber photometry console was connected to the LED driver to
668 control connectorized LED in Lock-in mode (CLEED 465 nm modulated at 220.537 Hz) that was connected
669 to its port on the Mini Cube (FMC4_AE(405)_E(460-490)_F(500-550)_S) through an optic patch cord
670 (MFP_200/220/LWMJ-0.37_1m_FC-FC_T0.20). Light stimulation and recorded fluorescence were
671 transmitted through an optical fiber (FT400EMT, 400 µm core, NA = 0.39, Thorlabs) connected both to

672 the animal's implanted optical fiber via a zirconia sleeve and to the sample (S) port on the Mini Cube.
673 Finally, the photoreceiver converting recorded light to electrical signals (AC Low setting, New Focus 2151
674 Visible Femtowatt Photoreceiver, New Focus, San Jose, CA, USA) was connected to the Mini Cube
675 through an optic path cord (600 μm core, NA = 0.48, FC-FC, Doric Lenses) fitted on a fiber optic adapter
676 (Doric Lenses) and to the fiber photometry console. Signal was acquired through Doric Neuroscience
677 Studio software (version 5.2.2.5) with a sampling rate of 12.0 kS/s (kilosamples per second) and a low-
678 pass filter with a cutoff frequency of 12.0 Hz.

679 We assessed changes in DA levels in NAcLSH or BLA in response to saline or nicotine injection in the tail
680 vein of the animal. After catheter implantation, the animal recovers in the plastic cylinder for 30 min. We
681 then started to record after at least 3 min baseline, 5 min after saline injection, 15 min after 30 $\mu\text{g}/\text{kg}$ or
682 60 $\mu\text{g}/\text{kg}$ nicotine injection. After the session, mice were re-anesthetized to carefully remove the catheter
683 and were allowed to rest for one day before the next recording session.

684 ***In vivo* electrophysiology on anesthetized mice**

685 Mice were deeply anesthetized with an IP injection of chloral hydrate (8%), 400 mg/kg, supplemented as
686 required to maintain optimal anesthesia throughout the experiment. The scalp was opened and a hole
687 was drilled in the skull above the location of the VTA. Intravenous administration of saline or nicotine
688 (30 $\mu\text{g}/\text{kg}$) was carried out through a catheter (30G needle connected to polyethylene tubing PE10)
689 connected to a Hamilton syringe, into the saphenous vein of the animal. For multiple doses of nicotine,
690 mice received first a dose of 30 $\mu\text{g}/\text{kg}$ and then one to four subsequent injections of nicotine at different
691 doses, either 10, 15, 60 and/or 90 $\mu\text{g}/\text{kg}$ (pseudo-randomly administered). Extracellular recording
692 electrodes were constructed from 1.5 mm outer diameter / 1.17 mm inner diameter borosilicate glass
693 tubing (Harvard Apparatus) using a vertical electrode puller (Narishige). The tip was broken straight and
694 clean under microscopic control to obtain a diameter of about 1 μm . The electrodes were filled with a
695 0.5% NaCl solution containing 1.5% of neurobiotin[®] tracer (VECTOR laboratories) yielding impedances
696 of 6-9 M Ω . Electrical signals were amplified by a high-impedance amplifier (Axon Instruments) and
697 monitored audibly through an audio monitor (A.M. Systems Inc.). The signal was digitized, sampled at 25
698 kHz, and recorded on a computer using Spike2 software (Cambridge Electronic Design) for later analysis.
699 The electrophysiological activity was sampled in the central region of the VTA (coordinates: between 3.1
700 to 4 mm posterior to bregma, 0.3 to 0.7 mm lateral to midline, and 4 to 4.8 mm below brain surface).
701 Individual electrode tracks were separated from one another by at least 0.1 mm in the horizontal plane.
702 Spontaneously active DA neurons were identified based on previously established electrophysiological
703 criteria (Grace and Bunney, 1984b; 1984a; Ungless and Grace, 2012).

704 After recording, nicotine-responsive cells were labelled by electroporation of their membrane: successive
705 current squares were applied until the membrane breakage, to fill the cell soma with neurobiotin
706 contained into the glass pipet (Pinault 1996). To be able to establish correspondence between neurons
707 responses and their localization in the VTA, we labeled one type of response per mouse: solely activated
708 neurons or solely inhibited neurons, with a limited number of cells per brain (1 to 4 neurons maximum, 2
709 by hemisphere), always with the same concern of localization of neurons in the VTA.

710 ***In vivo* electrophysiology on freely moving animals**

711 *Micro-drive and electrodes:* Hand-made poly-electrodes (bundle of 8 electrodes: "octrodes") were
712 obtained by twisting eight polyimide-insulated 17 μm Nickel-Chrome wires (A-M SYSTEMS, USA). The
713 use of eight channels relatively close to each other allows for a better discrimination of the different

714 neurons. Before implantation and recording, the octrodes were cut at suitable length and plated with a
715 solution of platinum (platinum black plating solution, Neuralynx; Bozeman, USA) and poly-ethylene glycol
716 (1 mg/mL) (25% platinum - 75% PEG) to lower their impedance to 200-500 kOhms and improve the
717 signal-to-noise ratio. The free ends of 2 octrodes were connected to the holes of an EIB-18 (electrode
718 interface board, Neuralynx) and fixed with pins. We designed and manufactured a micro-drive system
719 (home-made 3D conception and printing) consisting of a frame on which is mounted the EIB, and a
720 platform on which are glued the 2 octrodes. Using a driving screw, we were able to slide the platform up
721 and down within the frame, allowing to move through the VTA during chronic recordings in order to sample
722 neuronal populations.

723

724 *Micro-drive implantation:* After anesthetic procedure, the cranial bone of the mouse was exposed by a
725 midline incision of the scalp. The skull was drilled and recording electrodes were placed just above the
726 VTA (bregma - 3.2 ± 0.1 mm, lateral 0.5 ± 0.1 mm, ventral 4.1 ± 0.1 mm from the brain surface) (Paxinos
727 and Franklin, 2004). A small amount of petroleum jelly (Vaseline) was applied on top the hole and around
728 the recordings electrodes to prevent clotting and facilitate sliding for the following weeks. Monopolar
729 ground electrodes were laid over the cortical layer of the cerebellum, cemented to the skull with
730 SuperBond (Sun Medical) and pinned on the EIB during surgery. SuperBond and dental acrylic cement
731 were then used to fix the micro-drive to the skull for chronic recordings. The scalp was stitched and
732 buprenorphine was injected subcutaneously to facilitate awakening. Animals recovered until regaining
733 pre-surgery body weight, for at least one week.

734

735 *Neuronal recordings and characterization of DA neurons:* Recordings of extracellular potentials were
736 performed using a digital acquisition system (Digital Lynx SX; Neuralynx) together with the Cheetah
737 software. Signals from each wire were band-pass-filtered between 600 and 6000 Hz for multi-unit
738 recordings at 32 kHz sampling. Spikes sorting and clustering were performed using SpikeSort3D
739 (Neuralynx), and validation of clusters was done with custom-written Python routines based on activity
740 and waveform criteria as well as auto- and cross-correlograms. From the starting position after surgery
741 (around 4.10 mm), electrodes were lowered (75 µm steps) every other day to sample as many neurons
742 as possible until a depth of 5.0 mm was reached. The electrophysiological characteristics of VTA neurons
743 were assessed each time an active cell was encountered. Extracellular identification of putative DA
744 neurons (pDAn) was based on their location as well as on a set of unique electrophysiological properties
745 that characterize these cells in vivo: (1) a typical triphasic action potential with a marked negative
746 deflection; (2) a characteristic long duration (>2.0 ms) action potential; (3) an action potential width from
747 start to negative trough >1.1 ms; (4) a slow firing rate (1-10 Hz) with a regular single spiking pattern and
748 occasional short bursting activity. Putative GABA neurons were characterized by a characteristic short
749 duration of action potential from start to negative trough (<1.0 ms), and a high firing rate (>12Hz). D2
750 receptor (D2R) pharmacology was also used to confirm DA neuron identification: after a baseline (10 min)
751 and a saline (5 min) IP injection, 0.2 mL of quinpirole (1 mg/kg, D2R agonist) was injected (10 min
752 recording), followed by 0.2 mL-eticlopride (1 mg/kg, D2R antagonist) injection (10 min recording). Since
753 most DA, but not GABA neurons, express inhibitory D2 auto-receptors, neurons were considered as
754 pDAn, if quinpirole induced at least 30% decrease in their firing rate, while eticlopride restored firing above
755 the baseline. Nevertheless, as continuous D2 pharmacology could have affected DA neurons firing, we
756 allowed mice to recover two days after this experiment and we did not test all encountered pDAn. We
757 thus performed pharmacological confirmation when first encountering a pDA neuron in a given mouse or

758 at the end of the week if at least one putative neuron was present. Neurons were considered DA only if
759 they responded to the pharmacology, or if they presented electrophysiological characteristics defined
760 above and were recorded between two positive pharmacological experiments.

761 We assessed the pDAn responses to nicotine injection in the tail vein of the animal (catheter implantation
762 presented above see Fiber photometry section, Figure S2B). We let the animal recover after catheter
763 implantation and habituate to the plastic cylinder for 30 min, and then started to record VTA neurons. For
764 each session, we recorded 7 min of baseline, 7 min after saline injection, 15 min after 30 µg/kg nicotine
765 injection and 20 min after 60 µg/kg nicotine injection. After the session, mice were re-anesthetized to
766 carefully remove the catheter and were allowed to rest for one day before the next recording session. The
767 screw was turned to lower the octrodes into the VTA and try to sample new pDAn within the following
768 days.

769

770 **Ex vivo patch-clamp recordings**

771 For a functional verification of CatCh or Jaws expression, AAV5.EF1α.DIO.CatCh.YFP or
772 AAV5.EF1α.DIO.Jaws.eGFP virus was injected into 7 to 9-week-old male DAT^{CRE} mice. For the
773 characterization of NAc-projecting and Amg-projecting neurons, green retrobead tracers (Lumafluor) were
774 injected into 7-9 week old male WT mice. After 4 weeks (for DAT-Cre mice) or 2 weeks (for WT mice),
775 mice were deeply anesthetized by an intraperitoneal injection of a mix of ketamine (150 mg/kg Imalgene®
776 1000, Merial) and xylazine (60 mg/kg, Rompun® 2%, Bayer). Coronal midbrain sections (250 µm) were
777 sliced with a Compresstome (VF-200, Precisionary Instruments) after intracardial perfusion of cold (4°C)
778 sucrose-based artificial cerebrospinal fluid (SB-aCSF) containing (in mM): 125 NaCl, 2.5 KCl, 1.25
779 NaH₂PO₄, 5.9 MgCl₂, 26 NaHCO₃, 25 sucrose, 2.5 glucose, 1 kynurenate (pH 7.2, 325 mOsm). After 10
780 to 60 minutes at 35°C for recovery, slices were transferred into oxygenated artificial cerebrospinal fluid
781 (aCSF) containing (in mM): 125 NaCl, 2.5 KCl, 1.25 NaH₂PO₄, 2 CaCl₂, 1 MgCl₂, 26 NaHCO₃, 15 sucrose,
782 10 glucose (pH 7.2, 325 mOsm) at room temperature for the rest of the day, and individually transferred
783 to a recording chamber continuously perfused at 2 mL/minute with oxygenated aCSF. Patch pipettes (4-
784 8 MΩ) were pulled from thin wall borosilicate glass (G150TF-3, Warner Instruments) with a micropipette
785 puller (P-87, Sutter Instruments, Novato, CA) and filled with a potassium gluconate-based intracellular
786 solution containing (in mM): 116 K-gluconate, 20 HEPES, 0.5 EGTA, 6 KCl, 2 NaCl, 4 ATP, 0.3 GTP, and
787 biocytin 2 mg/mL (pH adjusted to 7.2). Neurons were visualized using an upright microscope coupled with
788 a Dodt contrast lens, and illuminated with a white light source (Scientifica). A 460 nm LED (pE-2, Cooled)
789 was used for visualizing GFP-, YFP- or RB-containing cells (using a bandpass filter cube, AHF). Whole-
790 cell recordings were performed with a patch-clamp amplifier (Axoclamp 200B, Molecular Devices)
791 connected to a Digidata (1550 LowNoise acquisition system, Molecular Devices). Signals were low-pass
792 filtered (Bessel, 2 kHz) and collected at 10 kHz using the data acquisition software pClamp 10.5
793 (Molecular Devices). Optical stimulation was applied through the microscope with two LEDs (460 nm and
794 525 nm, pE-2, CoolLED). To characterize CatCh expression, a 1 s continuous photostimulation was used
795 to evoke currents in voltage-clamp mode (-60 mV), and a 10 Hz - 5 ms/pulse photostimulation was used
796 to drive neuronal firing in current-clamp mode. Regarding Jaws expression, continuous photostimulation
797 (20 s) was used in current-clamp (-60 mV). To record nicotinic currents from RB+ DA neurons of the VTA,
798 local puffs (500 ms) of nicotine tartrate (100 µM in aCSF) were applied with a glass pipette (2-3 µm
799 diameter) positioned 20 to 30 µm away from the soma and connected to a picospritzer (World Precision
800 Instruments, adjusted to ~2 psi). All electrophysiological recordings were extracted using Clampfit
801 (Molecular Devices) and analyzed with R.

802 **Immunostaining**

803 After euthanasia, brains were rapidly removed and fixed in 4% paraformaldehyde. After a period of at
804 least three days of fixation at 4°C, serial 60-µm sections were cut from the midbrain with a vibratome.
805 Immunostaining experiments were performed as follows: free-floating VTA brain sections were incubated
806 for 1 hour at 4°C in a blocking solution of phosphate-buffered saline (PBS) containing 3% bovine serum
807 albumin (BSA, Sigma; A4503) (vol/vol) and 0.2% Triton X-100 (vol/vol), and then incubated overnight at
808 4°C with a mouse anti-tyrosine hydroxylase antibody (anti-TH, Sigma, T1299) and a chicken anti-GFP
809 antibody (Life technologies Molecular Probes, A-6455), both at 1:500 dilution, in PBS containing 1.5%
810 BSA and 0.2% Triton X-100. The following day, sections were rinsed with PBS, and then incubated for 3
811 hours at 22-25°C with Cy3-conjugated anti-mouse and Alexa488-conjugated anti-chicken secondary
812 antibodies (Jackson ImmunoResearch, 715-165-150 and 711-225-152) at 1:500 and 1:1000 dilution in a
813 solution of 1.5% BSA in PBS, respectively. After three rinses in PBS, slices were wet-mounted using
814 Prolong Gold Antifade Reagent (Invitrogen, P36930). Microscopy was carried out with a fluorescent
815 microscope, and images captured using a camera and analyzed with ImageJ.

816 In the case of electrophysiological recordings, the recorded neurons were identified by immunohisto-
817 fluorescence as described above, with the addition of 1:200 AMCA-conjugated streptavidin (Jackson
818 ImmunoResearch) in the solution. Immunoreactivity for both TH and neurobiotin (NB) allowed us to
819 confirm the neurochemical phenotype of DA neurons in the VTA (TH+ NB+).

820 In the case of optogenetic experiments on DAT^{iCRE} mice, identification of the transfected neurons by
821 immunofluorescence was performed as described above, with the addition of chicken-anti-GFP primary
822 antibody (1:500, ab13970, Abcam) in the solution. A goat-anti-chicken AlexaFluor 488 (1:500, Life
823 Technologies) was then used as secondary antibody. Immunoreactivity for TH, GFP and
824 neurobiotin/biocytyin allowed us to confirm the neurochemical phenotype of DA neurons in the VTA (TH+
825 NB+) and the transfection success (GFP+).

826 **Image acquisition**

827 For immunofluorescence pictures, all slices were imaged by acquisition on a Leica DMR epi-fluorescent
828 microscope, under identical conditions of magnification, illumination and exposure (using photometrics
829 coolsnap camera). Images were captured in gray level using MetaView software (Universal Imaging
830 Corporation, Ropper Scientific, France) and colored post-acquisition on ImageJ software.

831 **Elevated O-maze test**

832 All behavioral tests were conducted during the light period of the animal cycle (between 1:00 and 7:00PM).
833 The raw data for behavioral experiments were acquired as the time spent by animals in the different zones
834 of the environments. Animals were detected in their body center with a 2D USB camera, connected to the
835 Anymaze software for acquisition.

836 The elevated O-maze (EOM) apparatus consists of two open (stressful) and two enclosed (protecting)
837 elevated arms that together form a zero or circle (diameter of 50 cm, height of 58 cm, 10 cm-wide circular
838 platform). The time spent in exploring enclosed versus open arms indicates the anxiety level of the animal.
839 The first EOM experiment assessed the effect of an IP injection of Nic (0.5 mg/kg) on WT mice. The test
840 lasts 10 minutes: mice are injected 1 minute before the test, and then put in the EOM for 9 minutes. In

841 the second EOM experiment, mice received an IC infusion of Nic (100 ng/infusion) over 1 minute before
842 the 9-minute test. Finally, optogenetic EOM experiments consisted in 15 minute-test, alternating 5 minute-
843 periods of stimulation and non-stimulation (OFF-ON-OFF). For “rescue” experiment in EOM, nicotine was
844 injected IP to the mice with the same protocol as described above, the test lasted for 9 minutes with
845 continuous stimulation along the test (continuous for inhibition and 10Hz for activation).

846 **Real-time place preference test**

847 The real-time place preference (RTPP) protocols were performed in a Y-maze apparatus (Imetronic,
848 Pessac, France), using only two arms of the Y-maze as two distinct compartments (the third arm was
849 closed by a door and not available to the animal). The chamber in between is an equilateral triangle (side
850 of 11 cm) used as a neutral compartment, where the animal was never photo-stimulated. Each arm of the
851 maze measures 25 cm × 12 cm. The first arm displays black and white stripes with smooth walls and
852 floor, whereas the other arm displays uniform-gray rough walls and floor. Choices of the compartment
853 where the animals will be stimulated were counterbalanced across animals in the same test and YFP-
854 control groups.

855 The RTPP test consisted of a 20 minute-session where animals can freely navigate between the
856 compartments but are photo-stimulated only in one of the two compartments.

857 Implanted animals were connected with a bilateral fiber (diameter of 400 μm, NA = 0.39, Thorlabs)
858 attached to a rotor connecting the 470 nm-LED or 520 nm-LED (Prizmatix) with a fiber of diameter 500
859 μm and NA = 0.5 (Thorlabs). LED output was controlled using a Master-8 pulse stimulator (A.M.P.I.,
860 Jerus) which delivered a discontinuous stimulation of 5-ms light flashes at 10 Hz frequency and 470 nm
861 wavelength (for CatCh experiments), or a continuous stimulation at 520 nm (for Jaws experiments). Naive
862 mice were connected and placed at the center of the neutral compartment before starting the recording.
863 The time spent in the neutral compartment was not taken into account in the result. The results are
864 presented as preference score which is the difference of time spent between the stimulated compartment
865 over the “non-stimulated” compartment.

866 **Open field paradigm**

867 The open field (OF) is a square enclosure of 50 cm x 50 cm where animals can move freely. Animal
868 displacements were quantified by comparing the time spent in the center versus the periphery of the
869 square. When nicotine was injected to WT mice in the OF test (IP injection of nicotine tartrate at 0.5 mg/kg,
870 0.1 mL/10 g, 1 minute before the test), animals were placed in the center of the OF for a 9-minute test
871 duration, freely moving inside the enclosure. Regarding the optogenetic experiments conducted in the
872 OF, animals were placed in the maze for 15 minutes, while alternating between OFF, ON and OFF optical
873 stimulations periods of 5 minutes each.

874 **QUANTIFICATION AND STATISTICAL ANALYSIS**

875 **Measurements of neuronal activity**

876 Timestamps of action potentials were extracted in Spike 2 and analyzed using R, a language and
877 environment for statistical computing (Team, 2005, <http://www.r-project.org>). Spontaneous activity of DA
878 cell firing *in vivo* was analyzed with respect to the average firing frequency (in Hz) and the percentage of
879 spikes-within-burst (%SWB = number of spikes within burst divided by total number of spikes in a given
880 window). Neuronal basal activity was defined on at least three-minute recording. To determine whether

881 the spontaneous activity of VTA DA neurons could predict their responses to nicotine injection (activation
882 or inhibition), we analyzed 4 variables that characterize the firing patterns: the mean firing frequency, the
883 coefficient of variation of the firing frequency estimated on sliding windows, the %SWB and the burs event
884 frequency. For multiple logistic regression, glm function (R 4.0, with binomial family) was used for fitting
885 and predict.glm function was used to obtain prediction.

886 **Method for classifying VTA DA neurons subpopulations in response to nicotine injection**

887 Subpopulations of DA neurons were automatically classified using variation of firing frequency and the
888 following routine: First, we calculated the maximal variation from the baseline per neuron, within the first
889 3 (for anesthetized animals) or 5 minutes (for freely-moving mice) following injection. We then used a
890 bootstrapping method (see below) to exclude non-responding neurons. Two neurons included in Fig 1B
891 (n=245) did not show statistical variations after nicotine injections and were thus removed from the rest
892 of the study. Neurons displaying an increase in firing frequency ($\Delta f > 0$) were defined as “Nic+”, while
893 neurons displaying a decrease in firing frequency ($\Delta f < 0$) were defined as “Nic-”. For the dose-response
894 curve, neurons were classified as Nic+ or Nic- based on their response to a nicotine dose of 30 $\mu\text{g}/\text{kg}$ or
895 higher. For saline injections, only nicotine-responsive neurons were considered, and the polarity of the
896 variation was defined based on the response to nicotine (i.e. in Nic+ neurons, we consider that saline
897 increases activity). In $\beta 2^{-/-}$ mice, VTA DA neurons did not show a clear change in firing rate after nicotine
898 injection. In $\beta 2^{\text{Vec}}$ mice, lentivirus-mediated expression of $\beta 2$ is most likely heterogenous within the VTA,
899 hence not all recorded cells are expected to respond to nicotine. In $\beta 2^{-/-}$ and $\beta 2^{\text{Vec}}$ mice, we thus divided
900 populations of neurons using the threshold criteria ($\Delta f < 0$ or > 0) and evaluated the impact of re-expression
901 without using the bootstrapping method (Figure 3B and S8A-D). Responding neurons (bootstrapping at
902 2%) are shown in Figure S8E-F. Overall, for $\beta 2^{-/-}$ mice, only 22/46 neurons (47%) showed a response
903 (bootstrapping at 2%), while for $\beta 2^{\text{Vec}}$ mice this ratio increased to 65/90 (72%).
904

905 **Quantification of neuronal responses to nicotine injection**

906 Firing frequency was quantified on overlapping 60-second windows shifted by 15-second time steps
907 (except for Figure S1, in which windows are shifted by 1 sec steps). For each neuron, the firing frequency
908 was rescaled as a percentage of its baseline value averaged during 3 minutes before nicotine injection.
909 The responses to nicotine are thus presented as a percentage of variation from baseline (mean \pm S.E.M.).
910 The effect of nicotine was assessed by comparing the maximum of firing frequency variation induced by
911 nicotine and saline injection. For activated (respectively inhibited) neurons, the maximal (respectively
912 minimal) value of firing frequency was measured within the response period (3 to 5 minutes) that followed
913 nicotine or saline injection. The results are presented as mean \pm S.E.M. of the difference of maximum
914 variation after nicotine or saline. The mean responses to nicotine injections for recordings in freely moving
915 mice, both for inhibited and activated groups, pooled 7 responses at 30 $\mu\text{g}/\text{kg}$ Nic and one response at
916 60 $\mu\text{g}/\text{kg}$. Neurons that significantly responded to nicotine injections were identified by bootstrapping.
917 Baseline spike intervals were randomly shuffled 1000 times. Firing frequency was estimated on 60 sec
918 time windows, with 15 sec time steps. For each neuron we determined the percentile from the shuffled
919 data corresponding to the nicotine-evoked response (max or min frequency after nicotine injection).
920 Neurons were individually considered as responsive to nicotine injection if this percentile is ≥ 0.98 or
921 ≤ 0.02 .

922 **Quantification of juxtacellularly labeled neurons**

923 A total number of 245 neurons were recorded and labeled for Figure 1. Those 245 neurons were used in
924 Figure 1B. Two non-responding neurons were removed, so 243 neurons were used for Fig1C-D and G.
925 Among them, 101 neurons were shown in Figure 2B and E, with 49 neurons labeled in NAc-RB injected
926 mice and 52 in Amg-RB injected mice. The locations of the labeled neurons were manually placed on
927 sections of the Paxinos atlas georeferenced in a 2D grid using Adobe Illustrator rules. The medio-lateral
928 and dorso-ventral coordinates of the location of each neuron were extracted from the grid pattern and the
929 antero-posterior coordinates were estimated from the section of the Paxinos atlas on which the neurons
930 were placed. These three coordinates were used to make density histograms of location for nicotine-
931 activated and nicotine-inhibited DA neurons or NAc-projecting and Amg-projecting DA neurons.

932 **Quantification of fluorescence**

933 Data from fiber photometry experiments were first down-sampled by a 100-factor using custom Matlab
934 routine. Down-sampled data were then further analyzed on R software. First, we subtracted the mean
935 value of “autofluorescence” (signal acquired after each recording with the same parameters, but without
936 the optic fiber attached to the mouse) to the signal. We then fitted an exponential to this signal and
937 subtracted it before adding an offset equal to the mean of the signal before detrending to account for the
938 slow decay of the signal due to bleaching during recording. We defined a baseline fluorescence value
939 (F_0) as the mean fluorescence of the signal during 120 seconds before injection time, for each injection
940 (saline and nicotine) individually. We then calculated normalized variation in fluorescence ($\Delta F/F$) as $(F - F_0)/F_0$
941 for each injection. The analysis was carried out by averaging each $\Delta F/F$ obtained for each
942 condition (all saline or nicotine injections done in NAcLSh implanted mice, same for saline or nicotine in
943 BLA animals) and mean data were smoothed using a normal kernel.fit (bandwidth = 120). All Nic
944 responses ($n=7$) for BLA implantation were done at 30 $\mu\text{g}/\text{kg}$ recorded in 6 different animals. For NAcLSh
945 implantation, 6 animals received Nic injection at 30 or 60 $\mu\text{g}/\text{kg}$ ($n=8$, mean fluorescence pooled 2
946 injections at 60 $\mu\text{g}/\text{kg}$ and 6 injections at 30 $\mu\text{g}/\text{kg}$). For each injection (saline and nicotine), peak
947 fluorescence (maximum and minimum of $\Delta F/F$ for NAcLSh and BLA implanted mice respectively) were
948 detected within a 100 sec window after injection. For each paired injection, we calculated the difference
949 in peak fluorescence between nicotine and saline.

950 **Statistics: figure by figure**

951 All statistical analyses were done using the R software with home-made routines. Results are plotted as
952 mean \pm S.E.M. The total number (n) of observations in each group and the statistical tests used for
953 comparisons between groups or within groups are indicated on the figures directly or in the figure legends.
954 Comparisons between means were performed with parametric tests as Student’s t-test, or two-way
955 ANOVA for comparing two groups when parameters followed a normal distribution (Shapiro-Wilk
956 normality test with $p > 0.05$), or Wilcoxon non-parametric test as when the distribution was skewed. Holm’s
957 sequential Bonferroni *post hoc* analysis was applied, when necessary. Statistical significance was set at
958 $p < 0.05$ (*), $p < 0.01$ (**), or $p < 0.001$ (***), or $p > 0.05$ was considered not to be statistically significant.

959 Figure 1: Kolmogorov-Smirnov test was used to compare the responses of VTA DA neurons to saline or
960 nicotine injection. Wilcoxon test was used to demonstrate a significant increase or decrease of firing
961 frequency induced by nicotine injection compared to saline injection (B). Wilcoxon test was used to
962 compare the firing frequency before and after nicotine or saline injection. Wilcoxon test was used to
963 compare the firing frequency variation induced by nicotine or saline injection. (D). One-way ANOVA was

964 used to demonstrate a dose-effect of nicotine on activated or inhibited DA neurons (E). Wilcoxon test was
965 used to compare coordinates of nicotine-inhibited and nicotine-activated recorded neurons (G).

966 Figure 2: Wilcoxon test was used to compare the firing frequency before and after nicotine in RB+ and
967 RB- DA neurons. Wilcoxon test was used to compare firing frequency variations induced by nicotine in
968 RB+ and RB- DA neurons (C-F). Kolmogorov-Smirnov test was used to compare the responses of NAc-
969 projecting and Amg-projecting DA neurons to nicotine injection (G). Paired Student's t-test was used to
970 compare the peak of fluorescence induced by saline and nicotine injection in NAcLSh or BLA. Student's
971 t-test was used to compare the difference in $\Delta F/F$ (Nicotine – Saline) between NAcLSh and BLA (I).

972 Figure 3: For behavior (A-C), over time effect of nicotine or saline injection (IP and IC) on the time spent
973 by the mice in the open arms of the EOM was first tested with one-way repeated measures ANOVA for
974 each group of mice (shown in Figure S7A-D-G). Two-way repeated measures ANOVA (time/treatment or
975 time/genotype) were used to compare the difference between the groups. In case of significant interaction
976 effect between factors, Wilcoxon or Student's t-test with Holm's sequential Bonferroni corrections were
977 used for intra-group and inter-group *post hoc* analysis (as indicated in the figure). For electrophysiology
978 (B), Kolmogorov-Smirnov test was used to compare responses to nicotine of DA neurons in $\beta 2^{-/-}$ mice and
979 $\beta 2^{-/-}$ Vec mice. Wilcoxon tests with Bonferroni corrections are used to demonstrate a significant increase
980 or decrease of firing frequency induced by IV nicotine injection in $\beta 2^{-/-}$ Vec mice compared to saline and
981 nicotine injections in $\beta 2^{-/-}$ mice.

982 Figure 4 and 5: For EOM experiments (A-B), effect of light was first tested with one-way repeated
983 measures ANOVA for each group of mice (shown in Figure S11A-B and Figure S13A-B). Two-way
984 repeated measures ANOVA (time/opsin) were used to compare the difference between the groups. In
985 case of a significant interaction effect between factors, Wilcoxon or Student's t-test with Holm's sequential
986 Bonferroni corrections were used for intra-group and inter-group *post hoc* analysis (as indicated in the
987 figure). For EOM experiment under nicotine (C), over time effect of nicotine injection on the time spent by
988 the mice in the EOM open arms was first tested with one-way repeated measures ANOVA for each group.
989 Two-way repeated measures ANOVA (time/opsin) were used to compare the difference between the
990 groups. In case of a significant interaction effect between factors, Wilcoxon or Student's t-test with
991 Bonferroni corrections were used for intra-group and inter-group *post hoc* analysis (as indicated in the
992 figure). For RTPP experiments (D), preference scores between groups were compared with Student's t-
993 test.

994 Figure S2: Wilcoxon test was used to compare spontaneous activity of nicotine-inhibited and nicotine-
995 activated recorded neurons (C).

996 Figure S4: Wilcoxon test was used to compare coordinates of NAc- and Amg-projecting neurons (E).
997 Wilcoxon test was used to compare spontaneous activity of NAc- and Amg- projecting DA neurons (F).

998 Figure S5: Wilcoxon test was used to compare firing frequencies before and after nicotine in RB+ and
999 RB- DA neurons. Wilcoxon test was used to compare firing frequency variations induced by nicotine in
1000 RB+ and RB- DA neurons (D/H).

1001 Figure S6: Two-way repeated measures ANOVA (current, phenotype) was used to compare neuronal
1002 excitability (D). Wilcoxon test was used to compare nicotine-evoked currents (F).

1003 Figure S7: Two-way repeated measures ANOVA (time, treatment) was used to compare the distance
1004 traveled by mice in the OF after nicotine or saline injection (A). One-way repeated measures ANOVA
1005 were used to test the overtime effect of saline or nicotine intraperitoneal injection, or intracranial infusion,
1006 or the time spent by mice in the open arms of the EOM. Two-way repeated measures ANOVA (time,
1007 treatment) was used to compare number of entries in the open arms of the EOM after saline or nicotine
1008 injection (A, D, G). Two-way repeated measures ANOVA (time, genotype) was used to compare the time
1009 spent and the number of entries in the EOM open arms after nicotine injection between groups (A-D-F-
1010 G). In case of a significant interaction effect between factors, Wilcoxon or Student's t-test with Holm's
1011 sequential Bonferroni corrections were used for intra-group and inter-group *post hoc* analysis.

1012 Figure S8: Kolmogorov-Smirnov test was used to compare the responses of VTA DA neurons to saline
1013 or nicotine injection in $\beta 2^{-/-}$ (A) and $\beta 2^{-/-}$ Vec mice (C). Wilcoxon test was used to compare firing frequency
1014 before and after nicotine or saline injection. Wilcoxon test was used to compare firing frequency variation
1015 induced by nicotine or saline injection in $\beta 2^{-/-}$ (B-G-F) and $\beta 2^{-/-}$ Vec mice (D-G-F).

1016 Figure S11 and 13: For anxiety measurements, one-way repeated measures ANOVA were used to test
1017 the light effect on the time spent in the open arms of the EOM. Two-way repeated measures ANOVA
1018 were used to compare the stimulation effect depending on the position of the animal (closed arms or open
1019 arms) at the onset of the light and the number of entries in the open arms of the EOM between groups
1020 (A-B). For locomotor activity, two-way repeated measures ANOVA (time, opsin) were used to compare
1021 the difference of light effect on the distance traveled by the mice between the groups (C). In case of a
1022 significant interaction effect between factors, Wilcoxon or Student's t-test with Holm's sequential
1023 Bonferroni corrections were used for intra-group and inter-group *post hoc* analysis (as indicated in the
1024 figure).

1025 Figure S12: EOM experiments (C-D) and locomotor activity (E-F) were analyzed as previously described
1026 for Figure S9.

1027 Figure S14: For EOM experiments, the time spent in the open arms (cf. Figure 3), and the number of
1028 entries were analyzed as previously described (cf. Figure S11). Locomotor activity was analyzed as
1029 previously described in Figure S11. For RTPP experiments (E), preference scores between groups were
1030 compared with Student's t-test.

1031 **References**

- 1032 Aurnhammer, C., Haase, M., Muether, N., Hausl, M., Rauschhuber, C., Huber, I., Nitschko, H., Busch,
1033 U., Sing, A., Ehrhardt, A., et al. (2012). Universal real-time PCR for the detection and quantification of
1034 adeno-associated virus serotype 2-derived inverted terminal repeat sequences. *Hum Gene Ther*
1035 *Methods* 23, 18–28.
- 1036 Balerio, G.N., Aso, E., and Maldonado, R. (2006). Role of the cannabinoid system in the effects induced
1037 by nicotine on anxiety-like behaviour in mice. *Psychopharmacology* 184, 504–513.
- 1038 Beier, K.T., Gao, X.J., Xie, S., DeLoach, K.E., Malenka, R.C., and Luo, L. (2019). Topological
1039 Organization of Ventral Tegmental Area Connectivity Revealed by Viral-Genetic Dissection of Input-
1040 Output Relations. *CellReports* 26, 159–167.e6.
- 1041 Beier, K.T., Steinberg, E.E., DeLoach, K.E., Xie, S., Miyamichi, K., Schwarz, L., Gao, X.J., Kremer, E.J.,
1042 Malenka, R.C., and Luo, L. (2015). Circuit Architecture of VTA Dopamine Neurons Revealed by
1043 Systematic Input-Output Mapping. *Cell* 162, 622–634.
- 1044 Brischoux, F., Chakraborty, S., Brierley, D.I., and Ungless, M.A. (2009). Phasic excitation of dopamine
1045 neurons in ventral VTA by noxious stimuli. *Proc Natl Acad Sci USA* 106, 4894–4899.
- 1046 Changeux, J.-P., Bertrand, D., Corringier, P.J., Dehaene, S., Edelstein, S., Léna, C., Le Novère, N.,
1047 Marubio, L., Picciotto, M., and Zoli, M. (1998). Brain nicotinic receptors: structure and regulation, role in
1048 learning and reinforcement. *Brain Res Brain Res Rev* 26, 198–216.
- 1049 Changeux, J.-P. (2010). Nicotine addiction and nicotinic receptors: lessons from genetically modified
1050 mice. *Nat Rev Neurosci* 11, 389–401.
- 1051 Choi, V.W., Asokan, A., Haberman, R.A., and Samulski, R.J. (2007). Production of recombinant adeno-
1052 associated viral vectors. *Curr Protoc Hum Genet Chapter 12*, Unit12.9–12.9.21.
- 1053 Chuong, A.S., Miri, M.L., Busskamp, V., Matthews, G.A.C., Acker, L.C., Sørensen, A.T., Young, A.,
1054 Klapoetke, N.C., Henninger, M.A., Kodandaramaiah, S.B., et al. (2014). Noninvasive optical inhibition
1055 with a red-shifted microbial rhodopsin. (Nature Publishing Group).
- 1056 de Jong, J.W., Afjei, S.A., Pollak Dorocic, I., Peck, J.R., Liu, C., Kim, C.K., Tian, L., Deisseroth, K., and
1057 Lammel, S. (2019). A Neural Circuit Mechanism for Encoding Aversive Stimuli in the Mesolimbic
1058 Dopamine System. *Neuron* 101, 133–151.e137.
- 1059 Di Chiara, G., and Imperato, A. (1988). Drugs abused by humans preferentially increase synaptic
1060 dopamine concentrations in the mesolimbic system of freely moving rats. *Proc Natl Acad Sci USA* 85,
1061 5274–5278.
- 1062 Doyon, W.M., Dong, Y., Ostroumov, A., Thomas, A.M., Zhang, T.A., and Dani, J.A. (2013). Nicotine
1063 Decreases Ethanol-Induced Dopamine Signaling and Increases Self-Administration via Stress
1064 Hormones. *Neuron* 1–11.
- 1065 Durand-de Cuttoli, R., Mondoloni, S., Marti, F., Lemoine, D., Nguyen, C., Naudé, J., d'Izarny-Gargas, T.,
1066 Pons, S., Maskos, U., Trauner, D., et al. (2018). Manipulating midbrain dopamine neurons and reward-
1067 related behaviors with light-controllable nicotinic acetylcholine receptors. *eLife* 7, 15991.
- 1068 Eddine, R., Valverde, S., Tolu, S., Dautan, D., Hay, A., Morel, C., Cui, Y., Lambolez, B., Venance, L.,
1069 Marti, F., et al. (2015). A concurrent excitation and inhibition of dopaminergic subpopulations in
1070 response to nicotine. *Sci. Rep.* 5, 8184.
- 1071 Ford, C.P., Mark, G.P., and Williams, J.T. (2006). Properties and opioid inhibition of mesolimbic
1072 dopamine neurons vary according to target location. *Journal of Neuroscience* 26, 2788–2797.

- 1073 Fowler, C.D., Lu, Q., Johnson, P.M., Marks, M.J., and Kenny, P.J. (2011). Habenular $\alpha 5$ nicotinic
1074 receptor subunit signalling controls nicotine intake. *Nature* 471, 597–601.
- 1075 Frahm, S., Ślimak, M.A., Ferrarese, L., Santos-Torres, J., Antolin-Fontes, B., Auer, S., Filkin, S., Pons,
1076 S., Fontaine, J.-F., Tsetlin, V., et al. (2011). Aversion to Nicotine Is Regulated by the Balanced Activity
1077 of $\beta 4$ and $\alpha 5$ Nicotinic Receptor Subunits in the Medial Habenula. *Neuron* 70, 522–535.
- 1078 Grace, A.A., and Bunney, B.S. (1984a). The control of firing pattern in nigral dopamine neurons: burst
1079 firing. *J Neurosci* 4, 2877–2890.
- 1080 Grace, A.A., and Bunney, B.S. (1984b). The control of firing pattern in nigral dopamine neurons: single
1081 spike firing. *J Neurosci* 4, 2866–2876.
- 1082 Grenhoff, J., Aston-Jones, G., and Svensson, T.H. (1986). Nicotinic effects on the firing pattern of
1083 midbrain dopamine neurons. *Acta Physiol. Scand.* 128, 351–358.
- 1084 Grieder, T.E., George, O., and Tan, H. (2012). Phasic D1 and tonic D2 dopamine receptor signaling
1085 double dissociate the motivational effects of acute nicotine and chronic nicotine withdrawal.
- 1086 Grieder, T.E., Besson, M., Maal-Bared, G., Pons, S., Maskos, U., and van der Kooy, D. (2019). $\beta 2^*$
1087 nAChRs on VTA dopamine and GABA neurons separately mediate nicotine aversion and reward. *Proc*
1088 *Natl Acad Sci USA* 116, 25968–25973.
- 1089 Grieder, T.E., Sellings, L.H., Vargas-Perez, H., Ting-A-Kee, R., Siu, E.C., Tyndale, R.F., and van der
1090 Kooy, D. (2010). Dopaminergic signaling mediates the motivational response underlying the opponent
1091 process to chronic but not acute nicotine. *Neuropsychopharmacology* 35, 943–954.
- 1092 Khabou, H., Garita-Hernandez, M., Chaffiol, A., Reichman, S., Jaillard, C., Brazhnikova, E., Bertin, S.,
1093 Forster, V., Desrosiers, M., Winckler, C., et al. (2018). Noninvasive gene delivery to foveal cones for
1094 vision restoration. *JCI Insight* 3, D358.
- 1095 Kleinlogel, S., Feldbauer, K., Dempski, R.E., Fotis, H., Wood, P.G., Bamann, C., and Bamberg, E.
1096 (2011). Ultra light-sensitive and fast neuronal activation with the Ca^{2+} -permeable channelrhodopsin
1097 CatCh. *PLoS One* 6, 1–5.
- 1098 Klink, R., de Kerchove d'Exaerde, A., Zoli, M., and Changeux, J.P. (2001). Molecular and physiological
1099 diversity of nicotinic acetylcholine receptors in the midbrain dopaminergic nuclei. *J Neurosci* 21, 1452–
1100 1463.
- 1101 Kutlu, M.G., and Gould, T.J. (2015). Nicotine Modulation of Fear Memories and Anxiety: Implications for
1102 Learning and Anxiety Disorders. *Biochem Pharmacol* 1–58.
- 1103 Lammel, S., Hetzel, A., Häckel, O., Jones, I., Liss, B., and Roeper, J. (2008). Unique properties of
1104 mesoprefrontal neurons within a dual mesocorticolimbic dopamine system. *Neuron* 57, 760–773.
- 1105 Lammel, S., Lim, B.K., Ran, C., Huang, K.W., Betley, M.J., Tye, K.M., Deisseroth, K., and Malenka,
1106 R.C. (2012). Input-specific control of reward and aversion in the ventral tegmental area. *Nature* 491,
1107 212–217.
- 1108 Luscher, C. (2016). The Emergence of a Circuit Model for Addiction. *Annu Rev Neurosci* 39, annurev-
1109 neuro-070815-013920.
- 1110 Mameli-Engvall, M., Evrard, A., Pons, S., Maskos, U., Svensson, T.H., Changeux, J.-P., and Faure, P.
1111 (2006). Hierarchical control of dopamine neuron-firing patterns by nicotinic receptors. *Neuron* 50, 911–
1112 921.
- 1113 Mansvelder, H.D., and McGehee, D.S. (2000). Long-term potentiation of excitatory inputs to brain
1114 reward areas by nicotine. *Neuron* 27, 349–357.

- 1115 Margolis, E.B., Hjelmstad, G.O., Fujita, W., and Fields, H.L. (2014). Direct bidirectional μ -opioid control
1116 of midbrain dopamine neurons. *Journal of Neuroscience* 34, 14707–14716.
- 1117 Margolis, E.B., Mitchell, J.M., Ishikawa, J., Hjelmstad, G.O., and Fields, H.L. (2008). Midbrain dopamine
1118 neurons: projection target determines action potential duration and dopamine D(2) receptor inhibition.
1119 *Journal of Neuroscience* 28, 8908–8913.
- 1120 Maskos, U., Molles, B.E., Pons, S., Besson, M., Guiard, B.P., Guilloux, J.-P., Evrard, A., Cazala, P.,
1121 Cormier, A., Mameli-Engvall, M., et al. (2005). Nicotine reinforcement and cognition restored by targeted
1122 expression of nicotinic receptors. *Nature* 436, 103–107.
- 1123 Mejias-Aponte, C.A., Ye, C., Bonci, A., Kiyatkin, E.A., and Morales, M. (2015). A Subpopulation of
1124 Neurochemically-Identified Ventral Tegmental Area Dopamine Neurons Is Excited by Intravenous
1125 Cocaine. *J Neurosci* 35, 1965–1978.
- 1126 Mineur, Y.S., Fote, G.M., Blakeman, S., Cahuzac, E.L.M., Newbold, S.A., and Picciotto, M.R. (2016).
1127 Multiple Nicotinic Acetylcholine Receptor Subtypes in the Mouse Amygdala Regulate Affective
1128 Behaviors and Response to Social Stress. *Neuropsychopharmacology* 41, 1579–1587.
- 1129 Molas, S., DeGroot, S.R., Zhao-Shea, R., and Tapper, A.R. (2017). Anxiety and Nicotine Dependence:
1130 Emerging Role of the Habenulo-Interpeduncular Axis. *Trends Pharmacol Sci* 38, 169–180.
- 1131 Morales, M., and Margolis, E.B. (2017). Ventral tegmental area: cellular heterogeneity, connectivity and
1132 behaviour. *Nat Rev Neurosci* 18, 73–85.
- 1133 Morel, C., Fattore, L., Pons, S., Hay, Y.A., Marti, F., Lambolez, B., De Biasi, M., Lathrop, M., Fratta, W.,
1134 Maskos, U., et al. (2014). Nicotine consumption is regulated by a human polymorphism in dopamine
1135 neurons. *Mol Psychiatry* 19, 930–936.
- 1136 Morel, C., Fernandez, S.P., Pantouli, F., Meye, F.J., Marti, F., Tolu, S., Parnaudeau, S., Marie, H.,
1137 Tronche, F., Maskos, U., et al. (2017). Nicotinic receptors mediate stress-nicotine detrimental interplay
1138 via dopamine cells' activity. *Mol Psychiatry* 23, 1597–1605.
- 1139 Pascoli, V., Terrier, J., Hiver, A., and Lüscher, C. (2015). Sufficiency of Mesolimbic Dopamine Neuron
1140 Stimulation for the Progression to Addiction. *Neuron* 88, 1054–1066.
- 1141 Paxinos, G., and Franklin, K.B.J. (2004). *The Mouse Brain in Stereotaxic Coordinates* (Gulf Professional
1142 Publishing).
- 1143 Picciotto, M.R., Zoli, M., Rimondini, R., Léna, C., Marubio, L.M., Pich, E.M., Fuxe, K., and Changeux,
1144 J.P. (1998). Acetylcholine receptors containing the beta2 subunit are involved in the reinforcing
1145 properties of nicotine. *Nature* 391, 173–177.
- 1146 Picciotto, M.R., and Mineur, Y.S. (2013). Molecules and circuits involved in nicotine addiction: The many
1147 faces of smoking. *Neuropharmacology*.
- 1148 Pinault, D. (1996). A novel single-cell staining procedure performed in vivo under electrophysiological
1149 control: morpho-functional features of juxtacellularly labeled thalamic cells and other central neurons
1150 with biocytin or Neurobiotin. *J. Neurosci. Methods* 65, 113–136.
- 1151 Poulin, J.-F., Caronia, G., Hofer, C., Cui, Q., Helm, B., Ramakrishnan, C., Chan, C.S., Dombeck, D.A.,
1152 Deisseroth, K., and Awatramani, R. (2018). Mapping projections of molecularly defined dopamine
1153 neuron subtypes using intersectional genetic approaches. *21*, 1–17.
- 1154 Radke, A.K., and Gewirtz, J.C. (2012). Increased dopamine receptor activity in the nucleus accumbens
1155 shell ameliorates anxiety during drug withdrawal. *Neuropsychopharmacology* 37, 2405–2415.
- 1156 Schultz, W. (2007). Multiple dopamine functions at different time courses. *Annu Rev Neurosci* 30, 259–
1157 288.

1158 Su, M., Li, L., Wang, J., Sun, H., Zhang, L., Zhao, C., Xie, Y., Gamper, N., Du, X., and Zhang, H.
1159 (2019). Kv7.4 Channel Contribute to Projection-Specific Auto-Inhibition of Dopamine Neurons in the
1160 Ventral Tegmental Area. *Front Cell Neurosci* 13, 557.

1161 Sun, F., Zeng, J., Jing, M., Zhou, J., Feng, J., Owen, S.F., Luo, Y., Li, F., Wang, H., Yamaguchi, T., et
1162 al. (2018). A Genetically Encoded Fluorescent Sensor Enables Rapid and Specific Detection of
1163 Dopamine in Flies, Fish, and Mice. *Cell* 174, 481–496.e19.

1164 Sun, F., Zhou, J., Dai, B., Qian, T., Zeng, J., Li, X., Zhuo, Y., Zhang, Y., Tan, K., Feng, J., et al. (2020).
1165 New and improved GRAB fluorescent sensors for monitoring dopaminergic activity &em>in
1166 vivo. *bioRxiv* 2020.03.28.013722.

1167 Tolu, S., Eddine, R., Marti, F., David, V., Graupner, M., Pons, S., Baudonnat, M., Husson, M., Besson,
1168 M., Reperant, C., et al. (2013). Co-activation of VTA DA and GABA neurons mediates nicotine
1169 reinforcement. *Mol Psychiatry* 18, 382–393.

1170 Turiault, M., Parnaudeau, S., Milet, A., Parlato, R., Rouzeau, J.-D., Lazar, M., and Tronche, F. (2007).
1171 Analysis of dopamine transporter gene expression pattern -- generation of DAT-iCre transgenic mice.
1172 *Febs J.* 274, 3568–3577.

1173 Ungless, M.A., and Grace, A.A. (2012). Are you or aren't you? Challenges associated with
1174 physiologically identifying dopamine neurons. *Tins* 35, 422–430.

1175 Watabe-Uchida, M., Zhu, L., Ogawa, S.K., Vamanrao, A., and Uchida, N. (2012). Whole-Brain Mapping
1176 of Direct Inputs to Midbrain Dopamine Neurons. *Neuron* 74, 858–873.

1177 Wolfman, S.L., Gill, D.F., Bogdanic, F., Long, K., Al-Hasani, R., McCall, J.G., Bruchas, M.R., and
1178 McGehee, D.S. (2018). Nicotine aversion is mediated by GABAergic interpeduncular nucleus inputs to
1179 laterodorsal tegmentum. *Nature Communications* 9, 2710.

1180 Yang, H., de Jong, J.W., Tak, Y., Peck, J., Bateup, H.S., and Lammel, S. (2018). Nucleus Accumbens
1181 Subnuclei Regulate Motivated Behavior via Direct Inhibition and Disinhibition of VTA Dopamine
1182 Subpopulations. *Neuron* 97, 434–449.e434.

1183 Zarrindast, M.R., Khalifeh, S., Rezayof, A., Rostami, P., Aghamohammadi Sereshki, A., and
1184 Zahmatkesh, M. (2012). Involvement of rat dopaminergic system of nucleus accumbens in nicotine-
1185 induced anxiogenic-like behaviors. *Brain Res* 1460, 25–32.

1186 Zhao-Shea, R., Liu, L., Pang, X., Gardner, P.D., and Tapper, A.R. (2013). Activation of GABAergic
1187 neurons in the interpeduncular nucleus triggers physical nicotine withdrawal symptoms. *Curr Biol* 23,
1188 2327–2335.

1189 Zhao-Shea, R., Liu, L., Soll, L.G., Improgo, M.R., Meyers, E.E., McIntosh, J.M., Grady, S.R., Marks,
1190 M.J., Gardner, P.D., and Tapper, A.R. (2011). Nicotine-mediated activation of dopaminergic neurons in
1191 distinct regions of the ventral tegmental area. *Neuropsychopharmacology* 36, 1021–1032.

1192 Zhuang, X., Masson, J., Gingrich, J.A., Rayport, S., and Hen, R. (2005). Targeted gene expression in
1193 dopamine and serotonin neurons of the mouse brain. *J. Neurosci. Methods* 143, 27–32.

KEY RESOURCES TABLE

REAGENT or RESOURCE	SOURCE	IDENTIFIER
Antibodies		
Anti-tyrosine Hydroxylase produced in mouse	Sigma-Aldrich	Cat# T1299, RRID:AB_477560
Anti-GFP produced in chicken	Aveslabs	Cat# GFP-1020, RRID:AB_10000240
Anti-rabbit Cy2-conjugated produced in donkey	Jackson ImmunoResearch	Cat# 711-225-152, RRID:AB_2340612
Anti-mouse Cy3-conjugated produced in donkey	Jackson ImmunoResearch	Cat# 715-165-150, RRID:AB_2340813
Anti-chicken Alexa488-conjugated	Jackson ImmunoResearch	Cat# 703-545-155, RRID:AB_2340375
AMCA-Streptavidin	Jackson ImmunoResearch	Cat# 016-150-084, RRID:AB_2337243
Bacterial and virus strains		
Lenti-pGK-B2-IRES-GFP	Maskos et al., 2005 https://doi.org/10.1038/nature03694 : Provided by Institut Pasteur, Paris, France	Virus (Lentivirus)
Lenti-pGK-IRES-GFP	Maskos et al., 2005 https://doi.org/10.1038/nature03694 : Provided by Institut Pasteur, Paris, France	Virus (Lentivirus)
pAAV.Ef1a.DIO.CatCh.YFP	This paper : Provided by Institut de la vision, Paris France	plasmid
AAV5-flox-EF1a-hCatCh-YFP	This paper : Provided by Institut de la vision, Paris France	Virus (AAV)
pAAV.Ef1a.DIO.Jaws.eGFP	Adgene	65014 -Plasmid
AAV5-CAG-Flex-Jaws-eGFP	This paper : Provided by Institut de la vision, Paris France	Virus (AAV)
pAAV-Ef1a-DIO-YFP	This paper Provided by Institut de la vision, Paris France	Plasmid
AAV5-CAG-Flex-Jaws-eGFP	This paper Provided by Institut de la vision, Paris France	Virus (AAV)
pAAV-Ef1a-DIO-YFP	Adgene	105539-Plasmid
AAV5-flox-EF1a-YFP	This paper Provided by Institut de la vision, Paris France	Virus (AAV)
pAAV-CAG-Jaws-KGC-GFP-ER2	Adgene	99233-Plasmid
AAV2-CAG-Jaws-GFP	This paper Provided by Institut de la vision, Paris France	Virus (AAV)

pAAV-CAG-GFP	Adgene	83279--Plasmid
AAV2-7m8-CAG-GFP	This paper Provided by Institut de la vision, Paris France	Virus (AAV)
pAAV-flox-Ef1a-hChr2-YFP	This paper Provided by Institut de la vision, Paris France	Plasmid
AAV9-flox-Ef1a-hChr2-YFP	This paper Provided by Institut de la vision, Paris France	Virus (AAV)
AAV5-hSyn-hChr2(H134R)-eYFP	Adgene	26973-AAV5
AAV5.hSyn.eGFP.WPRE.bGH	Adgene	105539-AAV5
AAV5-hsyn-Jaws-KGC-GFP-ER2	Adgene	65014-AAV5
psAAV-hSyn-GRABDA2m	Sun et al., 2020 https://doi.org/10.1101/2020.03.28.013722	Plasmid
AAV1-hSyn-GRABDA2m	This paper Provided by Institut de la vision, Paris France	Virus (AAV)
Chemicals, peptides, and recombinant proteins		
NaCl	Sigma-Aldrich	S7653
KCl	Sigma-Aldrich	P9333
NaH ₂ PO ₄	Sigma-Aldrich	S8282
MgCl ₂	Sigma-Aldrich	M2670
CaCl ₂	Sigma-Aldrich	233506
NaHCO ₃	Sigma-Aldrich	S6297
Sucrose	Sigma-Aldrich	S0389
Glucose	Sigma-Aldrich	49159
Kynurenic Acid	Sigma-Aldrich	K3375
Albumin, from bovine serum	Sigma-Aldrich	A4503
KGlu	Sigma-Aldrich	P1847
HEPES	Sigma-Aldrich	H3375
EGTA	Sigma-Aldrich	E3889
ATP	Sigma-Aldrich	A9187
GTP	Sigma-Aldrich	G8877
Biocytin	Sigma-Aldrich	B4261
Nicotine tartrate	Sigma-Aldrich	N5260
Glucose	Sigma-Aldrich	G8270
DPBS 10x	Life Technologies	14200-067
Neurobiotin Tracer	Vector laboratories	SP-1120
Prolong Gold Antifade Reagent	Invitrogen	P36930
Chloral Hydrate	Sigma-Aldrich	302-17-0
Sodium Acetate	Sigma-Aldrich	57654611
Quinpirole	Tocris	55397
Eticlopride	Tocris	57266
Critical commercial assays		
EasyTag EXPRESS 35S Protein Labeling Kit	PerkinElmer	NEG772014MC

CaspaseGlo 3/7	Promega	G8090
TruSeq ChIP Sample Prep Kit	Illumina	IP-202-1012
Deposited data		
Raw and analyzed data	This paper	GEO: GSE63473
B-RAF RBD (apo) structure	This paper	PDB: 5J17
Human reference genome NCBI build 37, GRCh37	Genome Reference Consortium	http://www.ncbi.nlm.nih.gov/projects/genome/assembly/grc/human/
Nanog STILT inference	This paper; Mendeley Data	http://dx.doi.org/10.17632/wx6s4mj7s8.2
Affinity-based mass spectrometry performed with 57 genes	This paper; Mendeley Data	Table S8; http://dx.doi.org/10.17632/5hvpvpspw82.1
Experimental models: Organisms/strains		
strain (mouse) , strain background (mus musculus) - males	Janvier Laboratories, France	C57Bl/6j SC-C57J-M
strain (mouse) , strain background (mus musculus) - males	Maskos et al., 2005 https://doi.org/10.1038/374065a0	ACNB2 KO maintained on a C57BL6/J background
strain (mouse) , strain background (mus musculus) - males	Turiault et al., 2007 https://doi.org/10.1111/j.1742-4658.2007.05886.x	DAT1cre maintained on a C57BL6/J background
Software and algorithms		
R Project for Statistical Computing	http://www.r-project.org/	RRID:SCR_001905
Fiji	http://fiji.sc	RRID:SCR_002285
PyCharm	CE version 2020.3.4 (Python 3.8)	RRID:SCR_018221
Adobe Illustrator 2020	Adobe	RRID:SCR_010279
Spike 2 Software	CED	RRID:SCR_000903
Spike sort 3D	5.6.3	Neuralynx acquisition
Spike extractor	2.5.0.0	Neuralynx acquisition
Cheetah software	version 3.01 2.5.4	Neuralynx acquisition
Doric Neuroscience Studio	Doric	RRID:SCR_018569
Clampfit (pClamp suite)	Molecular Devices	RRID:SCR_011323

Figure 1

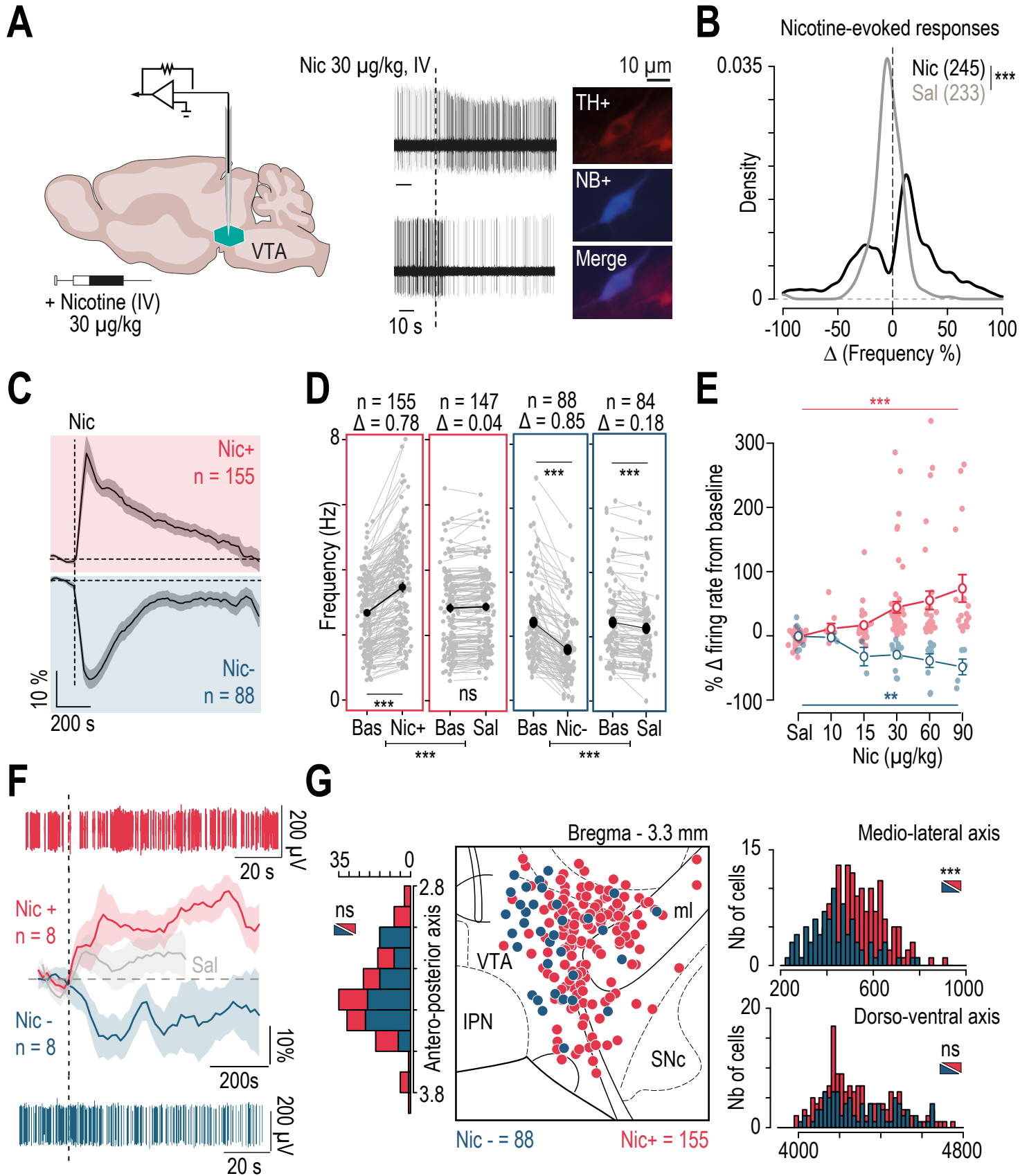


Figure 1

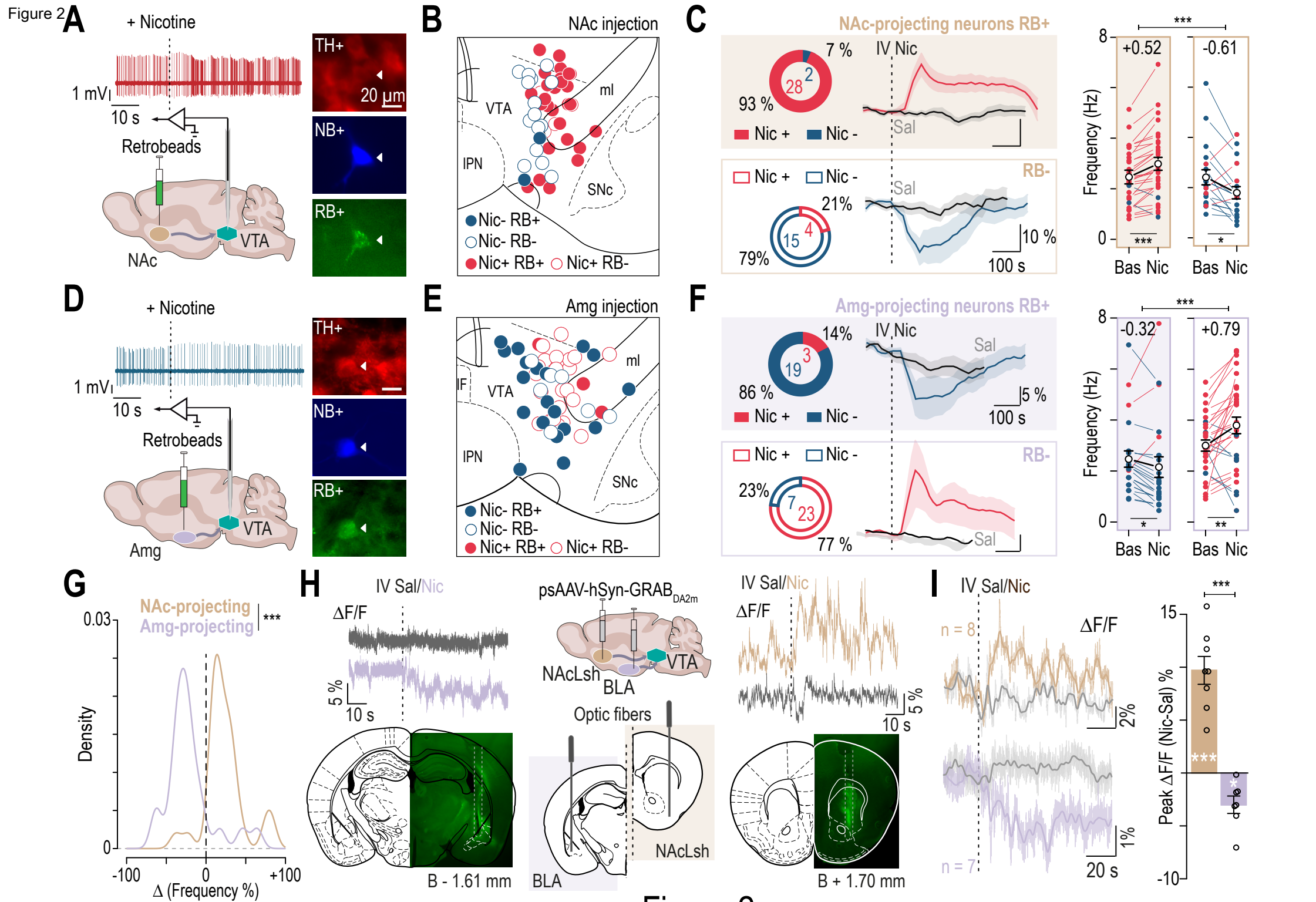


Figure 2

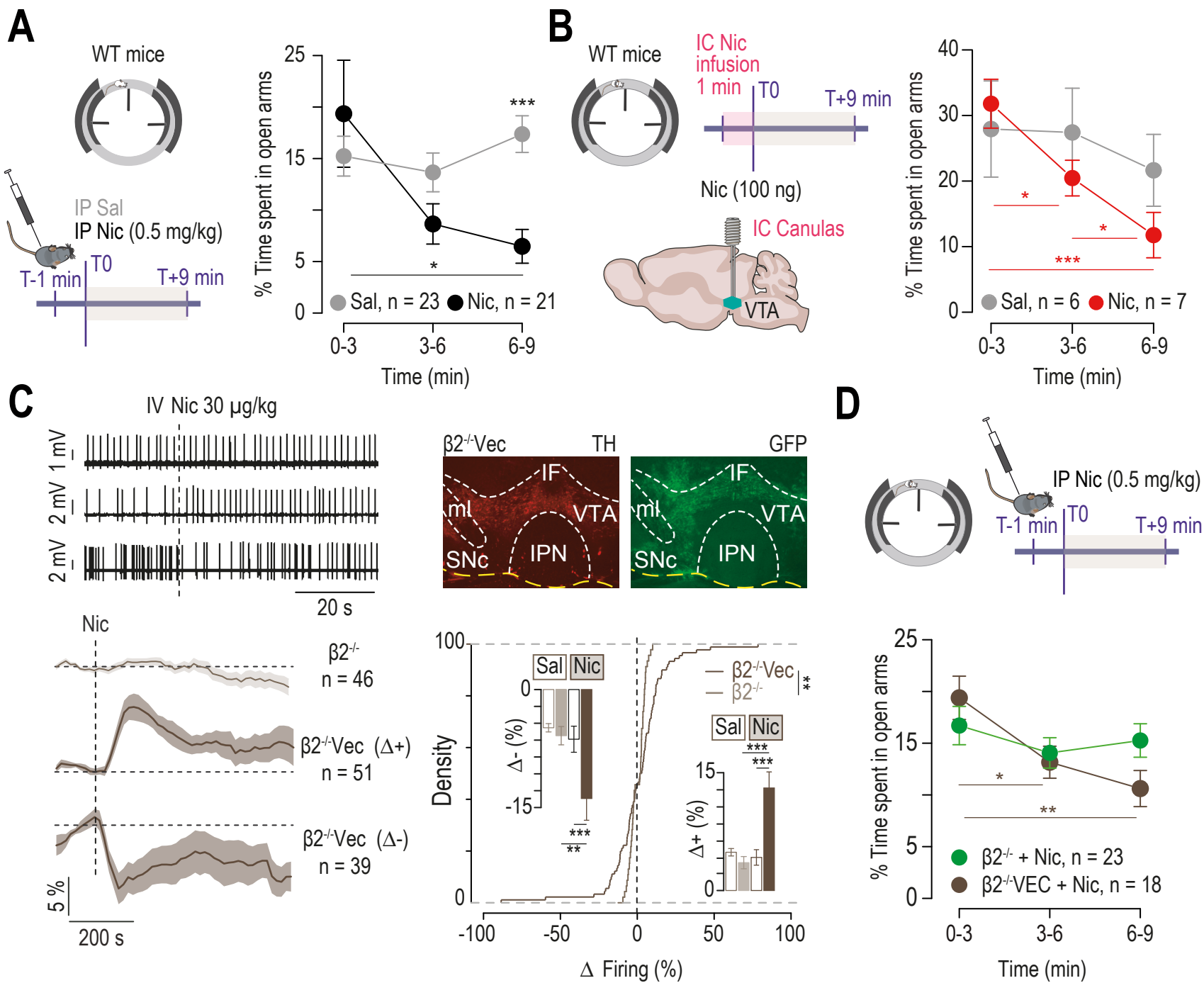


Figure 3

Figure 4

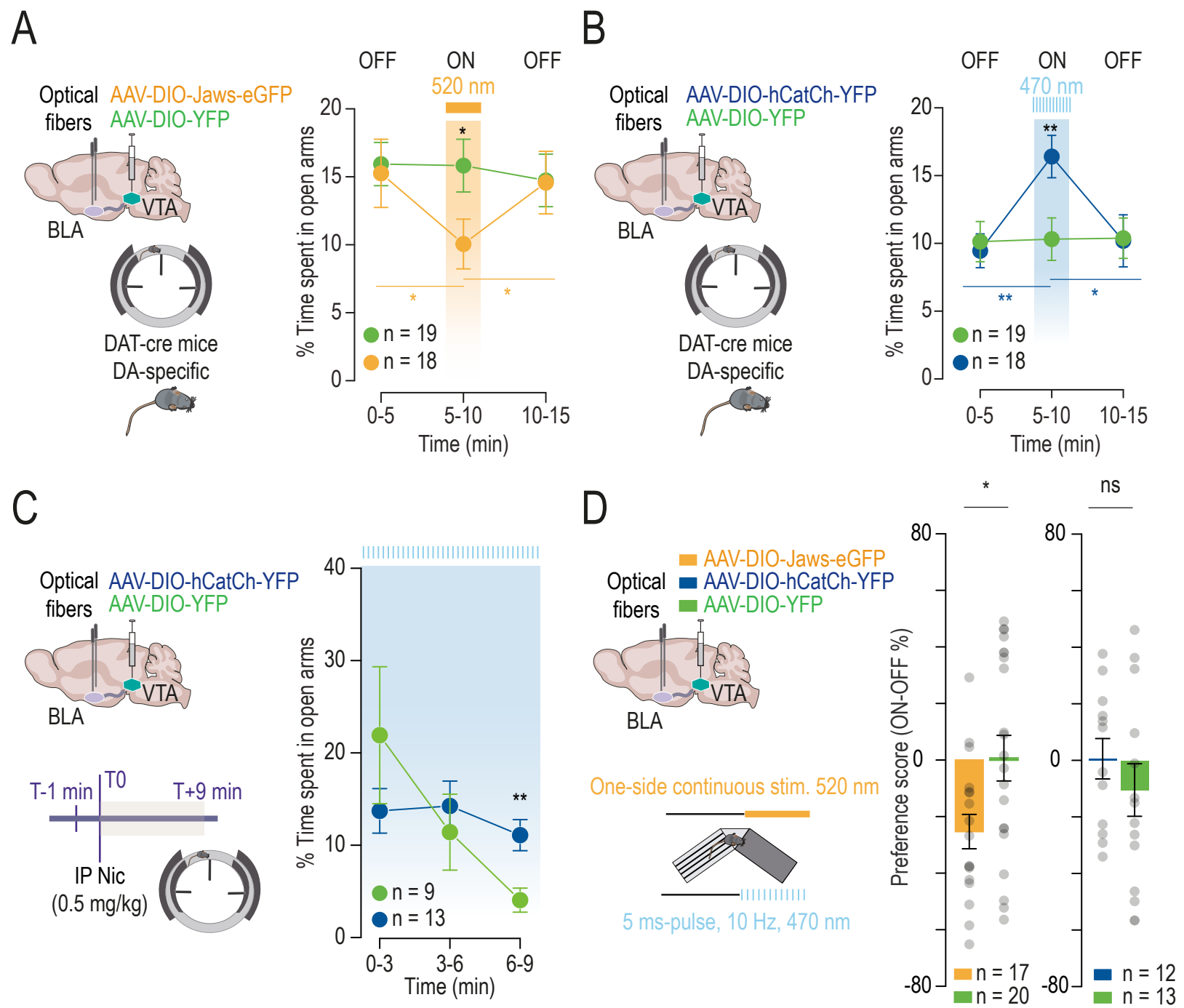


Figure 4

Figure 5

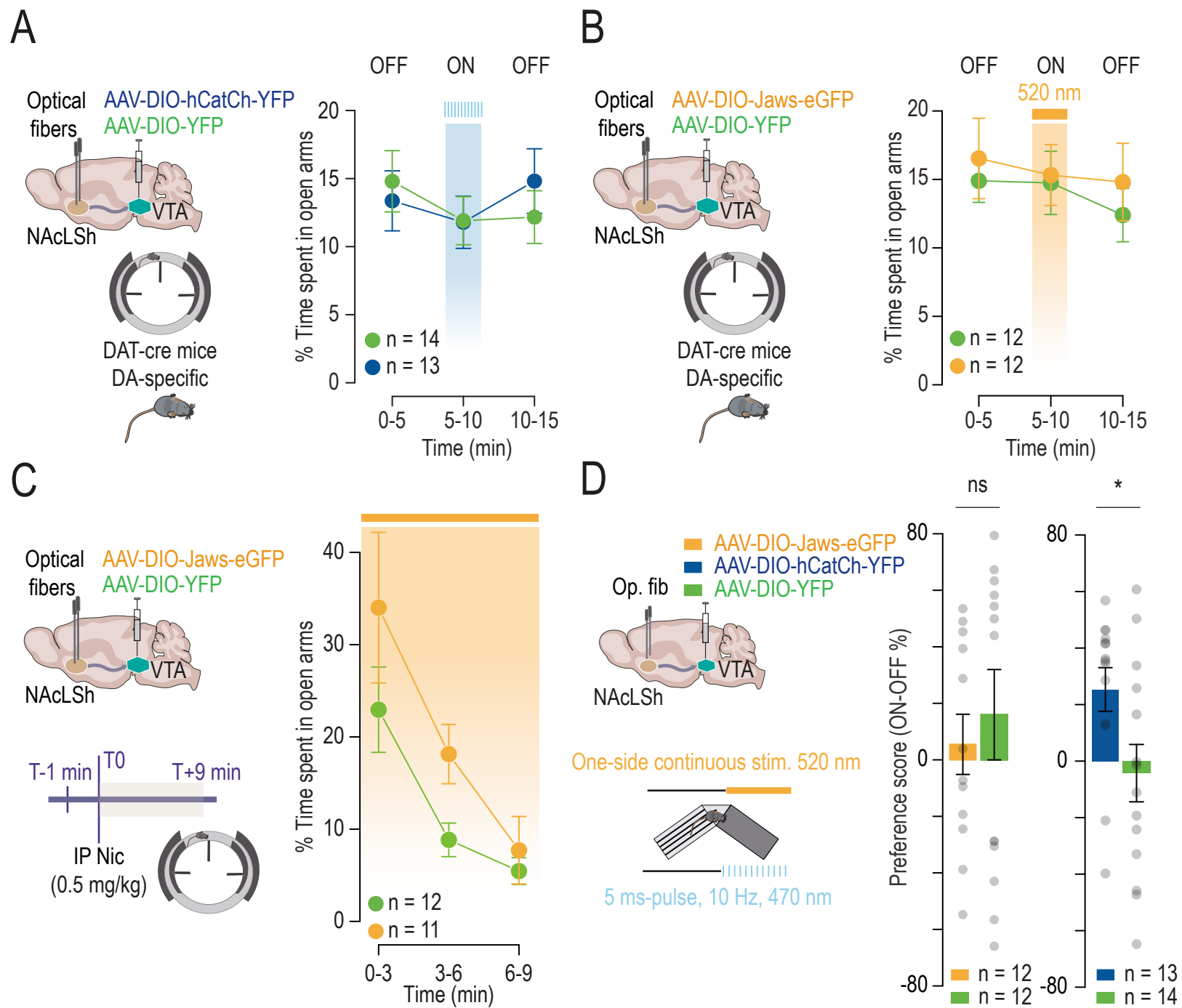


Figure 5

Supplemental Information

Nicotine inhibits the VTA to Amygdala dopamine pathway to promote anxiety

Nguyen C, Mondoloni S, Le Borgne T, Centeno I, Come M, Jehl J, Solié C, Reynolds LM, Durand-de Cuttoli R, Tolu S, Valverde S, Didienne S, Hanneke B, Fiancette JF, Pons S, Maskos U, Deroche-Gamonet V, Dalkara D, Hardelin JP, Mourot A, Marti F & Faure P

Supplemental Information consists of:

Supplementary Figure S1, related to Figure 1.

Supplementary Figure S2, related to Figure 1.

Supplementary Figure S3, related to Figure 1.

Supplementary Figure S4, related to Figure 2.

Supplementary Figure S5, related to Figure 2.

Supplementary Figure S6, related to Figure 2.

Supplementary Figure S7, related to Figure 3.

Supplementary Figure S8, related to Figure 3.

Supplementary Figure S9, related to Figure 4.

Supplementary Figure S10, related to Figure 4.

Supplementary Figure S11, related to Figure 4.

Supplementary Figure S12, related to Figure 4.

Supplementary Figure S13, related to Figure 5.

Supplementary Figure S14, related to Figure 5.

Figure S1: Paired responses to saline and nicotine injections of *in vivo* recorded DA neurons in anesthetized mice. Related to Figure 1.

Responses of VTA DA neurons to saline (left) and nicotine (right) injections. Responses are rank ordered based on the response to nicotine, from the most inhibited (below) to the most excited (above). *Left*: Colored scale of amplitude responses. *Right*: Examples of individual responses to nicotine (10 neurons), horizontal dotted lines indicate 0, vertical dotted lines the nicotine injections.

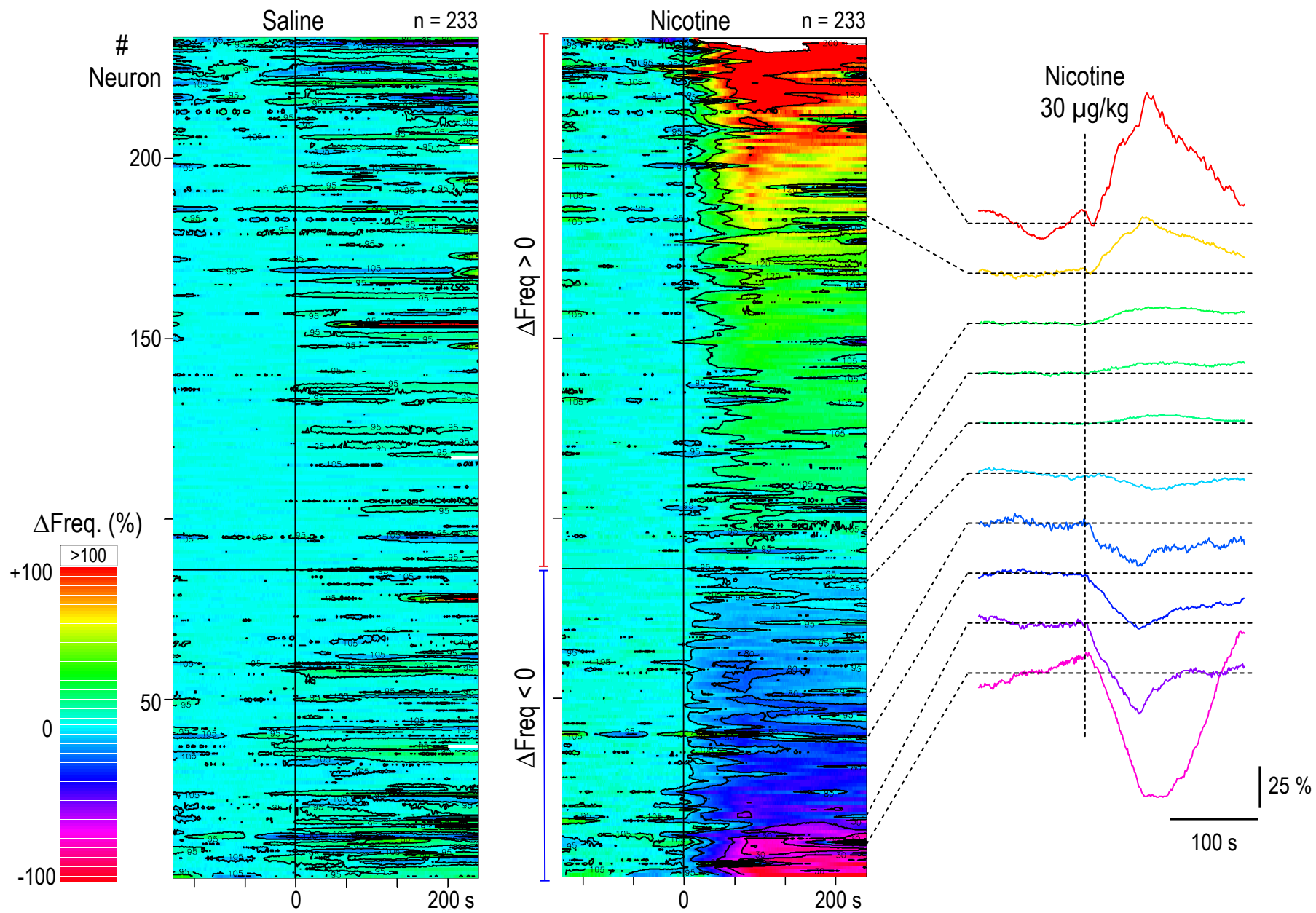
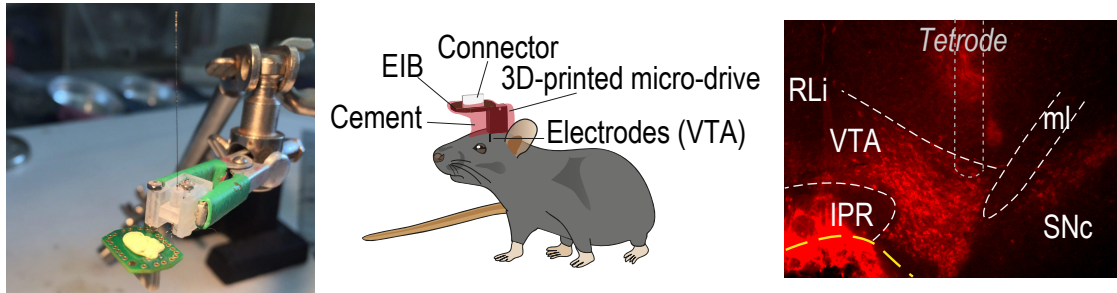


Figure S1

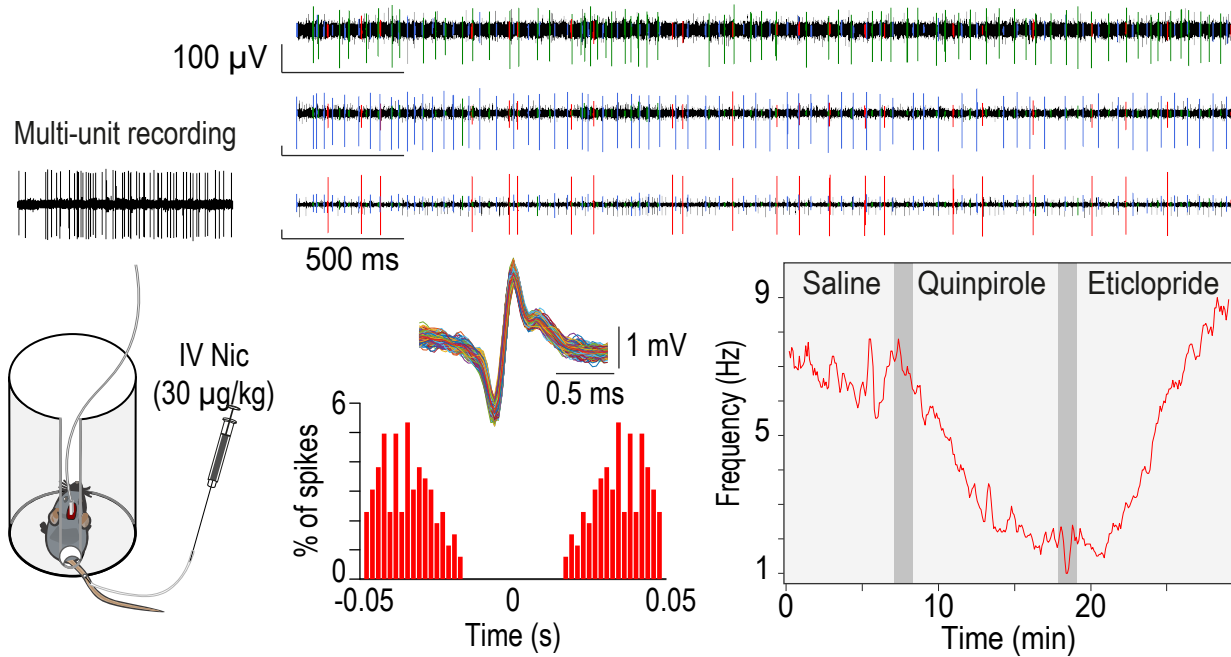
Figure S2: *In vivo* recordings of DA neurons: anesthetized and freely moving experiments. Related to Figure 1.

(A) From left to right: Picture of the micro-drive (upside-down view). Schematic of micro-drive implantation for *in vivo* recordings of freely moving mice. Histological slice showing tetrode implantation in the VTA. **(B)** Left: Schematic of the plastic cylinder used for IV nicotine injection into the tail vein during tetrode and fiber photometry recordings in freely moving animals. Right: Example of one multi-channel recording of three VTA neurons (color-coded after clustering on all channels, top). GABAergic neurons are in green and blue and a putative DA neuron is in red. DA neurons are characterized by electrophysiological criteria (firing frequency, bursting activity, regularity of firing and large refractory period as seen in the auto-correlogram, bottom) and their response to Quinpirole/Eticlopride (D2R selective agonist and antagonist respectively, bottom right). **(C)** Analysis of the spontaneous activity of NB-labeled DA neurons that were either activated (red) or inhibited (blue) by the nicotine injection. Top: Basal firing rates and percentage of spikes-within-burst (%SWB) between activated and inhibited neurons were not statistically different (Wilcoxon test $p = 0.051$ and $p = 0.064$). Bottom: Interval between SWB (in ms) as a function of the length of the burst (from two to seven action potentials).

A



B



C

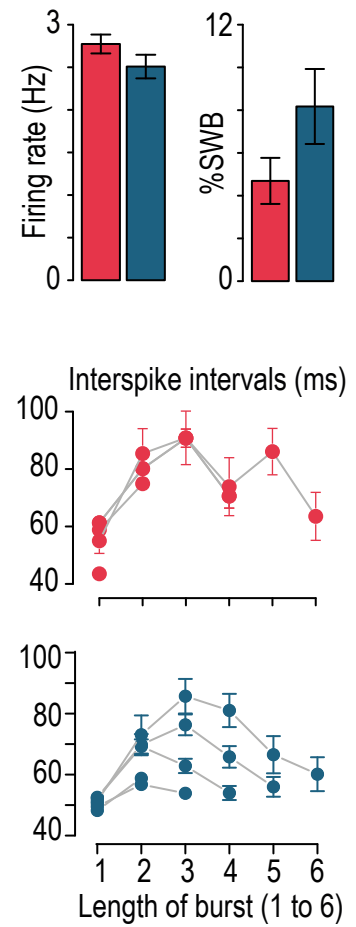
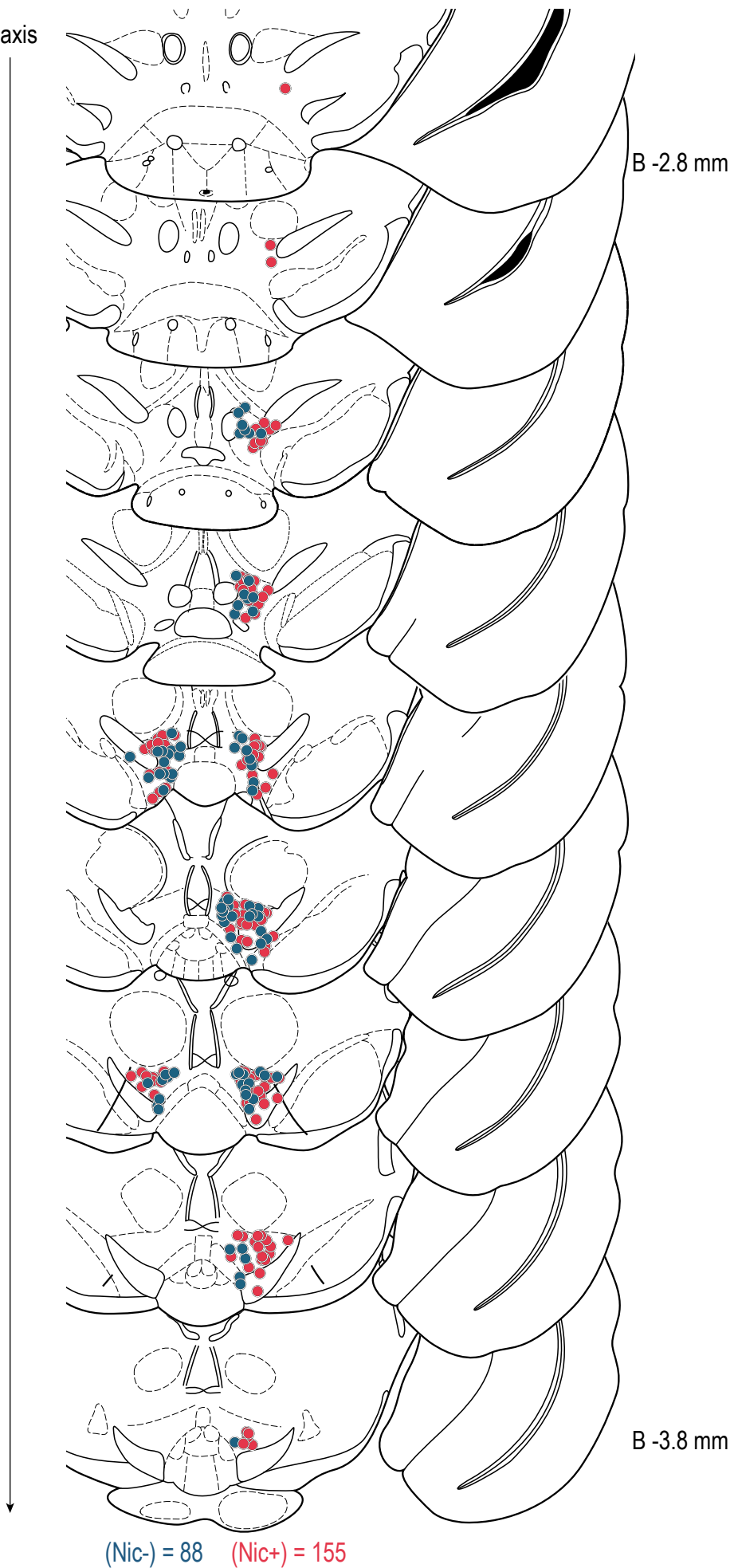


Figure S2

Figure S3: Localization of *in vivo* labeled DA neurons on anesthetized mice. Related to Figure 1.

Localization of VTA DA neurons labeled *in vivo* after juxtacellular recordings on anesthetized animals. Neurons are color-coded according to their responses to nicotine injection (activated in red, n = 155 and inhibited in blue, n = 88), and positioned according to the antero-posterior axis on the Paxinos atlas from Bregma -2.8 to -3.8 mm.

Antero-posterior axis



(Nic-) = 88 (Nic+) = 155

Figure S3

Figure S4: Retrobead injections into the NAc and Amg. Related to Figure 2.

(A, C) Examples of retrograde tracer (retrobeads RB, in yellow) injected in all of the NAc (A) and Amg sites (C), reported onto different Paxinos atlas slices. (B, D) Representative immunofluorescence images of VTA slices (TH+, red) revealing neurons containing RB (RB+, green), after RB injection into the NAc (B) or into the Amg (D). (E) *Left*: A Paxinos atlas slice at 3.3 mm from bregma, onto which neurobiotin-filled cell bodies of all recorded neurons from RB-injected mice were positioned (NAc-projecting neurons n = 30, gold and Amg-projecting neurons n = 22, purple). *Right*: Medio-lateral distribution (shown as density) of the neurons shown in E) that project either to the NAc (gold) or to the Amg (purple). Amg-projecting neurons were located more medially in the VTA than NAc-projecting neurons (Wilcoxon test, *** p < 0.001). (F) Analysis of the spontaneous activity of NB-labeled DA neurons that were found RB+ after either NAc injection (n = 30, gold) or Amg injection (n = 22, purple). NAc-projecting DA neurons and Amg-projecting DA neurons displayed similar firing frequency (Wilcoxon test, p = 0.8). The Amg-projecting neurons tend to have a higher bursting activity even though it is not statistically different than the NAc-projecting neurons (Wilcoxon test, p = 0.28). IF: *interfascicular nucleus*; IPN: *interpeduncular nucleus*; ml: *medial lemniscus*; SNc: *substantia nigra pars compacta*

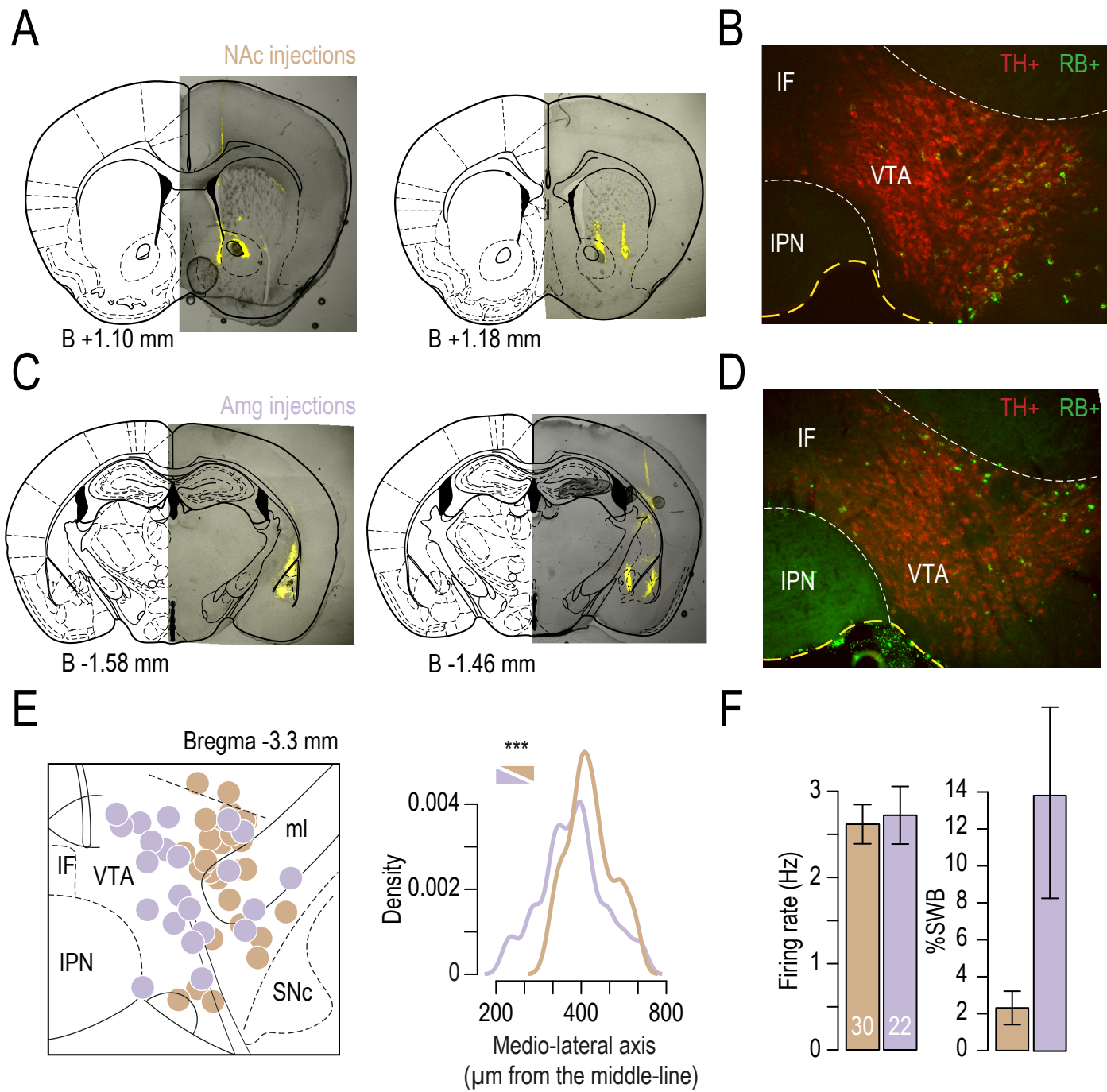


Figure S4

Figure S5: DA neurons projecting to either NAcMSh or NAcLSh are activated by nicotine injection. Related to Figure 2.

(A) Retrobeads (RB) were injected in the NAc Medial Shell (NAcMSh) of WT mice and VTA DA neuron responses to an IV nicotine injection (30 $\mu\text{g}/\text{kg}$) were recorded *in vivo* on anesthetized animals, and labeled with neurobiotin. Example of RB site in the NAcMSh (top) and retrobeads labelling in the VTA two weeks after injection (bottom). **(B)** *Post hoc* identification of NAcMSh-projecting DA neurons by immunofluorescent co-labeling of tyrosine hydroxylase (TH), neurobiotin (NB) and RB (scale bar 20 μm). Localization on the Paxinos atlas at bregma - 3.4 mm of NB-labeled DA neurons (NB+ TH+, n = 22) following RB injection (\bullet RB+, \circ RB-) into the NAcMSh. Red and blue colors denote nicotine-activated (Nic+) and nicotine-inhibited (Nic-) neurons, respectively. (RB+ Nic+, n = 14, RB+ Nic-, n = 0; RB- Nic+, n = 5; RB- Nic-, n = 3). **(C)** *Top*: Percentage and number of Nic+ (red) and Nic- (blue) cells among NAcMSh-projecting DA neurons (RB+). Mean change in firing frequency of NAcMSh-projecting DA neurons in response to an IV injection of nicotine (red) or saline (grey). *Bottom*: Percentage and number of Nic+ (red) and Nic- (blue) cells in non-RB-labeled neurons (RB-). Mean change in firing frequency of RB- DA neurons in response to an IV injection of nicotine (black) or saline (grey). **(D)** Firing rate variation (Δ) from baseline (Bas) induced by nicotine (Nic) injection in RB+ (*left*, mean $\Delta = +0.50$ Hz) or RB- (*right*, mean $\Delta = +0.05$ Hz) DA neurons. (Comparison between mean firing rate during baseline and maximum firing rate after injection: paired Wilcoxon test, *** p (RB+) < 0.001, p (RB-) = 0.64; Comparison between nicotine-induced firing rate variation evoked in RB+ and RB- DA neurons: Wilcoxon test, ** p = 0.004). Mean scores are represented in black, and individual scores in red or blue. **(E)** RB were injected in the NAc Lateral Shell (NAcLSh) of WT mice and VTA DA neuron responses to an IV nicotine injection were recorded as in (A). **(F)** Localization of NB-labeled DA neurons (NB+ TH+, n = 12) following RB injection into the NAcLSh. (RB+ Nic+, n = 6; RB+ Nic-, n = 0; RB- Nic+, n = 4; RB- Nic-, n = 3) and example of NB- labelled identified DA neuron (scale bar 20 μm). **(G)** Same as in (C) for NAcLSh -projecting (RB+) DA neurons (*top*) and for non-RB-labeled (RB-) neurons (*bottom*) when RB were injected in the NAcLSh. **(H)** Same as in (D) for NAcLSh -projecting (RB+) DA neurons (*left*, mean $\Delta = +0.73$ Hz) and for non-RB-labeled (RB-) neurons (*right*, mean $\Delta = -0.23$ Hz). (Comparison between mean firing rate during baseline and maximum firing rate after injection: paired Wilcoxon test, * p (RB+) = 0.03, p (RB-) = 0.8; Comparison between nicotine-induced firing rate variation evoked in RB+ and RB- DA neurons: Wilcoxon test, p = 0.13). Mean scores are represented in black, and individual scores in red or blue.

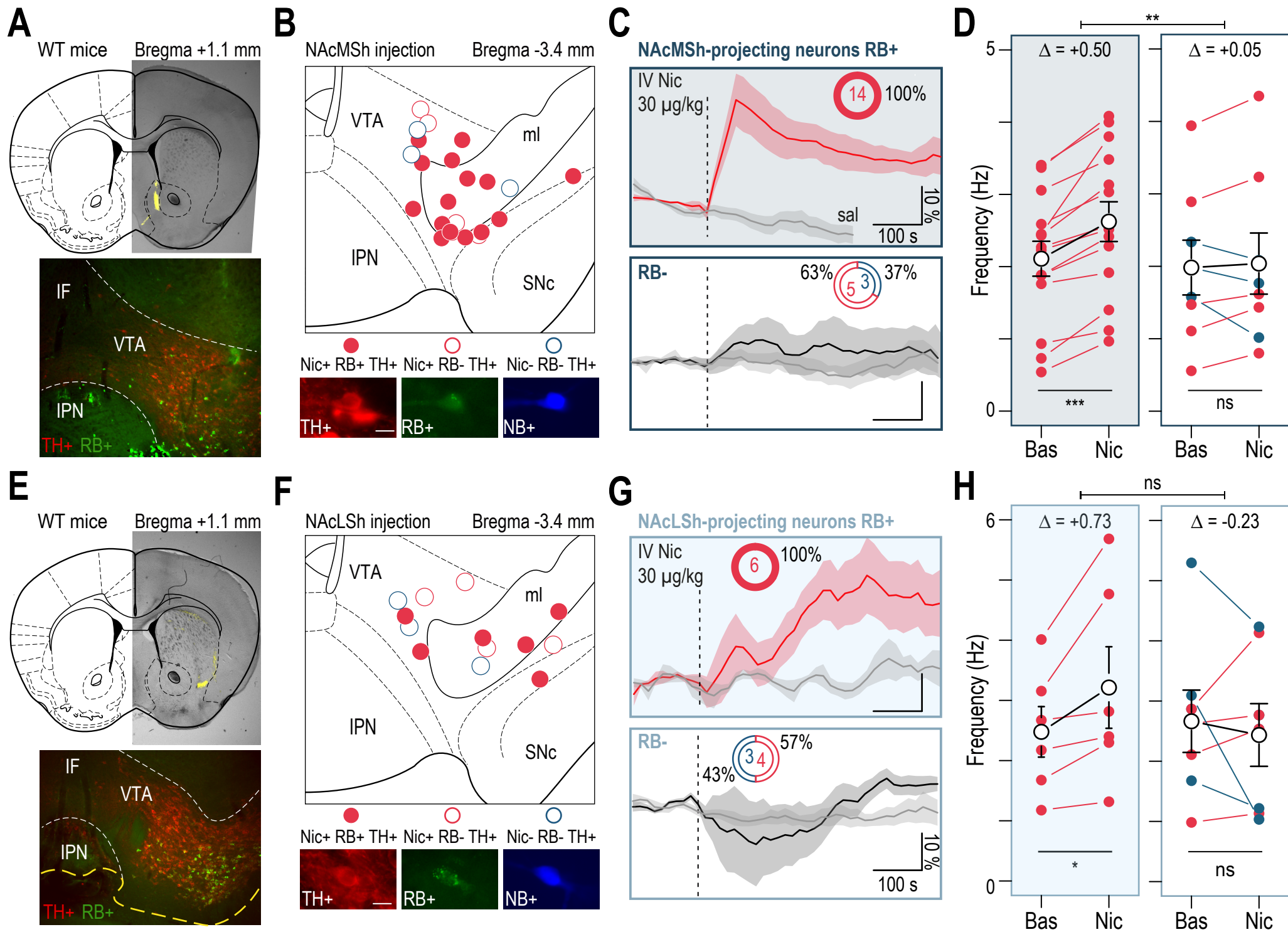


Figure S5

Figure S6: VTA DA neurons projecting to the Amg are more excitable but not more reactive to nicotine than NAc-projecting DA neurons. Related to Figure 2.

(A) Immunofluorescence image of VTA DA (TH+) neurons projecting to the NAc (retrobeads, RB+) labeled after patch-clamp recording (neurobiotin, NB+). **(B)** Immunofluorescence image of an Amg-projecting (RB+) VTA DA (TH+) neuron labeled after patch-clamp recording (neurobiotin, NB+). **(C)** Firing of NAc-projecting and Amg-projecting VTA DA neurons after current injections (20, 60 and 100 pA). **(D)** Higher excitability of Amg-projecting (n = 15, purple) compared to NAc-projecting (n = 13, gold) DA neurons (two-way RM ANOVA main effect phenotype $F(1,26) = 4.96$, * $p = 0.035$, current $F(4,104) = 15.97$, *** $p < 0.001$, current x phenotype interaction $F(4,104) = 13.78$, *** $p < 0.001$). **(E)** Nicotine-evoked currents (local puff 100 μM) in RB+-identified, NAc- or Amg-projecting VTA DA neurons recorded in brain slices (whole-cell voltage-clamp mode -60 mV). **(F)** Mean currents evoked by nicotine in either NAc-projecting (n = 16, gold, 33.0 ± 19.8 pA) or Amg-projecting (n = 17, purple, 22.4 ± 13.3 pA) VTA DA neurons were not statistically different (Student's t-test, $p = 0.08$).

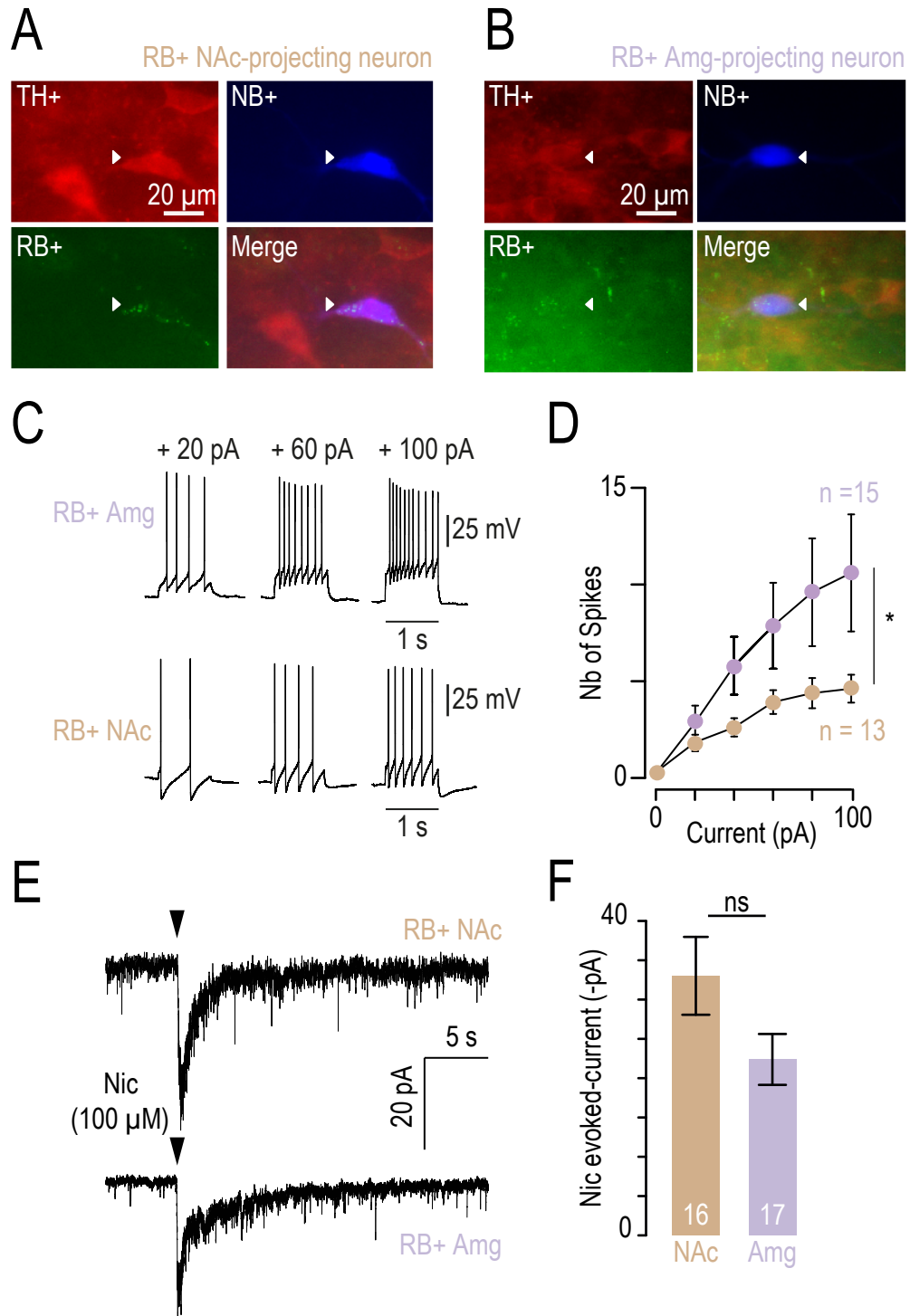


Figure S6

Figure S7: Detailed analysis of nicotine-induced anxiety-like behaviors and the role of $\beta 2$ subunit-containing nAChR. Related to Figure 3.

(A) Left: Individual data for Figure 3A, Sal (grey, $n = 23$) or Nic (black, $n = 21$), solid colors indicate group means, individual data with open gray dots (one-way RM ANOVA Nic: $F_{(2,40)} = 5.18$, ** $p = 0.01$; Sal: $F_{(2,44)} = 1.65$, $p = 0.2$). **Right:** Mean number of open arm entries during elevated O-maze (EOM) test (two-way RM ANOVA main time effect $F_{(2,84)} = 8.02$, *** $p < 0.001$). **(B)** Locomotor activity was measured in a square open field (OF) following an intraperitoneal (IP) injection of either saline (IP Sal, grey, $n = 6$) or nicotine (IP Nic 0.5 mg/kg, black, $n = 6$) in WT mice. No difference was observed in the distance traveled over time (two-way RM ANOVA no time, no treatment or interaction effect, $p > 0.05$) or in the total distance traveled during 9 minutes (*inset*, Student's t-test, $p > 0.05$). **(C)** Example of *post hoc* verification of intracranial guide cannula implantations in WT mice. Bilateral injection cannulas (0.5 μm longer than the guide cannulas) are inserted on the day of the experiment for local infusion into the VTA. Tyrosine hydroxylase (TH) labeling is shown in yellow. **(D) Left:** Individual data for Figure 3B, intracranial (IC) infusion of Sal (grey, $n = 6$) or Nic (red, $n = 7$) 1 mg/mL 1 minute before the test (one-way RM ANOVA Nic: $F_{(2,12)} = 26.11$, *** $p < 0.001$; Sal: $F_{(2,10)} = 0.01$, $p = 0.99$). Group means are shown by solid color points, individual data with open gray dots. **Right:** Mean number of open arm entries during EOM test (two-way RM ANOVA main time effect $F_{(2,20)} = 8.25$, ** $p = 0.002$). **(E)** Schematic of $\beta 2$ subunit re-expression by lentiviral vectorization in the VTA of $\beta 2^{-/-}$ mice. Lentiviruses encoding either pGK- $\beta 2$ -IRES-GFP ($\beta 2^{-/-}$ Vec) or pGK-GFP ($\beta 2^{-/-}$ GFP, used as a control) were injected into the VTA. Representative immunofluorescence image of a $\beta 2^{-/-}$ Vec mouse brain labeled for TH (red) and GFP (green). **(F)** Percentage of time spent in the open arms of the EOM by $\beta 2^{-/-}$ GFP mice ($n = 6$, green) and $\beta 2^{-/-}$ mice ($n = 17$, grey) was not different (two-way RM ANOVA no time, no treatment or interaction effect, $p > 0.05$). **(G) Left:** Individual data for Figure 3D, $\beta 2^{-/-}$ mice ($n = 23$, green) and $\beta 2^{-/-}$ Vec mice ($n = 18$, brown) after IP injection of Nic 0.5 mg/kg 1 minute before the test (one-way RM ANOVA for $\beta 2^{-/-}$ Vec mice: $F_{(2,34)} = 8.65$, *** $p < 0.001$; and for $\beta 2^{-/-}$ mice: $F_{(2,44)} = 1.08$, $p = 0.3$). Group means are shown by solid color points, individual data with open gray dots. **Right:** Mean number of open arm entries from $\beta 2^{-/-}$ GFP or $\beta 2^{-/-}$ mice in this test (two-way RM ANOVA main time effect $F_{(2,78)} = 7.26$, ** $p = 0.001$).

IF: *interfascicular nucleus*; IPN: *interpeduncular nucleus*; SNc: *substantia nigra pars compacta*; ml: *medial lemniscus*; SNc: *substantia nigra pars compacta*.

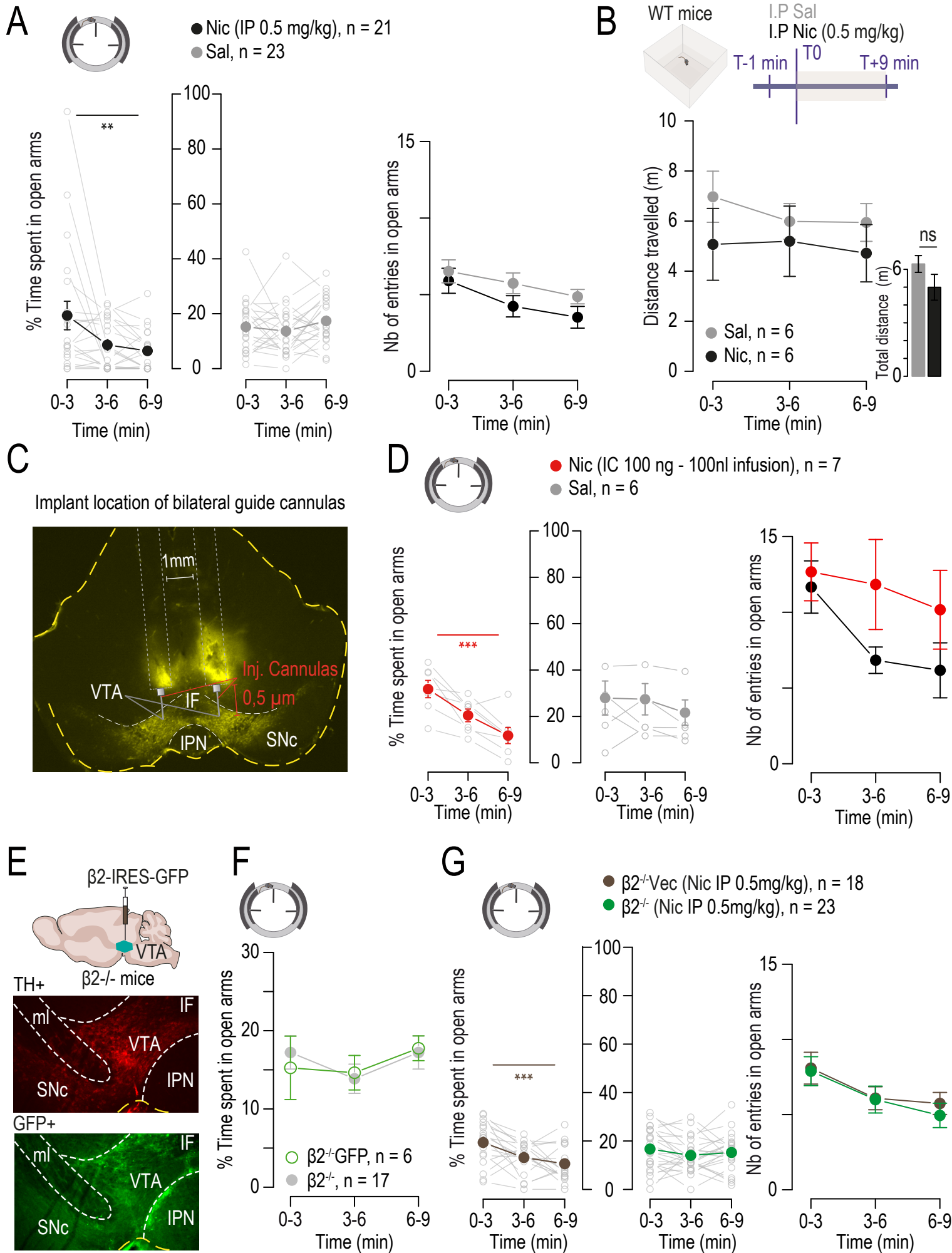


Figure S7

Figure S8: $\beta 2$ nAChR subunit re-expression in the VTA restores DA neuron response to nicotine injection. Related to Figure 3.

(A) Density plot of percentage of firing variation induced by IV injection of either saline (Sal, grey, $n = 46$) or nicotine (Nic, black, $n = 46$) in $\beta 2^{-/-}$ mice (Kolmogorov-Smirnov test, $p = 0.7$). (B) Firing rate variation (Δ) from baseline (Bas) induced by Nic and Sal injection in $\beta 2^{-/-}$ Vec mice DA neurons with increase ($\Delta fr > 0$) or decrease ($\Delta fr < 0$) in firing frequency after Nic injection. Comparison between mean firing rate during baseline and maximum firing rate after injection (paired Wilcoxon test, *** $p < 0.001$), comparison between saline-induced and Nic-induced firing rate variation (Wilcoxon test, $p(\Delta fr > 0) = 0.07$, $p(\Delta fr < 0) = 0.4$). (C) Density plot of percentage of firing variation induced by IV Sal or Nic injection in $\beta 2^{-/-}$ Vec mice (Sal: grey, $n = 79$, Nic: black, $n = 90$). (Kolmogorov-Smirnov test, * $p = 0.024$). (D) Firing rate variation (Δ) from baseline (Bas) induced by Nic and Sal injection in $\beta 2^{-/-}$ Vec mice DA neurons with increase ($\Delta fr > 0$) or decrease ($\Delta fr < 0$) in firing frequency after Nic injection. Comparison between mean firing rate during baseline and maximum firing rate after injection (paired Wilcoxon test, *** $p < 0.001$), comparison between saline-induced and Nic-induced firing rate variation (Wilcoxon test, *** $p < 0.001$). Mean scores are represented in black, and individual scores in grey. (E) Time course for the average change in firing frequency upon saline (grey) or nicotine injection for activated (Nic+, in red) and inhibited (Nic-, in blue) VTA DA neurons in $\beta 2^{-/-}$ and $\beta 2^{-/-}$ Vec mice. Comparison between saline-induced and nicotine-induced firing rate variation (paired Wilcoxon test, ** $p = 0.0015$, *** $p < 0.001$). (F) Firing rate variation (Δ) from baseline (Bas) induced by Nic injection in Nic+ or Nic- DA neurons in $\beta 2^{-/-}$ and $\beta 2^{-/-}$ Vec mice. Comparison between mean firing rate during baseline and maximum firing rate after Nic injection (paired Wilcoxon test, * $p = 0.015$, *** $p < 0.001$), comparison between Nic-induced firing rate variation in $\beta 2^{-/-}$ and $\beta 2^{-/-}$ Vec mice (Wilcoxon test, *** $p < 0.001$). Mean scores are represented in black, and individual scores in grey. In panels B and D, all neurons are considered, while in E and F only responding neurons (i.e those with a statistically significant increase (Nic+) or decrease (Nic-) in firing rate in response to Nic injection, see bootstrapping in Methods) are included.

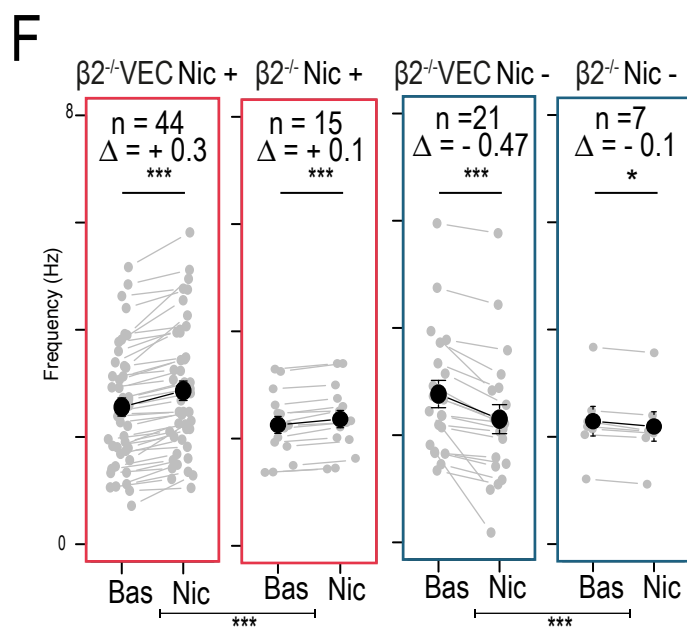
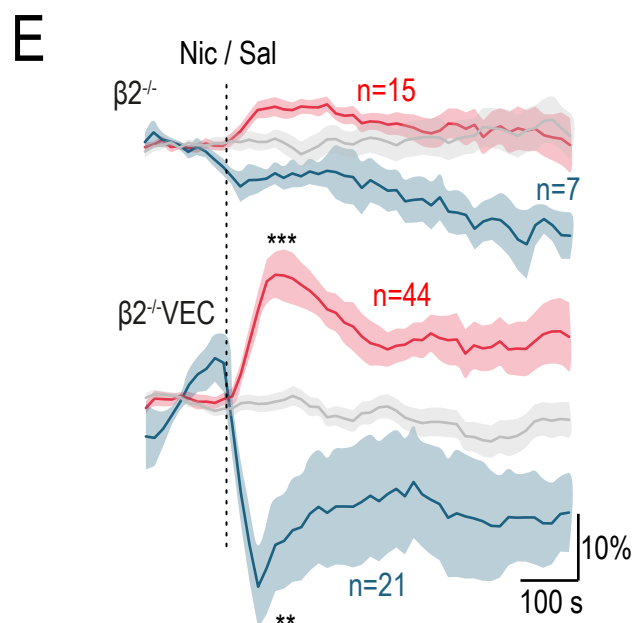
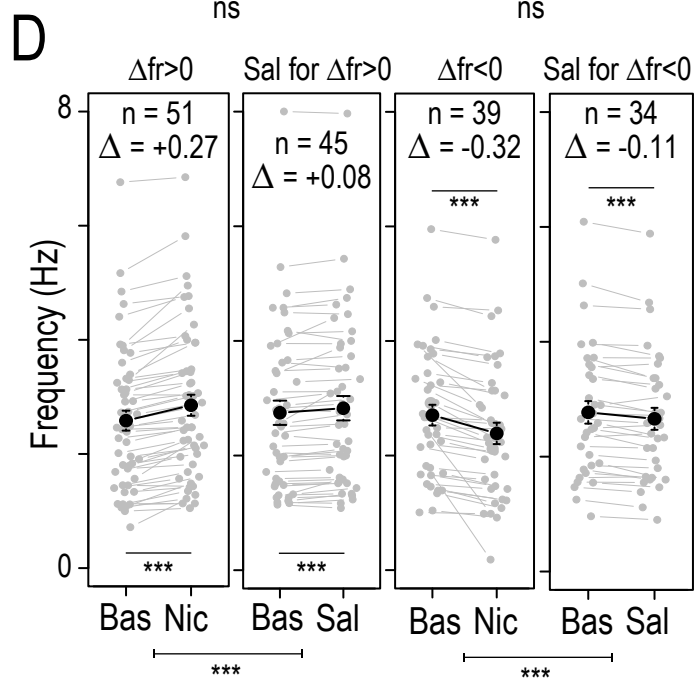
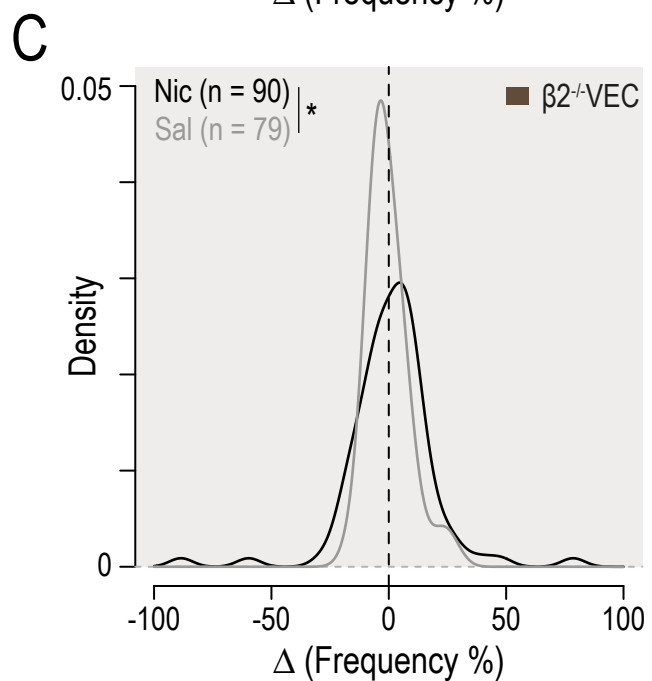
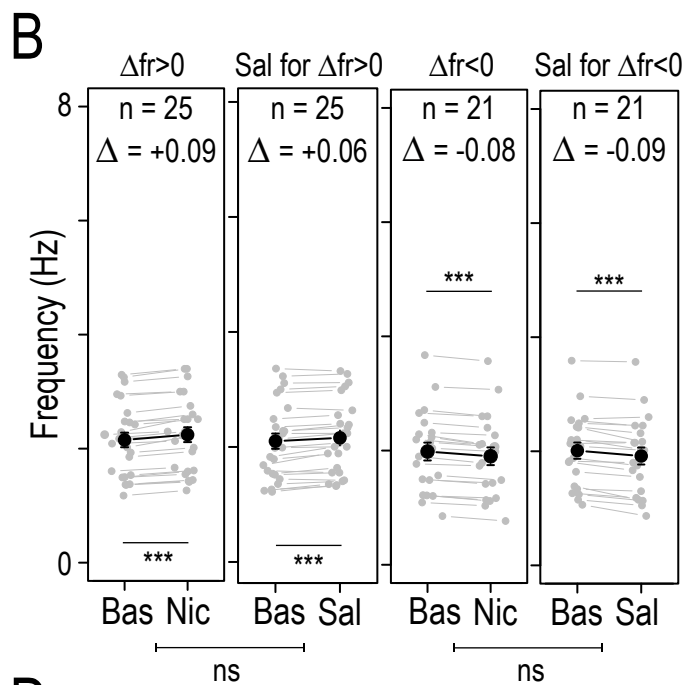
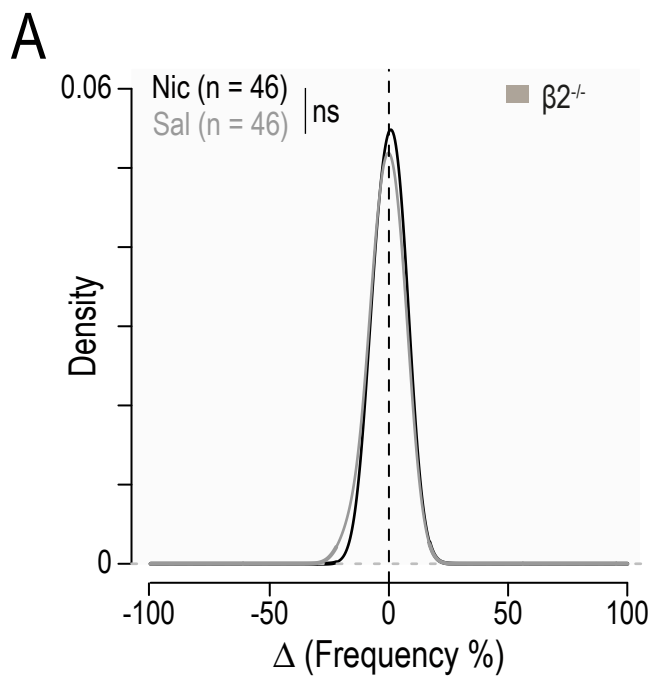


Figure S8

Figure S9: Temporally specific control of DA neuron firing with Jaws and CatCh. Related to Figure 4.

(A) Representative immunofluorescence image of VTA DA neurons after patch-clamp recordings in mice injected with AAV-Ef1 α -DIO-Jaws-eGFP into the VTA. Neurobiotin (NB, blue), tyrosine hydroxylase (TH, red), GFP (green) (scale bar 20 μ m). **(B)** Example of a recording trace of a VTA DA neuron during continuous light stimulation (highlighted in yellow, 20 s, 520 nm) and raster plot of action potentials showing light-induced inhibition in Jaws-expressing DA neurons (n = 7). **(C)** Representative immunofluorescence image of VTA DA neurons (NB, blue; TH, red; GFP, green) after patch-clamp recording in mice injected with AAV-DIO-hCatCh-YFP into the VTA (scale bar 20 μ m). **(D)** Example of recording trace of a DA neuron of the VTA during light stimulation (10 Hz, 5-ms pulse, 470 nm) and light-evoked inward current in DA neurons expressing CatCh. Mean light-evoked currents in seven DA neurons.

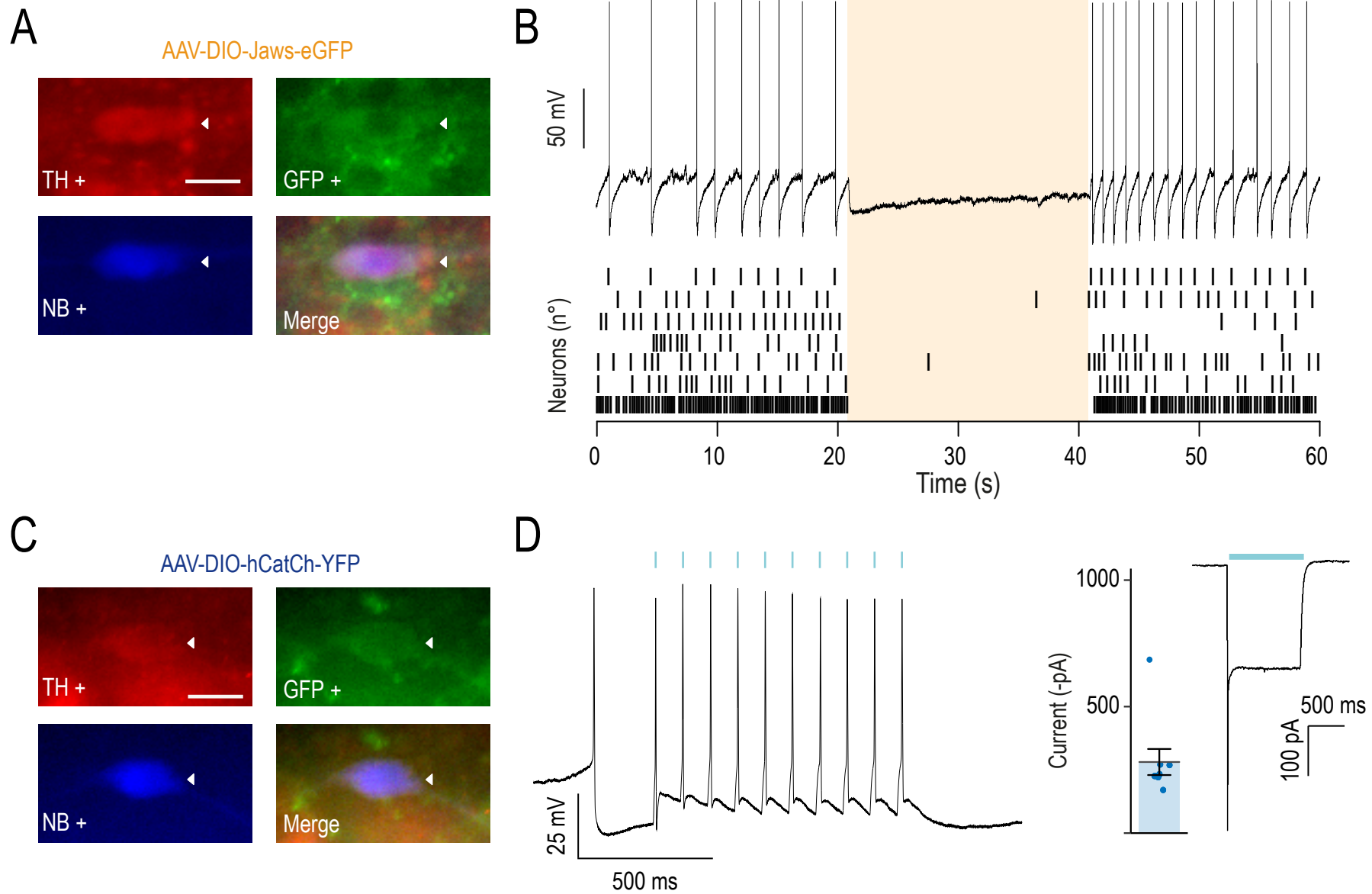


Figure S9

Figure S10: Fiber locations for optogenetic experiments. Related to Figure 4.

(A) Representative immunofluorescence images of VTA sections after AAV-DIO-Jaws-eGFP or AAV-DIO-YFP injection into the VTA. **(B)** Representative immunofluorescence images of VTA sections after AAV-Ef1 α -DIO-hCatCh-YFP or AAV-Ef1 α -DIO-YFP injection into the VTA. **(C)** Verification of fiber implantations into the basolateral Amygdala (BLA) of mice used in optogenetic experiments, positioned onto Paxinos atlas slices from bregma -1.22 to -1.82 mm. *Left side:* orange dots indicate fiber tip location for mice injected with Jaws (n = 13), and green dots indicate fiber location in YFP controls (n = 10). *Right side:* blue dots indicate fiber tip location for mice injected with CatCh (n = 16), and green dots indicate fiber location in YFP controls (n = 11). **(D)** Verification of fiber implantations into the Nucleus Accumbens lateral shell (NAcLSH) of mice used in optogenetic experiments, positioned onto Paxinos atlas slices from bregma + 0.86 to + 1.54 mm. *Left side:* blue dots indicate fiber tip location for mice injected with CatCh (n = 13), and green dots indicate fiber tip positions in YFP controls (n = 14). *Right side:* orange dots indicate fiber tip location for mice injected with Jaws (n = 11), and green dots indicate fiber tip location in YFP controls (n = 12).

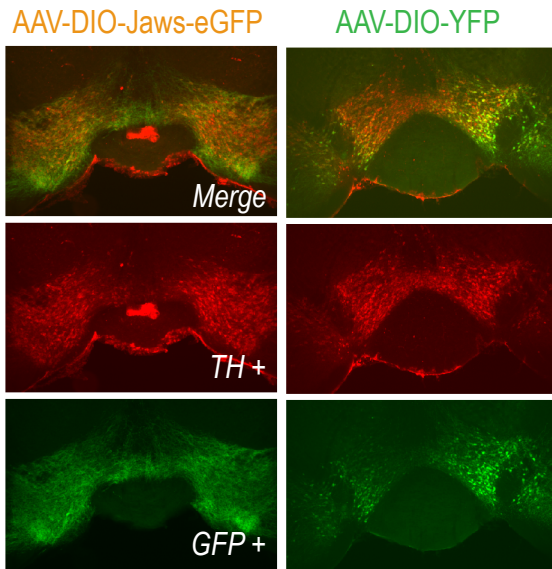
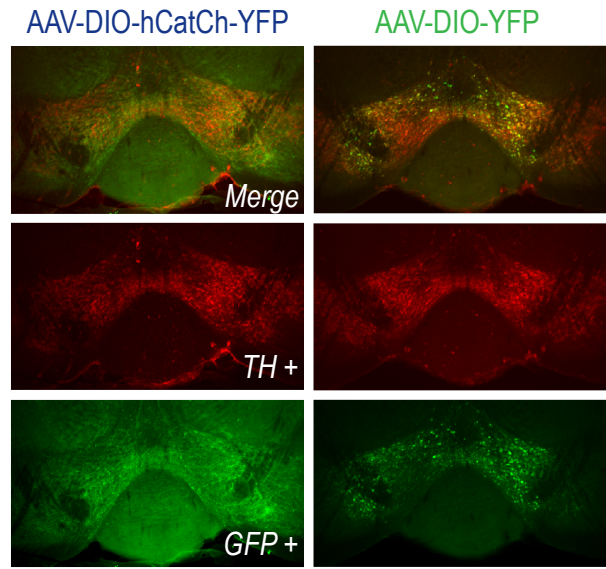
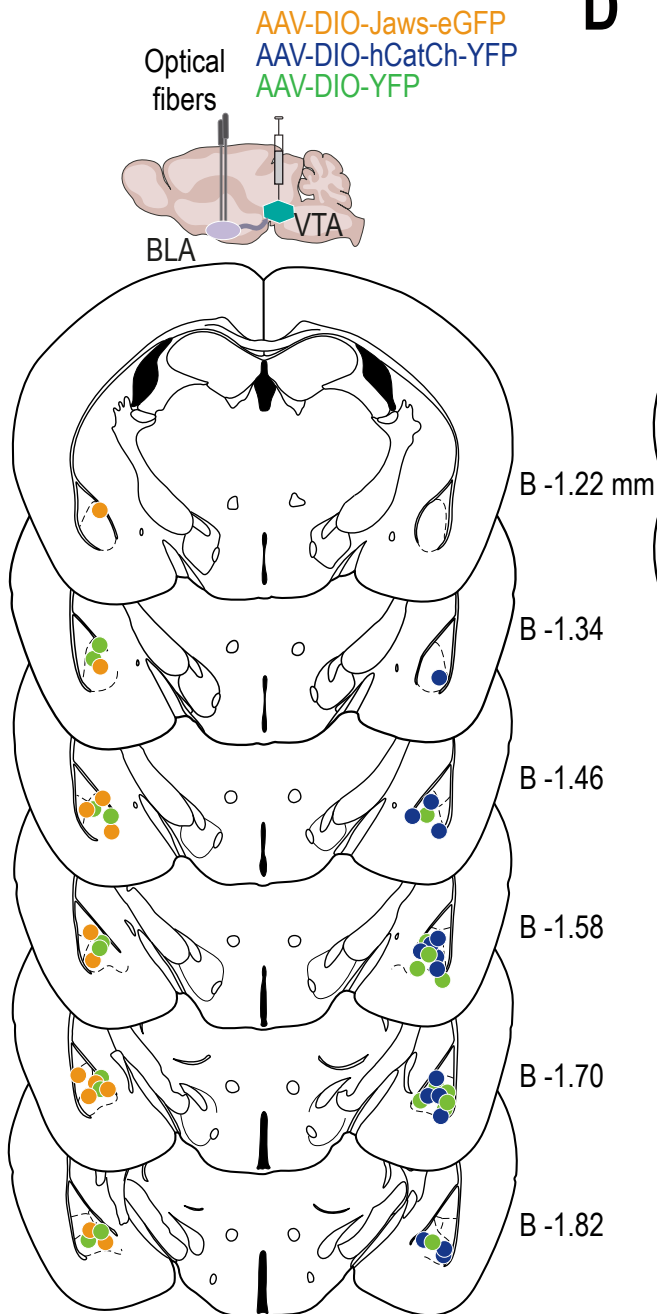
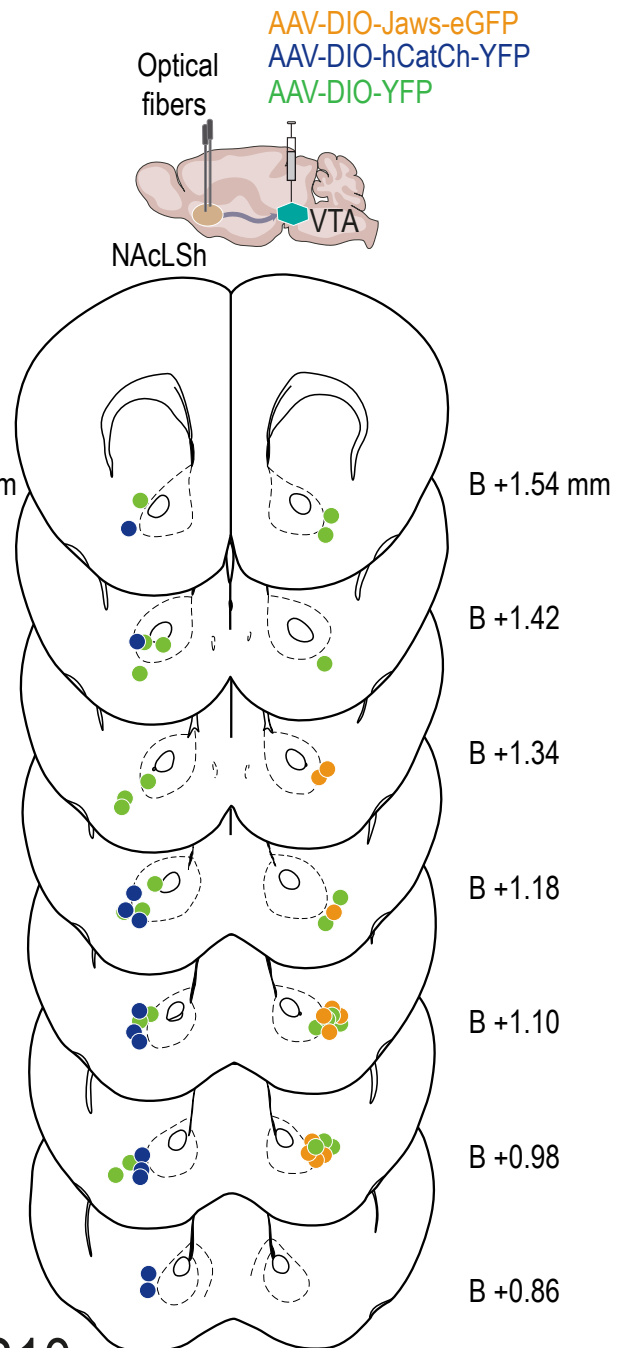
A**B****C****D**

Figure S10

Figure S11: Detailed analysis of optogenetic effects on elevated O-maze test and locomotor behavior. Related to Figure 4.

(A) Left: Individual data for Figure 4A (Jaws, $n = 18$, orange, one-way RM ANOVA $F_{(2,34)} = 5.28$, ** $p = 0.01$; YFP, $n = 19$, green, one-way RM ANOVA $F_{(2,36)} = 0.32$, $p = 0.7$). **Middle:** Time spent in open arms for mice injected with Jaws during the 10 first minute of EOM, divided in two groups depending on the location of the animal, either in open arms (OA, white) or closed arms (CA, gray) at the onset of the stimulation (two-way RM ANOVA OA vs CA main light effect $F_{(1,17)} = 9.02$, ** $p = 0.008$, no effect of position $F_{(1,17)} = 0.003$, $p = 0.96$). **Right:** Open arm entries during EOM (two-way RM ANOVA Jaws vs YFP no effect of time or opsin). Group means are shown by solid color points, individual data with open gray dots. **(B) Left:** Individual data for Figure 4B (CatCh, $n = 18$, blue, one-way RM ANOVA $F_{(2,34)} = 9.27$, *** $p < 0.001$; YFP, $n = 19$, green, one-way ANOVA $F_{(2,36)} = 0.01$, $p = 0.99$). **Middle:** Time spent in open arms for mice injected with CatCh during the 10 first minutes of EOM, divided in two groups depending on the location of the animal, either in open arms (OA, white) or closed arms (CA, gray) at the onset of the stimulation (two-way RM ANOVA OA vs CA main light effect $F_{(1,16)} = 16.56$, *** $p < 0.001$, no effect of position $F_{(1,16)} = 0.32$, $p = 0.57$). **Right:** Open arm entries during EOM (two-way RM ANOVA CatCh vs YFP no effect of time or opsin). Group means are shown by solid color points, individual data with open gray dots. **(C)** Locomotor activity was assessed in a novel open field (OF) in the three paired groups. **Top:** Jaws-injected ($n = 20$) and YFP-injected mice ($n = 20$) with fibers implanted in the BLA (two-way RM ANOVA, main time effect $F_{(2,76)} = 44.27$, *** $p < 0.001$, no opsin or interaction effect). **Bottom:** CatCh-injected ($n = 13$) and YFP-injected mice ($n = 10$) implanted in the BLA (two-way RM ANOVA, main time effect $F_{(2,42)} = 25.17$, *** $p < 0.001$, no opsin or interaction effect).

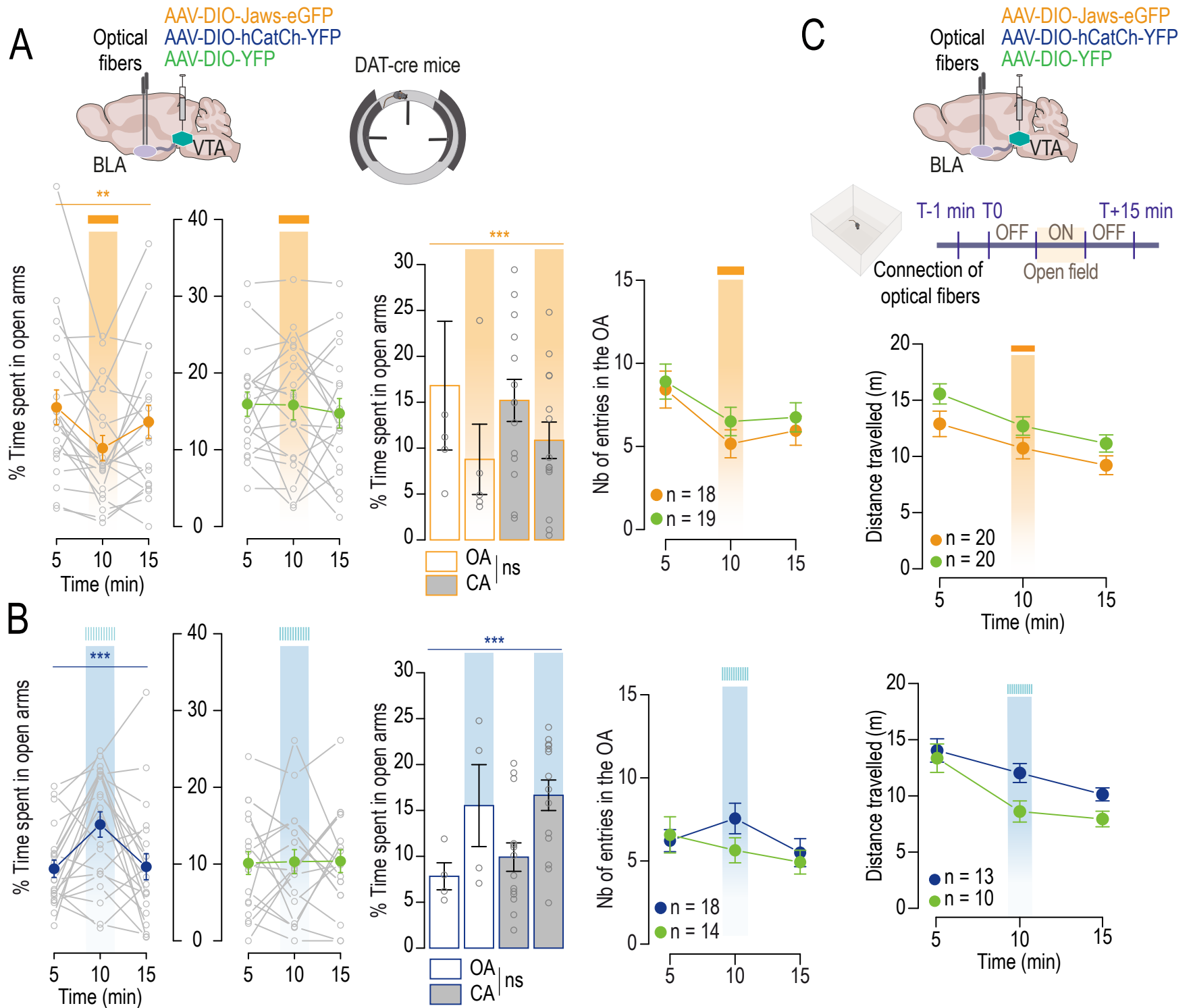


Figure S11

Figure S12: Inhibition of VTA terminals in the BLA, but not the CeA, produces anxiety-like behavior. Related to Figure 4.

(A) *Left*: Representative immunofluorescence image of a VTA section with AAV-CAG-Jaws-GFP (Jaws) expression (GFP: green labeling, TH: red labeling). *Right*: Optical fibers were implanted in the basolateral Amygdala (BLA) of wild-type (WT) mice injected either with Jaws (orange dots represent the fiber tip location, $n = 7$) or with AAV-CAG-GFP (GFP, green dots, $n = 3$) in the VTA. **(B)** *Left*: Representative immunofluorescence image of a VTA section with Jaws expression (GFP: green labeling, TH: red labeling). *Right*: Optical fibers were bilaterally implanted in the central amygdala (CeA) of a separate group of WT mice injected with either Jaws (orange dots represent the fiber tip location, $n = 7$) or with GFP (green dots, $n = 7$) in the VTA. **(C)** Photo-inhibiting VTA axon terminals in the BLA using Jaws during the EOM in the same mice induced a decrease in the time spent in the open arms compared to the control group (two-way RM ANOVA, time x opsin interaction $F_{(2,42)} = 3.44$, * $p = 0.04$, *post hoc* Student's t-test p (ON Jaws vs GFP) = 0.056; *post hoc* Student's t-test with Bonferroni corrections Jaws * p (5 minutes vs 10 minutes) = 0.01; ** p (10 minutes vs 15 minutes) = 0.005). **(D)** Photo-inhibiting VTA terminals in the CeA did not produce any difference in the amount of time spent in the open arm of the EOM test (two-way RM ANOVA, time x opsin interaction $F_{(2,32)} = 3.67$, * $p = 0.04$, *post hoc* Student's t-test with Bonferroni corrections $p > 0.05$). **(E)** Mice implanted in the BLA were tested for any difference in locomotor activity between groups in the open field (OF). The test lasted 15 minutes and consisted of a 5-minute period of photostimulation (continuous at 520 nm) in between two non-stimulation periods (OFF-ON-OFF). During both OFF- and ON-periods, the groups did not present any statistically significant difference in the distance traveled in the OF (two-way RM ANOVA main time effect $F_{(2,44)} = 5.89$, ** $p = 0.005$, no opsin or interaction effect, *post hoc* Student's t-test with Bonferroni corrections, $p > 0.05$). **(F)** Photo-inhibiting VTA terminals in the CeA did not produce any statistically significant difference in locomotor activity in the OF test between the Jaws- and GFP-expressing groups (two-way RM ANOVA main time effect $F_{(2,32)} = 23.11$, *** $p < 0.001$, time x opsin interaction $F_{(2,32)} = 3.8$, * $p = 0.03$, no opsin effect, *post hoc* Student's t-test with Bonferroni corrections, $p > 0.05$).

IF: *interfascicular nucleus*; IPN: *interpeduncular nucleus*; ml: *medial lemniscus*; SNc: *substantia nigra pars compacta*.

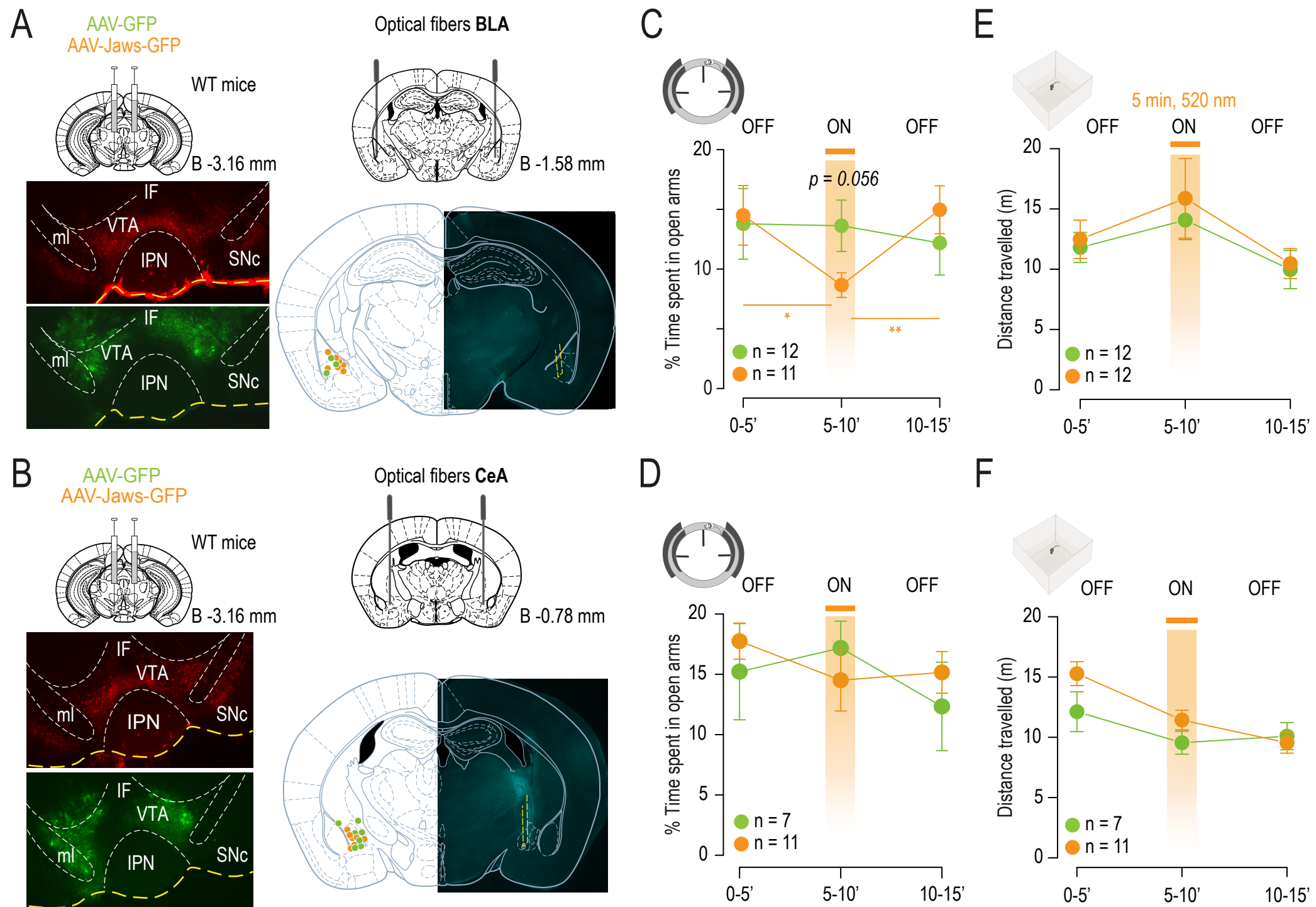


Figure S12

Figure S13: Detailed analysis of optogenetic stimulations of NAcLSH in elevated O-maze test and locomotor behavior. Related to Figure 5.

(A) Left: Individual data for Figure 5A (CatCh, $n = 13$, blue, one-way RM ANOVA $F_{(2,24)} = 0.61$, $p = 0.6$; YFP, $n = 14$, green, one-way RM ANOVA $F_{(2,26)} = 1.47$, $p = 0.3$). **Middle:** Time spent in open arms for mice injected with CatCh during the 10 first minute of EOM, divided in two groups depending on the location of the animal, either in open arms (OA, white) or closed arms (CA, gray) at the onset of the stimulation (two-way RM ANOVA OA vs CA no effect of light $F_{(1,11)} = 0.46$, $p = 0.5$, or position $F_{(1,11)} = 1.35$, $p = 0.27$). **Right:** Open arm entries during EOM (two-way RM ANOVA CatCh vs YFP no effect of time or opsin). Group means are shown by solid color points, individual data with open gray dots. **(B) Left:** Individual data for Figure 5B (Jaws, $n = 12$, orange, one-way RM ANOVA $F_{(2,22)} = 0.25$, $p = 0.8$; YFP, $n = 12$, green, one-way RM ANOVA $F_{(2,22)} = 0.93$, $p = 0.4$). **Middle:** Time spent in open arms for mice injected with Jaws during the 10 first minute of EOM, divided in two groups depending on the location of the animal, either in open arms (OA, white) or closed arms (CA, gray) at the onset of the stimulation (two-way RM ANOVA OA vs CA no effect of light $F_{(1,11)} = 0.18$, $p = 0.67$, or position $F_{(1,11)} = 1.9$, $p = 0.19$). **Right:** Open arm entries during EOM (two-way RM ANOVA Jaws vs YFP no effect of time or opsin). Group means are shown by solid color points, individual data with open gray dots. **(C) Locomotor activity was assessed in a novel open field (OF) in the three paired groups. Top:** CatCh-injected ($n = 13$) and YFP-injected mice ($n = 14$) implanted in the NAcLSH (two-way RM ANOVA, main time effect $F_{(2,50)} = 14.27$, *** $p < 0.001$, time x opsin interaction $F_{(2,50)} = 4$, * $p = 0.02$, *post hoc* Wilcoxon test for CatCh vs YFP at 5 minutes, * $p = 0.04$). **Bottom:** Jaws-injected ($n = 12$) and YFP-injected mice ($n = 12$) implanted in the NAcLSH (two-way RM ANOVA, main time effect $F_{(2,44)} = 12.47$, *** $p < 0.001$).

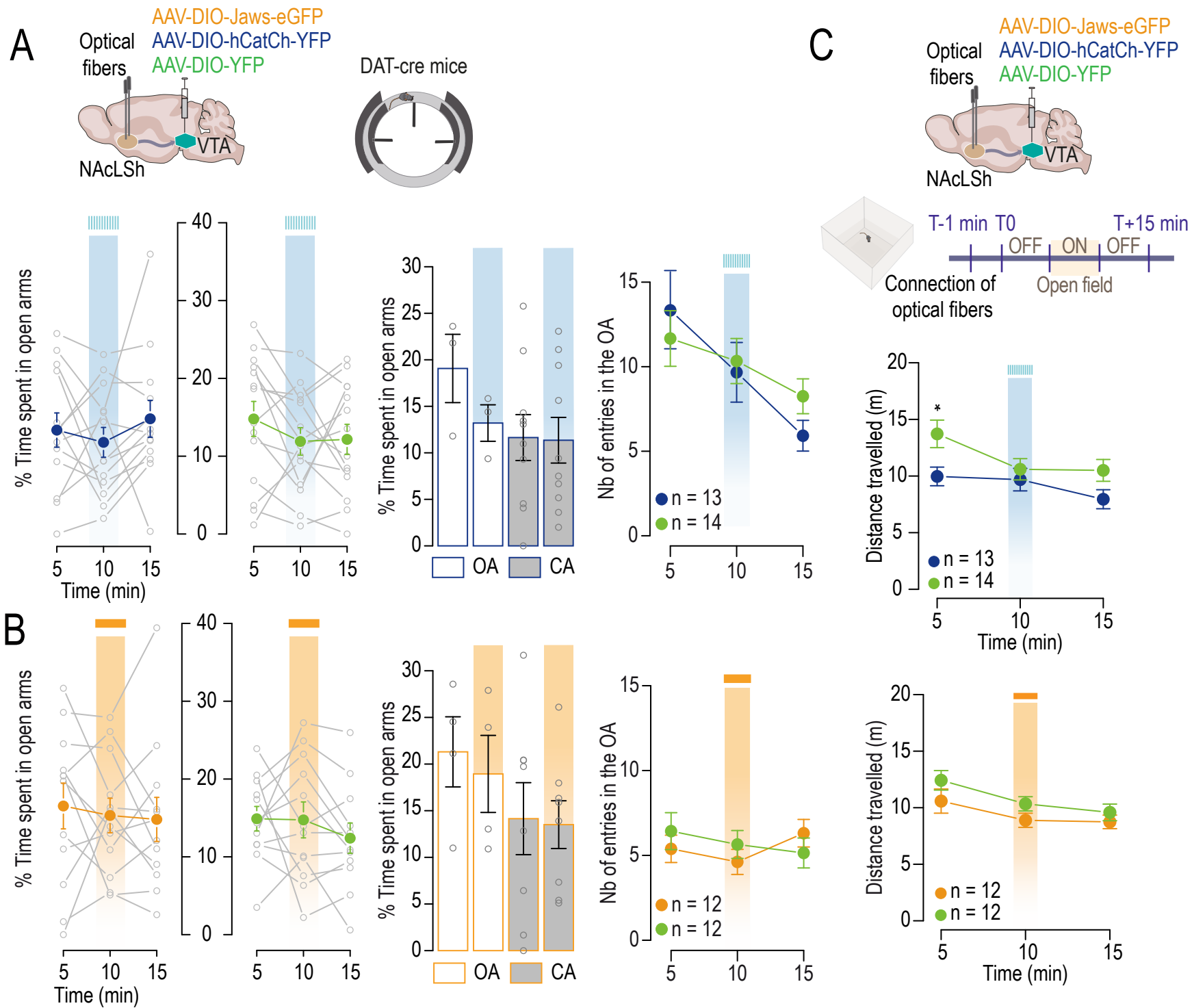


Figure S14: Activation of VTA terminals in the NAcMSh changes the EOM exploration and increases locomotor activity but not place preference. Related to Figure 5.

(A) Top: Representative immunofluorescence image of a VTA section with AAV-hSyn-Jaws-GFP (Jaws) expression (GFP: green labeling, TH: red labeling). **Bottom:** Optical fibers were bilaterally implanted in the NAc medial shell (NAcMSh: bregma 1.7; lateral 1.75; ventral 4.25 mm, angle 12°) of wild-type (WT) mice injected into the VTA with either AAV-hSyn-ChR2-eYFP (ChR2, blue dots represent fiber tip locations, n = 8), Jaws (orange dots, n = 7) or AAV-hSyn-eGFP as a control (GFP, green dots, n = 10) into the VTA. **(B) Top:** Activating VTA axon terminals in the NAcMSh by ChR2 photostimulation during the EOM task induced an increase in both the number of entries into the open arm (two-way RM ANOVA main time effect $F_{(2,28)} = 15.68$, *** $p < 0.001$, time x opsin interaction $F_{(2,28)} = 7.59$, ** $p = 0.002$; *post hoc* Student's t-test for ChR2 vs GFP mice: ** p (ON) = 0.007 ; *post hoc* Student's t-test with Bonferroni corrections for ChR2 mice, *** p (5 vs 10 minutes) < 0.001, *** p (10 vs 15 minutes) = 0.001) and in the percentage of time spent by the mice in the open arms compared to the control group (two-way RM ANOVA main time effect $F_{(2,28)} = 7.28$, ** $p = 0.003$, opsin $F_{(1,14)} = 5.26$, * $p = 0.038$, time x opsin interaction $F_{(2,28)} = 4.53$, * $p = 0.02$; *post hoc* Student's t-test for ChR2 vs GFP mice: *** p (ON) < 0.001; *post hoc* Student's t-test and Wilcoxon test with Bonferroni corrections for ChR2 mice, p (5 vs 10 minutes) = 0.06, *** p (10 vs 15 minutes) < 0.001). **Bottom:** Inhibiting VTA axon terminals in the NAcMSh by Jaws photostimulation during the EOM task did not alter the number of entries into the open arm, nor the percentage of time mice spent in the open arms (two-way RM ANOVA no time or opsin effect, nor interaction effect). **(C) Top:** Locomotor activity assessed in ChR2- and GFP-expressing groups in a square novel open field (OF). The OF test lasts 15 minutes, with 10 Hz photostimulation at 470 nm, 5-ms pulses, during a 5-minute ON period in between two non-stimulation periods (OFF-ON-OFF). Activating VTA terminals in the NAcMSh by ChR2 photostimulation produced a significant increase of locomotor activity compared to GFP-expressing mice (two-way RM ANOVA main time effect $F_{(2,28)} = 38.45$, *** $p < 0.001$, opsin $F_{(1,14)} = 17.93$, *** $p < 0.001$, time x opsin interaction $F_{(2,28)} = 18.45$, *** $p < 0.001$; *post hoc* Student's t-test with Bonferroni corrections for ChR2 mice, *** p (5 vs 10 minutes) < 0.001, *** p (10 vs 15 minutes) < 0.001). **Bottom:** Locomotor activity assessed in Jaws- and GFP-expressing groups, where the stimulation occurs continuously at 520 nm over the 5-minute ON period. Inhibiting VTA terminals in the NAcMSh by Jaws photostimulation did not alter locomotor activity in comparison to GFP-expressing mice (two-way RM ANOVA no time or opsin effect nor interaction effect). **(D)** The number of entries in the open arms (two-way RM ANOVA main time effect $F_{(2,20)} = 5.27$, * $p = 0.014$) and the percentage of time spent in the open arms of the EOM after nicotine IP injection in Jaws or GFP injected mice stimulated continuously throughout the test in the NAcMSh (two-way RM ANOVA main time effect $F_{(2,20)} = 7.88$, ** $p = 0.003$, and effect of opsin $F_{(1,10)} = 7.79$, * $p = 0.019$). **(E)** Preference score in 20min-RTPP defined by the % of time spent in the compartment where the animals are photo-stimulated compared to the compartment where they are not (ON-OFF). Neither activation (Student t-test, $p = 0.4$) nor inhibition (Student t-test, $p = 0.9$) of the DA axon terminals in the NAcMSh induced place preference or aversion.

IF: *interfascicular nucleus*; IPN: *interpeduncular nucleus*; ml: *medial lemniscus*; SNc: *substantia nigra pars compacta*; VTA: *ventral tegmental area*

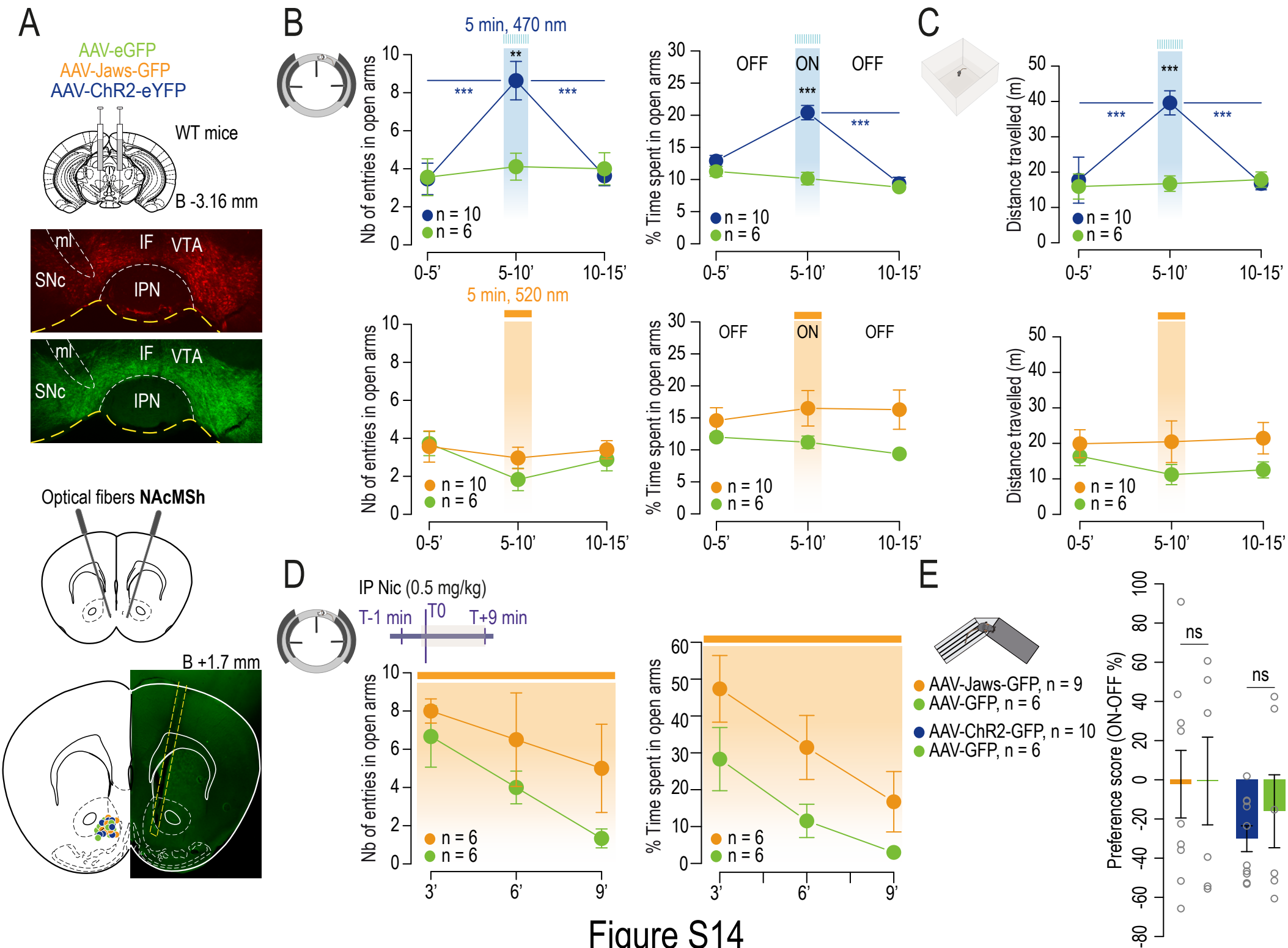


Figure S14